# Dissecting Treg Heterogeneity in Human Cancer to find Novel Targets of Immunotheraphy

## Thesis

Giorgia Alvisi

# DISSECTING TREG HETEROGENEITY IN HUMAN CANCER TO FIND NOVEL TARGETS OF IMMUNOTHERAPY

For the Degree of Doctor of Philosophy

International PhD Program in Immunology

HUMANITAS CLINICAL AND RESEARCH INSTITUTE

(Milan, Italy)

Affiliated Research Centre to “The Open University”

(Milton Keynes, UK)

Under the supervision of

Director of Studies: Dr. Enrico Lugli

Supervisor: Professor Marinos Kallikourdis

External Supervisor: Awen Gallimore, University Hospital of Wales, Cardiff

July 2022

# Abstract

T cell dysfunction in the tumor microenvironment (TME) mediated by the hyper-activation of inhibitory subpopulations such as regulatory T cells (Treg) represents a major obstacle to effective antitumor immunity and immunotherapy. The molecular mechanisms at the basis of the increased immunosuppressive capacity of Treg cells in the TME are currently not clear. Preclinical data shows that bulk Treg depletion improves T cell infiltration and its antitumor activity but simultaneously results in deleterious autoimmune responses. Targeting hyperactive Treg specifically present in the tumor would improve antitumor immunity while reducing toxicity. To this aim, we developed 30-parameter FACS to profile millions of single T cells from chemotherapy-naïve cancer patients. Computational algorithms applied to single-cell data identified T cell subsets preferentially enriched in tumors compared to adjacent normal lung tissue and peripheral blood. We found that the Interferon regulatory factor 4 (IRF4) defines a novel specific subpopulation of tumor infiltrating Tregs with superior immunosuppressive capacity. Integration of transcriptomic data and whole genome binding sites of transcription factors further revealed that IRF4, either alone or in combination with its partner BATF, directly controlled a molecular program responsible for Treg hyperproliferation and suppressive functions that included CTLA-4, ICOS, TNFRSF9 (4-1BB) and IL1R2. Accordingly, deletion of Irf4 exclusively in Tregs resulted in delayed tumor growth in mice while the abundance of IRF4+ Tregs correlated with poor prognosis in patients with multiple human cancers. We further identify mesenchyme homeobox 1 (MEOX1), a transcription factor novel to Treg biology, as sufficient to reprogram circulating Tregs to a tumor-infiltrating 4-1BB+ phenotype. MEOX1 activity sustains hyper-activated Treg gene expression and immunosuppression by favoring chromatin accessibility at sites regulated by AP-1/IRF4/BATF. Thus, Interfering with IRF4-dependent molecular program, which is shared by several solid tumors, may represent a novel immunotherapeutic approach capable to block immunosuppression in the tumor microenvironment.

# Table of contents

# 1. Introduction

## 1.1. Adaptive T cell responses

T lymphocytes are crucial players of the cell-mediated adaptive immune responses against infections and malignancies. They are characterized by a cell surface specific receptor, namely T cell receptor (TCR) recognizing cognate antigens (Ag) presented by major histocompatibility complex (MHC) on the surface of antigen presenting cells (APCs) or target cells (Morris and Allen, 2012). Recombination of TCR genes results in remarkably broad repertoire of distinct antigen specificities.

T cells originate from bone marrow deriving precursors that home to the thymus to undergo a process of maturation including TCR $\alpha\beta$ (or less frequently $\gamma\delta$) genes rearrangement (Robey and Fowlkes, 1994). Once into the thymus, the T cell precursors lack expression of CD4 and CD8 co-stimulatory proteins and are called double negative (DN) (Spits, 2002). The DN thymocytes rearrange variable (V), diversity (D) and joining (J) segments of the variable TRB locus and express a pre-TCR complex composed of β chain and an invariant pre-Tα chain on the cell surface. The variable pre-TCR-αβ is associated with the invariable intracellular CD3/ζ-complex, which is involved in the intracellular transduction of the signal. Biochemical changes in the cytoplasmic portions of the CD3 complex such as the phosphorylation of the tyrosine-based activation motifs (ITAMs), trigger the rearrangement of the TCRβ chain which in turn stimulates thymocyte proliferation, rearrangement of the TCRα chain locus and induction of the two TCR co-receptors CD4 and CD8. At the Double-positive (DP) stage, $CD8^+CD4^+$ thymocytes undergo a random rearrangement of V and J chain of the TCRα locus generating diversity in TCR specificities. Although theoretical models calculate that the human genome is capable of generating over $10^{15}$ different TCRs, the actual observed diversity is estimated at $2.5x10^8$ (Robins et al., 2009), leading to hypothesize that high levels of TCR degeneracy are required to cover a full spectrum of possible peptides. Accordingly, it has been shown that a single TCR is able to recognize $>10^6$ diverse peptides (Wooldridge et al., 2012).

DP cells located in the cortex region of the thymus can recognize self-

peptides presented by the major histocompatibility complex (MHC). This interaction with “self” is crucial for thymocytes survival. Indeed, only those with low but sufficient affinity to self-peptide:MHC (p:MHC) complexes expressed on thymic epithelial cells will be positively selected. By contrast, T cells which bind MHC with high affinity are harmful as potentially autoreactive, thus are negative selected and die by apoptosis. Around 70% of thymocytes are eliminated by negative selection while the remaining fractions maturate into single-positive (SP) naïve ($T_N$) CD4+ and CD8+ T cells. The commitment towards the CD4+ or CD8+ functionally divergent T cell lineages depends on the interaction with two different classes of MHC: DP thymocytes with TCRs that recognize peptide complexed with MHC class I on the surface of APC develop toward CD8 SP thymocytes, whereas those recognizing peptide complexed with MHC class II develop toward CD4 SP thymocytes (Starr et al., 2003).

After arrangement of the mature TCR within the thymus, $T_N$ migrate to the periphery and patrol secondary lymphoid organs (SLOs) where they continuously scan antigen presenting cells in search of their cognate-Ag (Mannie et al., 1991). After Ag recognition, $T_N$ cells get activated and generate more differentiated effector cells (expansion phase) whose function is to eliminate exogenous threats. $CD8_+$ ‘killer’ effector T cells are key players of cell-mediated immune responses against intracellular pathogens and tumor cells (Jaime-Sanchez et al., 2020; Nu Zhang at al., 2011; Anne M. van der Leun, Daniela S. Thommen and Ton N. Schumacher, 2020). They are able to destroy target cells through direct cellular cytotoxicity, but much of their function can also be attributed to effector cytokines release (eg. TNF, IFNγ) (Zhang & Bevan, 2011). $CD4_+$ T ‘helper’ ($T_H$) cells orchestrate adaptive immunity via juxtracrine and cytokine signalling. They differentiate into specific subtypes depending mainly on the cytokine milieu of the microenvironment. For instance, transforming growth factor β (TGFβ) and interleukin 6 (IL6) direct the development of IL-17 producing $T_H17$ cells during extracellular bacterial and fungal infection; IFNγ and IL12 drive the differentiation of IFNγ-$T_H1$ cells that help to combat intracellular pathogens; IL-4 induces IL4-producing $T_H2$ cells during infection with large mucosal parasites. The functional specialization of these subsets is associated with master

transcription factors (TF), including retinoic acid receptor related orphan receptor-γt (RORγt) for $T_H17$, GATA-binding protein 3 (GATA3) and interferon regulatory factor 4 (IRF4) for $T_H2$ and T-box transcription factor TBX21 (T-bet) for $T_H1$ (Brummelman*; Pilipov* et al., 2018).

After infection, the vast majority of T cells (95%) dies (contraction phase), while a small fraction survives and generates memory cells, which persist in the long term (Reinhardt et al, 2001). Memory cells are clonally expanded and activate more rapidly than $T_N$ cells after a subsequent antigen encounter, thus ensuring enhanced protection in case of re-infection.

## 1.2. Immune tolerance

T cells can recognize and eradicate a large variety of pathogens while remaining unresponsive towards self-tissue. This phenomenon is known as immune tolerance and it is ensured by central and peripheral mechanisms. Tolerance mechanisms that operate in the thymus before the maturation and circulation of T cells are referred to as “central tolerance” while mechanisms that act on mature circulating T cells and are referred to as “peripheral tolerance.”

Central tolerance is achieved by the abovementioned negative selection of thymocytes with high affinity for self-peptide:MHC and it is only ~70% efficient. Indeed, not all self-Ags are expressed in the thymus to ensure a complete elimination of potentially self-reactive specificities (Bouneaud et al., 2000). Also the first layer of peripheral tolerance concerns the affinity threshold of the TCR-p:MHC interaction. Indeed clonal deletion in the thymus requires a lower affinity compared to the one that is sufficient to induce T cell activation in the periphery (Pircher et al., 1991) and for this reason, mature $T_N$ cells show low-reactivity to self-Ags and are refractory to peripheral activation. After Ag-specific TCR triggering, extrinsic mechanisms contributes to self-tolerance maintenance. Specifically, in the absence of pathogens, antigen presenting cells such as dendritic cells (DC) are quiescent and express low levels of co-stimulatory molecules such as CD80 and CD86 that bind the T cells co-stimulatory receptor CD28 (Steinman et al., 2003). In the absence of this co-stimulatory signal, T cells are eliminated by clonal deletion or enter in a long-term state of

hypo-responsiveness and repression of TCR activation signalling called “anergy” (Redmond and Sherman et al., 2005).

An additional dominant mechanism of peripheral tolerance involves regulatory T cells (Treg), a highly immunosuppressive subset of CD4+ T cells (Sakaguchi et al, 1995). Treg cells express high levels of the IL2-receptor α chain (CD25) and the forkhead box transcription factor 3 (Foxp3), which acts as a lineage-specifying factor by determining the unique suppressive function of these cells (Rudensky, 2011; Hori et al., 2003). Humans with a mutation in the *FOXP3* gene are affected by Treg dysfunction and develop X-linked (IPEX) syndrome characterized by multiple autoimmune disorders (Bennett et al., 2001). Similarly, mice that lack Foxp3 expression are deficient in Treg cell and develop lethal auto-immunity and lymphoproliferative diseases (Brunkow et al., 2001; Fontenot et al., 2003). Thus, Tregs are indispensable to maintain immune homeostasis and prevent autoimmunity and immunopathology. Expression of IL-7 receptor subunit (CD127) is inversely correlated with the expression of Foxp3 and the suppressive function of human Treg, and it is currently used in conjunction with CD25 as a surface phenotypic marker in the purification of Treg cells, defined in humans as CD4+CD25+CD127- T cells (Liu et al., 2006).

The neonatal thymectomy showed that the majority of Treg cells develop in the thymus (tTreg): according to a current model, a thymocyte with intermediate-affinity TCR for a self-peptide/MHC is driven to the Treg cell lineage, while developing T cell with low-affinity TCR generate naïve T cell and one with high-affinity TCR is deleted by the abovementioned negative selection (**Figure 1**).

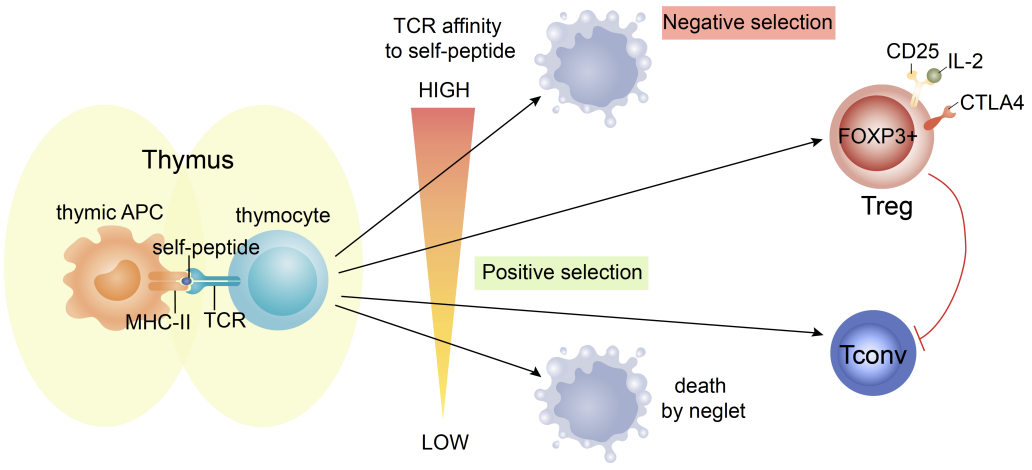

**Figure 1: Treg development.** Treg development is initiated by TCR signalling that is activated upon recognition of self-antigen presented by MHC class II molecules expressed on thymic APCs. Specifically, intermediate TCR stimulation in precursor thymocytes is followed by sequential activation of IL-2 receptor α chain, IL-2 signalling and expression of Foxp3, which orchestrate differentiation of these cells into Treg. Immature T cells with higher affinity for self-antigen are potentially auto-reactive T cells and are negative selected while T cells with lower but sufficient affinity for MHC molecules are positively selected. Thymocytes with too low affinity for self-peptide-MHC complex cannot survive without TCR signalling and are eliminated by a process called death by neglect.

*Figure 1*

tTreg cells undergo further differentiation and functional specialization in the periphery, featuring their migration into non-lymphoid tissues and their maintenance under inflammatory conditions. Additionally, strong TCR signalling, suboptimal co-stimulation and high amounts of TGFβ and retinoic acid promote the induction of FOXP3 in peripheral naïve CD4 T cells (pTreg) (Josefowicz et al., 2012; Abbas et al., 2013). tTregs are mainly involved in tolerance to self-antigens while pTreg restrain immune responses against non-self antigens such as allergens, commensal microbiota and paternal alloantigens.

Noteworthy, CD4+FOXP3+ Treg cells are not the only suppressive cells that mediate immune tolerance. Other immune types with immunosuppressive functions include CD8+FOXP3+ Treg cells, IL-10 producing type 1 regulatory T cells (Tr1) (Bonnal et al., 2021), TGFβ-producing CD4+ Th3 cells, regulatory γδ T cells, regulatory B (Breg) cells, myeloid derived suppressor cells (MDSCs), immunosuppressive plasmocites, regulatory invariant natural killer (NK) cells and subsets of innate lymphoid cells. Although these cells might play specific roles in infections or cancer, FOXP3+ seems to be the dominant population involved in peripheral tolerance as demonstrated by studies showing that bulk depletion of Tregs results in detrimental autoimmunity, allergy and immunopathology (Chinen et al., 2016; McHugh et al., 2002; Sethoguchi et al., 2005).

### 1.2.1 Treg-mediated immune-suppression

Tregs maintain immune homeostasis in physiology by inhibiting immune cells via different modes of action, including expression of cell-surface inhibitors, such as cytotoxic T Lymphocyte Antigen 4 (CTLA-4) (Wing et

al., 2008); depletion of IL-2 by overexpression of CD25; production of inhibitory cytokines, such as IL-10 (Larmonier et al., 2006), TGF-β (Chen et al., 2005) or IL-35 (Collison et al., 2007); purine-mediated suppression by CD39-dependent ATP degradation (Deaglio et al., 2007); or direct cytotoxicity through granzymes and/or perforin (Grossman et al., 2004) (**Figure 2**). The combinatorial mechanisms that Tregs use to exert their suppressive activity depend on the disease setting, inflammatory status of the local environment, and their anatomical localization.

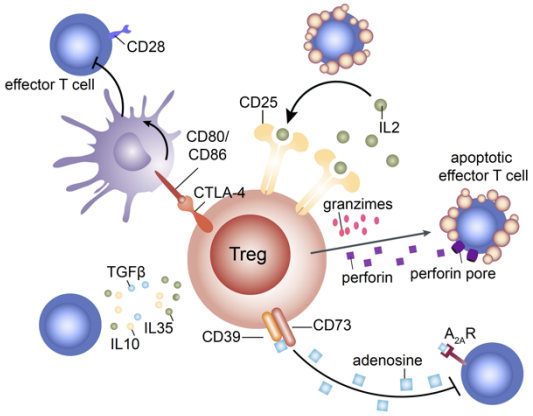


**Figure 2: Treg-mediated immune suppression.** Tregs constitutively express IL2Rα (CD25) and thus bind to and deplete IL-2 from their surrounding environment, hence reducing the availability of this cytokine for other effector cells. They also constitutively express CTLA-4, which bind to CD80/CD86 on APC therefore reducing their ability to prime and activate effector cells. Furthermore, Tregs can produce immunosuppressive cytokines, such al IL-10, IL-35 and TGFβ, which dampen the activity of APC and effector T cells, and can secrete granzymes and perforins that directly kill these cells. Finally, Treg can convert ATP in adenosine via ectonucleoside triphosphate diphosphohydrolase 1 (CD39) and 5'-nucleotidase (CD73), thereby inhibiting effector cells through the adenosine $A_{2A}$ receptor ($A_{2A}R$) pathway.

*Figure 2*

Among all, competition for IL-2 consumption together with constitutive high expression of CTLA-4, are essential core mechanisms for the immunosuppressive functions of Treg on the basis of the following observations. First, neutralization of circulating IL-2 by administration of anti-IL-2 Abs hampers Treg function and survival, resulting in severe autoimmunity (Sakaguchi et al., 2008). Accordingly, high dose of IL-2 abrogates Treg cell-mediated immune suppression of T cell activation and proliferation in vitro (Takahashi et al., 1998; Thornton et al., 1998). Second, mice with Treg-specific CTLA4 deficiency develop severe autoimmune disorders involving multiple organs (Wing et al., 2008). Moreover, heterozygous *CTLA4* mutations cause multiple autoimmune manifestations associated with impairment in the immunosuppressive activity of Treg cells (Shubert et al., 2014; Kuehn et al., 2014). Mechanistically, CTLA4 binds CD80 and CD86 on APC with higher affinity

than CD28, thereby depriving Tconv cells of co-stimulatory signals (Walker et al., 2011). In addition, CTLA4 can deplete CD80/CD86 from the cell surface by trogocytosis. Through these mechanisms, Treg cells can suppress Tconv in an antigen specific-manner by inhibiting the maturation of APCs presenting antigens.

### 1.2.2. Human Treg heterogeneity

Human Tregs are broadly subdivided into two major populations according to their immunophenotypic landscape, activation status and localization in the body (**Figure 3A**; Miyara et al., 2009).

Resting Tregs (rTregs) are FOXP3$^{int}$CD45RA$^{hi}$CD25$^{int}$, represent the majority of Treg cells in the circulation and secondary lymphoid organs, and share phenotypic features with naïve and memory conventional T cells (Tconv), but are endowed with a baseline suppressive function and a history of antigen exposure. Upon TCR stimulation, resting Treg proliferate and further differentiate in highly immunosuppressive effector Treg (eTreg). eTregs are FOXP3$^{hi}$CD45RA$^{low}$CD25$^{hi}$, share phenotypic features with activated Tconv and are empowered by enhanced migration capacity to non-lymphoid tissues. Each non-lymphoid organ may house distinct populations of tissue-resident eTreg cells, which adopt functions according to local immune regulation (**Figure 3B**).

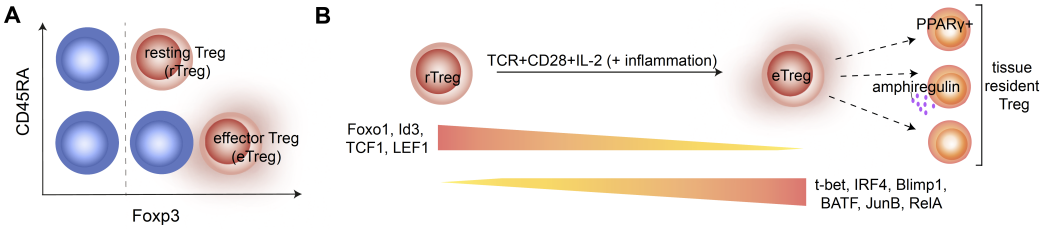


**Figure 3: Treg activation and differentiation. A.** In humans, CD4+FOXP3+ Treg cells can be divided into 2 main groups: FOXP3$^{int}$CD45RA$^{hi}$CD25$^{int}$resting Treg (rTregs) or FOXP3$^{hi}$CD45RA$^{low}$CD25$^{hi}$ effector Treg (eTreg). **B.** FOXP3+ Treg leave the thymus and recirculate through SLOSs as rTreg. Activation signals involving TCR ligation, CD28 co-stimulation and/or IL2 induce rTreg differentiation into eTreg. However, eTreg surveillance of SLOs is not sufficient to maintain immunological tolerance; therefore, specialization into discrete tissue-resident subsets is required. An example of long-term resident Treg cells are those present in adipose-tissue, which are marked by the expression of peroxisome proliferator-activated receptor gamma (PPAR-γ) and regulate insulin resistance (Cipolletta et al., 2012). Other examples are eTregs that reside in skeleton muscle. Here, they prevent inflammation and produce the grown factor amphiregulin that enhance the regeneration of muscle satellite cells and potentiate muscle repair after muscle injury (Burzyn at al., 2013).
*Figure 3*

In addition to rTreg and eTreg subsets, another FOXP3 expressing subset can be identified in the peripheral blood, ie $FOXP3^{low}CD45RA^{low}$ cells. Indeed, while in mice Foxp3 is an exclusive marker of Treg lineage, in humans it can be transiently expressed at low level upon TCR stimulation by Tconv cells that are not immunosuppressive but rather immunostimulatory, producing IFNγ and IL-17. Comprehensive screening of monoclonal antibodies reactive with human lymphocytes identified CD15s (syalyn Lewis x) as a candidate marker for separating FOXP3+ Treg and FOXP3+non-Treg cells. CD15s is a ligand for selectin that promotes binding to endothelial cells and subsequent migration to the tissues. CD15s+CD45RA-FOXP3+ cells are suppressive while CD15s-CD45RA-FOXP3+ counterpart is not and secretes cytokines such as IL2 and INFγ (Miyara et al., 2015). Other molecules such as HLA-DR, T-Cell Membrane Protein 3 (TIM3), Inducibile T Cell Costimulator (ICOS), which are induced upon activation, have also been proposed as markers relatively specific for highly suppressive FOXP3+ T cells (Sakaguchi et al., 2020).

The classification in resting, effector and non-Treg FOXP3+ expressing cells based on surface markers expression has a good correlation with Treg-specific epigenetic changes. A distinct DNA methylation pattern combined with the formation of characteristic histone modifications establishes an open chromatin structure at the Treg-specific demethylation region (TSDR) that allows binding of transcription factors (TF) and *FOXP3* expression. rTregs are stable Tregs with a de-methylated Foxp3 enhancer CNS2, which is more profoundly de-methylated in eTreg while methylated in Tconv transiently expressing Foxp3 (Ohkura et al., 2012; Ohkura et al., 2013). Moreover, both CD25 and CTLA4 are expressed by Treg as well as activated Tconv cells, but Tregs express these molecules constitutively and at high levels whereas Tconv non-constitutively and after TCR stimulation. This difference mirrors a clear difference in the CpG methylation status at the TSDR in Foxp3, CD25, CTLA-4, Helios and other Treg-signature genes. Thus, the Treg-specific epigenome, in particular Treg-specific CpG hypomethylation, is required for stable maintenance of the Treg phenotype and function and can be used to differentiate between Tregs and activated Tconv transiently expressing Foxp3.

### 1.2.3. Transcriptional control of Treg differentiation

FOXP3 is required for the establishment and maintenance of Treg lineage identity and function but it does not act alone. Several other TF cooperate with it to stabilize the expression of the Treg cell signature and/or polarize the effector Treg program differentiation (**Figure 3B**).

T cell specific transcription factor 1 (TCF1) and lymphoid enhancer binding factor 1 (LEF1) (Yang et al., 2019), Forkhead box protein O1 (FOXO1) (Ouyang et al., 2012) and DNA-binding protein inhibitor 3 (ID3) (Miyazaki et al., 2014) are essential for maintaining the resting Treg pool while their inactivation is required to relieve the eTreg differentiation path. Once activated by TCR, Tregs undergo a program of effector differentiation that mirrors $T_H$ cell differentiation by up-regulating TFs usually associated with $T_H$ polarization (Cretney et al., 2013). Specifically, T-bet is required for Treg cell homeostasis and function during polarized $T_H1$-type inflammatory responses (Koch et al., 2009). Indeed, T-bet+ Treg cells are enriched at sites of $T_H1$-type inflammation. Notably, T-bet-deficient Treg cells display impaired proliferation during $T_H1$ cell-mediated immune responses, ultimately failing to control expansion of IFNγ-producing $T_H1$ cells when transferred into FOXP3-deficient mice. Similarly, Treg cell expression of IRF4 is required for Treg cell-mediated control of $T_H2$-type inflammatory responses (Zheng et al., 2009). Mice in which *Irf4* is specifically deleted within FOXP3+ Treg cells down-regulate CTLA-4, B lymphocyte-induced maturation protein (BLIMP1), ICOS (Cretney et al., 2013) and develop a lymphoproliferative diseases associated with a selective increase of IL4 and IL5-producing $T_H2$-like CD4+ T cells (Zheng et al., 2009). IRF4 cooperates with other TFs in DNA binding and regulating transcription in Treg cells, namely the AP-1 family members Basic Leucine Zipper ATF-Like Transcription (BATF) and JunB (Li P et al., 2012). *Batf*-deficient Treg cells fail to differentiate into eTreg cells and to accumulate in peripheral tissues, such as colon and visceral adipose tissues (VAT) (Hayatsu et al., 2017; Vasanthakumar et al., 2015). Like BATF and IRF4, JunB is highly expressed in ICOS+ eTreg cells in vivo and can be induced by stimulation with anti-CD3 and anti-CD28 antibodies in the presence of IL2 in vitro (Koizumi et al., 2018). Mechanistically, JunB promotes DNA-binding of IRF4 at loci of eTreg-related genes containing AP-1 composite elements

(AICE) motifs, such as *Icos* and *Ctla4*, on which JunB colocalizes with BATF and IRF4. Treg-specific *JunB*-deficient mice exhibit severe inflammation in the colon and lung, aberrant activation of $T_H1$, $T_H2$, and $T_H17$ cells, and enhanced humoral immune responses.

Finally, TNFRSF-signalling induced activation of NF-kB transcription factor RelA is required in a non-redundant manner to maintain the pool of eTreg cells in lymphoid and non-lymphoid tissues in both mice and humans. Indeed RelA is essential for basic eTreg cellular process, including survival and metabolism, but it is not required for DNA binding and/or expression of IRF4 (Vasanthakumar et al., 2017).

In conclusion, Treg have a very diverse and dynamic repertoire of TF that changes depending on the inflammatory context as well as the location of the response. Further elucidation of specific transcriptional regulatory mechanisms involved in the differentiation of tissue resident eTreg may contribute to the development of drugs that target local Treg functions while preserving the systemic Treg-mediate homeostasis.

## 1.3. Natural antitumor T cell response

Cancer cells acquire mutations during tumorigenesis and establish their own protective environment, called tumor microenvironment (TME), which is highly immunosuppressive, tolerogenic, hypoxic and rich of angiogenic factors. Although antitumor immune cells, such as T cells and natural killer (NK) cells, normally infiltrate tumors, and their abundance correlates with better prognosis, suppression of the antitumor immune response in the TME is a major obstacle to tumor eradication. Specifically, T cells in the TME are exposed to chronic antigen stimulation and undergo a dysfunctional program generally referred to as “exhaustion” characterized by progressive loss of IL2, TNF and IFN$\gamma$ effector cytokine production capacity, decreased proliferation potential and increased expression of inhibitory receptors such as PD-1, CTLA-4, lymphocyte-activation gene 3 (LAG3), TIM3, the natural killer cell receptor 2B4 (CD244) and CD160 (Virgin et al., 2009; Wherry, 2011; Wolf et al., 2019). The gene expression profile of exhausted T cells ($T_{EX}$) differ from that of functional memory and effector T cell populations, nevertheless, genes that are involved in effector differentiation may also play a role during the development of

exhaustion. Although the exhausted state may have evolved to protect against detrimental immunotoxicity and autoimmunity, cancer cells exploit these adaptive traits to promote immunosuppression.

Despite chronic T cell receptor activation, other critical immune-regulatory mechanisms driving T cell exhaustion at the tumor sites include: defective help from CD4+ cells; hyper-activation of suppressive cells (ie. Tregs, MDSCs); abundance of soluble mediators (ie. IL10, TGFβ, adenosine); metabolic restrictions (ie. hypoxia) (Tanaka et al., 2017; Speiser et al., 2016; Zorour et al. 2016). Among others, the ratio of Treg cells to CD8+ T cell in tumor tissues is a reliable indicator of prognosis (Roychoudhuri et al., 2015), with a high ratio generally indicating a poor prognosis and reduced survival of patients with different cancer types, including breast, ovarian cancer, lung cancer, pancreatic ductal adenocarcinoma, glioblastoma, melanoma and other malignancies (Galon et al., 2013).

### 1.3.1. Tregs in cancer

In the TME, eTregs are aberrantly enriched and dampen anti-tumor immunity (Tanaka & Sakaguchi, 2017; Gallimore et al., 2019). Transcriptome analysis of human cancer specimens has further revealed that tumor-infiltrating Tregs express high levels of various activation markers, such as *LAG3, HAVCR2* (encoding TIM3), *ICOS*, Tumor Necrosis Factor Receptor Superfamily member 4 (*TNFRSF4*, encoding OX40), glucorticoid-induced TNFR-related protein (*TNFRSF18*, encoding GITR), compared to Tregs in the blood and healthy tissues (De Simone et al., 2016; Plitas et al., 2016). One possible mechanism of the aberrant activation of Treg in the TME is that proliferating and dying tumor cells present a larger number of self-antigens, which are preferentially recognized by Treg cells (Nishikawa et al., 2005; Oliveira et al., 2022). The TCR repertoire of Tregs infiltrating tumors in mice is skewed toward self-antigens and different from that of tumor infiltrating Tconv, suggesting that Treg are able to clonally expand in the TME (Hindley et al., 2011; Saint-Perez et al., 2012). These findings have been recapitulated in human breast cancer (Plitas et al., 2016) and melanoma (Ahmadzadeh et al., 2019).

An additional mechanism of Treg activation in the TME involves focal adhesion kinase (FAK). Indeed, it has been demonstrated that activation

of FAK in tumor cells drives exhaustion of CD8+ T cells and recruitment of Tregs in the tumor microenvironment by regulating chemokine/cytokine and ligand-receptor networks, including CCL5 (Serrels et al., 2015). Thus, signals provided by tumor intrinsic factors such as driver gene alterations can engage eTreg in the tumor lesions by changing chemokine milieu.

### 1.3.1.1. Targeting Treg cells to boost anti-tumor immunity

Since Treg critically promote tumor progression by preventing optimal function of effector cells, several potential strategies to restrain Treg-mediate immunosuppression in solid tumors have been clinically and/or pre-clinically tested (**Figure 4).**

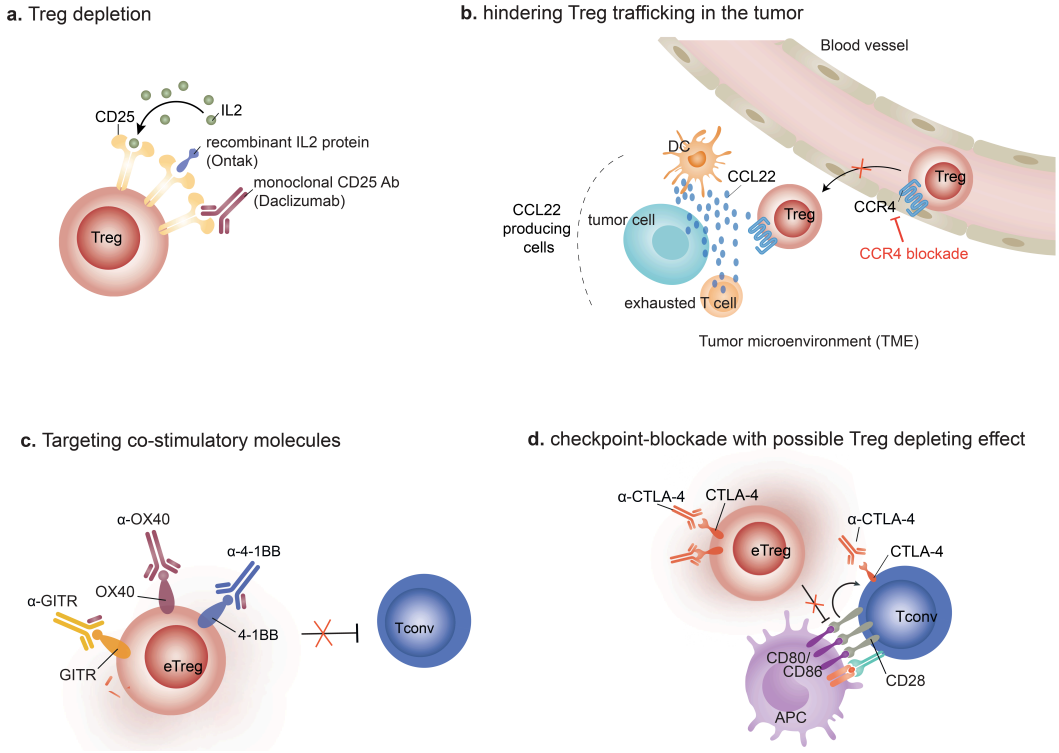


**Figure 4. Targeting Treg cells in cancer immunotherapy.** Tumor progression is determined by the tip of balance of host antitumor immunity versus immune suppression in the TME. Strategies directly against intratumoral Treg involve targeting molecules specifically over-expressed by eTregs such as CTLA-4, CCR4, OX40, GITR, or signals that are crucial for Treg survival and functions, such as TCR and IL2 signaling. Rational combinatorial strategies are others key matter of research.
*Figure 4*

a. **Treg depletion in tumor lesions.** Treg depletion by blocking IL2 or CD25 in mice resulted in enhanced antitumor activity but concomitant manifestations of autoimmunity, underlying that improved specificity for tumor Treg cells is required to preserve homeostasis (Chinen et al., 2016; McHugh et al., 2002; Sethoguchi

et al., 2005; Wei et al., 2005). In humans two drugs for Treg depletion by targeting CD25 have been developed: monoclonal antibodies against CD25 (Daclizumab) and a recombinant IL2 protein composed of IL2 linked with the active domain of diphtheria toxin (Ontak). Daclizumab, when combined with vaccines, had beneficial effects in patients with glioblastoma and breast cancer (Rech et al., 2012; Jacobs et al., 2010) but was reported to have marginal effect in metastatic melanoma (Dannull et al., 2005). Similarly, Ontak was effective in patients with renal carcinoma (RCC) but induced adverse effects in melanoma patients (Attia et al., 2005; Vargas et al., 2017). A possible explanation of these conflicting results is the unspecific effect of these drugs on Tconv expressing CD25. Further studies are required to specifically deplete tumor-resident Treg cells while sparing antitumor immunity. In this regard, newly developed CD25-targeting Ab optimized to deplete Tregs whilst preserving IL-2-STAT5 signalling on effector T cells (Solomon et al., 2020), are currently in clinical evaluation.

b. **Hindering Treg-trafficking to the tumor.** Treg homing to the TME is mediated through composite chemokine-receptor interactions (ie. CCL22-CCR4, CCL28-CCR10, CXCL12-CXCR4, CCL5-CCR5 and/or CCL1-CCR8), which differ among cancers (Togashi et al., 2017; Curiel et al., 2004; Tan et al.,2009; Hoelzinger et al., 2010). Macrophages and/or tumoral cells in the TME are the main producers of Treg-recruiting chemokines. For example, hypoxia-driven secretion of CCL28 from hepatocellular carcinoma cells promotes accumulation of Treg cells into liver tumors. Interestingly, also intratumoral exhausted CD8+ cells can produce such chemokines, such as CCL1 and CCL22 (Williams et al., 2017; Spranger et al., 2013). In mouse models, blockade of chemotactic signalling (ie. targeting CCR4) curtail Treg frequencies in the tumor lesions (Spranger et al., 2013). However, these chemokines can also recruit Tconv and other immune subsets that express similar chemokine receptors. For this reason, specific targeting of Treg chemotaxis is still challenging although promising.

c. **Targeting co-stimulatory molecules**. Co-stimulatory molecules, such as the tumor necrosis factor superfamily (TNFRSF) members OX40, GITR and 4-1BB, are highly expressed by eTregs in TME (De Simone et al., 2016) while induced upon activation in Tconv and represent relatively specific candidates for the deletion or functional regulation of Treg cells. Activation of these receptors dampens the immunosuppressive capacity of Treg while stimulating Tconv cells in mouse models (Piconese et al., 2008; Valzasina et al., 2005). In accordance with these promising results, OX40 and GITR agonists are being investigated alone or in combination with other therapies in patients with advanced stage solid tumors (Geva et al., 2020; Brendan et al., 2013). Unfortunately, the clinical efficacy of these drugs is limited to a minority of patients, requiring the identification of markers that can predict responder and non-responder patients.

d. **Checkpoint blockade therapy with possible Treg-depleting effects.** In the last decade, immune checkpoint blockade, an immunotherapeutic approach capable of blocking inhibitory receptors expressed by T lymphocytes in the cancer milieu (Sharma and Allison, 2015), has been approved in the clinical practice demonstrating the crucial role of the immune system in tumour regression. Both tumor-infiltrating Tconv and Treg cells express inhibitory receptors, thus monoclonal antibodies (mAbs) targeting these proteins could affect both cell types. The antitumor immunity elicited by anti-CTLA-4 mAb (ipilimumab) for instance was initially associated to the blocking inhibitory signals into activated CTLA-4 expressing Tconv. However, pre-clinical evidence indicates that these agents preferentially target CTLA-4+ Treg in the TME by antibody-dependent cellular toxicity (ADCC), thereby increasing the CD8+ T cell to Treg ratio (Bulliard et al., 2013; Selby et al., 2013; Simpson et al., 2013). Accordingly, a study in melanoma patients reveal that a polymorphism resulting in the expression of high-affinity variant of low-affinity immunoglobulin-γ-Fc (FcγRIIIA), which elicit enhanced ADCC activity compared with low-affinity variant, responded better to ipilimumab treatments and showed better

overall survival (Vargas et al., 2018). However, a lack of FOXP3+ cell depletion in tumor specimens after treatment of patients with ipilimumab has also been reported (Sharma et al., 2019). Moreover, a different anti-CTLA-4 mAb, tremelimumab, that does not have ADCC activity, had a similar therapeutic effect, suggesting that Treg depletion may not be the main mechanism of ipilimumab. Thus, further analyses to address the mechanism of actions of treatments targeting CTLA-4 are warranted.

Like CTLA-4, PD1 is an inhibitory receptor highly expressed by tumor infiltrating T cells. PD1 hinders excessive activation of T cells by suppression of TCR/CD28 signalling. As a result, blockade of PD1 enhances the function of PD1+ cells, including that of Tregs. Accordingly, total PD1 deficiency in mice lead to autoimmunity (Dong et al., 2002; Freeman et al., 2000) and Treg-specific loss of PD1 expression enhance Treg suppressive function and proliferation (Sage et al., 2013), meaning that anti-PD1 therapy is able to boost anti-tumor immunity but at the same time enhance Treg function. Accordingly, hyper progressive disease (HPD) in patients with gastric cancer treated with anti-PD1 mAbs was positively associated with the abundance of proliferative eTreg in the TME (Togashi et al., 2018). Despite this, anti PD1 has been proven to be effective in a subset of cancer patients (Topalian et al., 2012). It may be the case that anti-PD1 is primarily targeting $PD1^{hi}$ Tconv in responder patients and that the effect on these cells outweighs the effect on Treg cells. In agreement with this hypothesis, Kumagai et al. (2020) have recently shown that when PD-1 is predominantly expressed in CD8+ T cells in the TME, blocking PD1 converts PD1+CD8+ T cells into CD8+ Teff cells with potent effector function, leading to tumor regression. Conversely, when PD1 is predominantly expressed by Treg cells in the TME, PD1 blockade converts them into activated eTreg cells with potent suppressor function, leading to tumor progression. Thus, the balance of PD1 expression between CD8+ effector cells and eTreg in the TME might be used as a biomarker to predict response to the PD1-blocking immunotherapy. These results further suggest that $PD1^{hi}$ Treg depletion would enhance anti-PD1-treatment efficacy,

underlying the need to better characterize these cells in the TME. How anti-PD1 affects $PD1^{hi}$ Treg in the periphery also warrant further elucidation in order to reduce drugs toxicity.

In conclusion, specific depletion or functional ablation of Treg cells trigger effective anti-tumor response but concurrently can correlate with autoimmunity, allergy and immunophatology. Thus, the key issue in Treg-targeted anti-cancer therapy is how specifically target intratumoral eTreg while preserving circulating Tregs and thus maintaining immune homeostasis. The pre-requisite to do so is the identification of a specific molecular program or molecules that are specifically expressed by eTreg that are predominant in the cancer tissues. Transcriptional profiling recently revealed that CD4+ Treg isolated from colon, lung and breast tumors are different from those isolated from adjacent tissue and the blood (De Simone et al., 2016), but the molecular mechanisms leading to increase Treg activity in tumors remain poor defined.

## 2. Thesis scope and outline

Treg-dependent immunosuppression represents a major obstacle to effective anti-tumor immune responses. The aim of my PhD project is to characterize the molecular mechanisms at the basis of CD4+ Treg hyperactivity in the human tumor microenvironment (TME) and pinpoint those subsets with the most potent immunosuppressive capacity.

In the first part of the study we evaluated the functional heterogeneity of T cells in non-small cell lung cancer (NSCLC) patients' samples. Specifically, we used flow cytometry and cell sorting for the characterization and isolation of discrete subsets of human Tregs, as well as molecular technologies, functional assays (both in vitro and in vivo) and RNA sequencing to obtain an all-encompassing characterization of the identified populations. Although focusing on lung cancer, we show an effector Treg differentiation path that is common to at least two additional tumor types, i.e. hepatocellular carcinoma and melanoma, suggesting that a common mechanism underlies immunosuppression in the TME irrespective of the tumor type.

In the second part of the work, we used high-dimensional single cell technologies to characterize with precision the immune infiltrate of human cholangiocarcinoma, a rare, yet aggressive tumor of the biliary tract with little therapeutic options and poorly responding to checkpoint blockade, so to find novel targets of immunotherapy. We performed cellular and molecular assays to characterize the identified intratumoral Treg subsets at the functional, transcriptional and epigenetic level, in order to dissect their identity, fate commitment and prognostic value.

Results indicated as "part 1" are included in: Alvisi G*, Brummelman J*, Puccio S*, Mazza EMC, Paoluzzi Tomada E, Losurdo A, Zanon V, Peano C, Colombo FS, Scarpa A, Alloisio M, Vasanthakumar A, Roychoudhuri R, Kallikourdis M, Pagani M, Lopci E, Novellis P, Blume J, Kallies A, Veronesi G, Lugli E. *IRF4 instructs effector Treg differentiation and immune suppression in human cancer*. Journal of Clinical Investigation. 2020 Jun 1;130(6):3137-3150.

Results indicated as “part 2” are included in: Alvisi G*, Termanini* A, Soldani C, Portale F, Carriero R, Pilipow K, Costa G, Polidoro M, Franceschini B, Malenica I, Puccio S, Lise V, Galletti G, Zanon V, Colombo FS, De Simone G, Tufano M, Aghemo A., Di Tommaso L., Peano C, Cibella J, Iannacone M, Roychoudhuri R, MAnzo T, Donadon M, Torzilli G, Kunderfranco P, Di Mitri D, Lugli E, Lleo A. *Multimodal single-cell profiling of intrahepatic cholangiocarcinoma defines hyperactivated Tregs as a potential therapeutic target*. Journal of Hepatology. 2022.

*these authors contributed equally

# 3. Material and Methods

## 3.1. Study approval

The Humanitas Clinical and Research Center Istitutional Review Board approved all human experiments (approval no. 28/01/2016 for buffy coats from healthy donors, approval no. 146/20 for iCCA patients' samples, approval no. #1501 for NSCLC patients' samples). All donors were enrolled at Humanitas Research Hospital and provided written informed consent. Experiments in mice, performed in collaboration with Axel Kallies, University of Melbourne, were executed in accordance with the guidelines of the Walter and Eliza Hall Institute and approved by the institutional IACUC. The Italian Ministry of Health authorization number MI/IC/Op2/17/024 approved the use of recombinant plasmids.

## 3.2 Patients characteristics

In the first part of this study, we included patients with diagnosis of NSCLC who underwent a lung major resection (anatomical segmentectomy, lobectomy, or pneumonectomy) at the Humanitas Cancer Center. Information on the pathological stage (pStage), determined by an institutional pathologist was available for all patients, while results of the preoperative fluorodeoxyglucose (FDG) PET–computed tomography (CT) scan were available for 25 patients. PET scans were acquired 60 min after FDG administration in patients fasting for at least 6 h. Whole body images were obtained from the base of the skull to mid-thigh by means of integrated PET-CT tomographs. Images were displayed on a GE ADW4.6 workstation (GE Healthcare). $SUV^{max}$ was determined as the highest pixel value within the tumor mass that was identified with three-dimensional volumes of interest, as previously described (Lopci et al., 2016). $SUV^{max}$ high and low groups were defined based on the median value of this parameter across the entire cohort.

In the second part of this study, we included patients who had pathology proven iCCA. Hepatitis B or C positive patients were excluded. Samples (one tumoral and one peritumoral) were selected from areas without macroscopic evidence of necrosis or haemorrhage. For morphological analysis, sections were cut (2μm thick), stained with hematoxylin and

eosin and evaluated by an expert liver pathologist. Histological features evaluated included tumor grade, desmoplasia, resection margin, steatosis, perineural, and linfo-vascular invasion, and lymph node metastasis. Resected iCCA patients were followed up every 3 months, as per protocol in our Hospital, or until death, and major events were recorded.

None of patients received preoperative chemotherapy or radiotherapy. The characteristics of the cancer patients are further indicated in **Table 1.**

| Parameter | Subdivision | NSCLC patients (n=82) |
|---|---|---|
| Sex - no. (%) | Female | 34 (41.5%) |
| | Male | 48 (58.8%) |
| Age - mean (SD) | | 69 (10.3%) |
| Smoking status - no. (%) | Smoker | 42 (51.2%) |
| | Former | 29 (35.4%) |
| | Non-smoker | 10 (12.2%) |
| | Unknown | 1 (1.2%) |
| Tumor type - no. (%) | Adenocarcinoma | 62 (75.6%) |
| | Squamous cell carcinoma | 18 (21.95%) |
| | Other | 2 (2.4%) |
| pStage - no. (%) | IA1 | 4 (4.9%) |
| | IA2 | 10 (12.2%) |
| | IA3 | 9 (11%) |
| | IB | 8 (10%) |
| | IIA | 9 (11%) |
| | IIB | 18 (22%) |
| | IIIA | 12 (14.6%) |
| | IIIB | 10 (12.2%) |
| | IVA | 2 (2.4%) |
| Tumor location - no. (%) | R | 2 (2.4%) |
| | RLL | 12 (14.6%) |
| | RML | 4 (4.9%) |
| | RUL | 25 (30.5%) |
| | RML+RLL | 3 (3.6%) |
| | L | 9 (10.9%) |
| | LLL | 11 (13.4%) |
| | LUL | 16 (19.5%) |
| Results PET-CT scan available - no. (%) | Yes | 41 |
| | No | 41 |
| | | **iCCA Patients (n=20)** |
| Gender - no (%) | Female | 9 (45%) |
| | Male | 11 (55%) |
| Age - median (SD) | | 68 (10,21) |
| Body Mass Index - median (SD) | | 23,35 (4,16) |
| Tumor Grade - no (%) | 1 | 0 (0%) |
| | 2 | 11 (55%) |
| | 3 | 9 (45%) |
| Tumor Stage - no (%) | 1 | 7 (35%) |
| | 2 | 9 (45%) |
| | 3 | 3 (15%) |
| | 4 | 1(5%) |
| Tumor size (cm) - median (SD) | | 6,85 (4,35) |
| Margins - no (%) | Non-invasive | 12 (60%) |
| | Invasive | 8 (40%) |
| Etiology - no (%) | Hepatitis B Virus | 0 (0%) |
| | Hepatitis C Virus | 0 (0%) |
| Overall Survival (months) - median (SD) | | 15,89 (11,08) |

**Table 1: Patients characteristics**

## 3.3. Sample collection and processing

- Peripheral blood mononuclear cells (PBMCs) were isolated from buffy coats of healthy donors by density-gradient separation and

were either used fresh or cryopreserved in FBS supplemented with 10% dimethyl sulfoxide (DMSO) until use.

- Blood samples from patients were obtained by venipuncture at induction of anesthesia and collected in vacutainer EDTA Tubes (BD). Tissues were obtained in the operating room in a sterile field by the surgeon and collected in complete R10 medium: RPMI-1640 medium with 10% FBS (Sigma-Aldrich), 1% penicillin-streptomycin and 1% Ultra-glutamine (both from Lonza) RPMI 1640 media: 10% FBS (Sigma-Aldrich), 1% penicillin-streptomycin (Lonza) and 1% Ultra-glutamine (Lonza).
- The tumor and adjacent cancer-free tissue samples fromn NSCLC patients were processed into single cell suspensions by mechanical disaggregation. The samples were cut into small pieces (size 1 $mm^3$), after which further disaggregation was performed using gentleMACS dissociator (Miltenyi Biotec). Subsequently, samples were passed through a 70-µm cell-strainer (Falcon) and washed with physiological saline solution (NaCl 0.9%; Baxter). After centrifugation (300 *g*, 15 min), erythrocytes lysis was performed by incubating the cell suspension for 5 min in house made ACK lysis buffer (155 mM $NH_4Cl$, 10 mM $KHCO_3$, and 0.1 mM EDTA-2Na [all from Sigma-Aldrich] diluted in $H_2O$), and subsequently washed with saline. Before FACS sorting, NSCLC infiltrating leukocytes were further purified by centrifugation (790 g for 30 min without brake) on a 40%/70% Percoll (Sigma-Aldrich) gradient. After isolation of the interphase between the two layers, the cells were washed with HBSS without $Ca^{2+}$ or $Mg^{2+}$ (Lonza).
- Cell isolation from healthy human liver was performed by collagenase perfusion adapting a traditional two-step technique (Seglen, 1976). Briefly, non-tumoral tissue displaying the normal vascular architecture was perfused in order to collect the circulating intrahepatic blood (perfusate).
- The tumor liver samples were digested with collagenase, obtaining a single-cell suspension. Parenchymal cells were eliminated from the sample through appropriate centrifugations and the supernatant was stored. Cells were pelleted, counted, and frozen according to the slow freezing procedure in standard cryo-vials. Further

disaggregation of iCCA tissue into a single-cell solution for sequencing was completed using the MACS tumor dissociation kit (Miltenyi Biotec). The MACS tumor dissociation kit enzyme mix (300µl) was added to each sample. Next, samples were put into the gentleMACS Dissociator and ran through the tough tumor program. The cell suspension was then filtered with a 70-µm cell-strainer. Cells were pelleted, counted and frozen according to the slow freezing procedure in standard cryo-vials (1 ml cell suspension in the cryopreservation medium as above). Considering that prolonged blood storage leads to selective loss of cell populations with a short half-life time, such as eosinophils and neutrophils (Park and Bochner, 2010; Summers et al., 2010), those populations were excluded from the analysis.

We used two different strategies to generate single-cell suspension from tissues, namely gentleMACS dissociator for lung samples and MACS tumor dissociation kit for liver samples. The MACS tumor dissociation kit is optimized for high yield of tumor cells and tumor-infiltrating lymphocytes, while preserving important cell surface epitopes. I validated by FACS analysis the persistence of cell surface markers after both procedures (data not shown).

## 3.4 Flow cytometry

Fluorochrome-conjugated monoclonal antibodies (mAb) used in the study (**Table 2)** were titrated to determine optimal concentrations (Lugli et al., 2017). Intracellular molecules were measured with the FoxP3 Transcription Factor Staining Buffer Set (eBioscience). Flow cytometry data were compensated in FlowJo by using single stained controls (BD Compbeads incubated with fluorescently-conjugated antibodies; Lugli et al., 2017).
All data were acquired on a FACS Symphony A5 flow cytometer (BD Biosciences) equipped with 5 lasers (UV, 350 nm; violet, 405 nm; blue, 488; yellow/green, 561 nm; red, 640 nm; all tuned at 100 mW, except UV tuned at 60 mW) and capable to detect 30 parameters.

| Specificity | Fluorochrome | Clone | Manufacturer | Cat.no. |
|---|---|---|---|---|
| **Viability staining (15 min, RT)** | | | | |
| Aqua | BV510 | - | BioLegend | 423102 |
| **Chemokine receptor staining (20 min, 37°)** | | | | |
| CCR8 | BV421 | 433H | BD | 566380 |
| CCR5 | APC-Cy7 | 2DT/CCR5 | BD | 557755 |
| CXCR6 | PE-CY7 | K041E5 | BioLegend | 356012 |
| CCR7 | BB660 | 150503 | BD | 625454 |
| CCR4 | PECF594 | 1G1 | BD | 565391 |
| CCR2 | BV650 | LS132.1D9 | BD | 747849 |
| CXCR5 | BV785 | J252D4 | BioLegend | 356936 |
| CCR7 | BV711 | 150503 | BD Biosciences | 563921 |
| CXCR3 | APC | G025H7 | BioLegend | 353708 |
| **Surface staining (15 min, RT)** | | | | |
| TIGIT | PerCP-eF710 | MBSA43 | eBioscience | 46-9500-42 |
| CD25 | BV711 | BC96 | BioLegend | 302636 |
| OX4O | BV650 | ACT35 | BD | 563658 |
| Tim3 | BV605 | 7D3 | BioLegend | 345018 |
| CD27 | BV570 | O323 | BioLegend | 356936 |
| PD-1 | BV480 | EH12.1 | BD | 566112 |
| CD8 | BUV805 | SK1 | BD | 564312 |
| CD28 | BUV737 | Cd28.2 | BD | 564438 |
| CD4 | BUV615 | SK3 | BD | 624297 |
| CD45RA | BUV563 | HI100 | BD | 565702 |
| ICOS | BUV395 | DX29 | BD | 564777 |
| CD127 | PE-Cy5 | eBioRDR5 | eBioscience | 15-1278-42 |
| CD98 | BB515 | UM7F8 | BD Biosciences | 565103 |
| CD73 | APC-Cy7 | AD2 | BioLegend | 344022 |
| CD25 | APC-R700 | 2A3 | BD Biosciences | 565106 |
| CD57 | BV605 | NK-1 | BD Biosciences | 563895 |
| PD-1 | BV421 | EH12.2H7 | BioLegend | 329919 |
| CD95 | BUV737 | DX2 | BD Biosciences | 564710 |
| HLA-DR | BUV661 | G46-6 | BD Biosciences | 565073 |
| CD69 | BUV395 | FN50 | BD Biosciences | 564364 |
| CD27 | BV570 | O323 | BioLegend | 302825 |
| CD71 | PE-Cy5 | M-A712 | BD Biosciences | 551143 |
| CD39 | APC-H7 | EBioA1 | eBioscience | 47-0399-41 |
| CD28 | BV786 | CD28.2 | BioLegend | 302950 |
| CD45RO | BV570 | UCHL1 | BioLegend | 304226 |
| CD161 | BV605 | HP-3G10 | Biolegend | 339915 |
| CD25 | BUV563 | 2A3 | BD | 612918 |
| CD69 | BUV737 | FN50 | BD | 564439 |
| CD103 | BUV661 | Ber-ACT8 | BD | 749993 |
| 2B4 | PE-Cy5.5 | C1.7 | Beckman Coulter | B21171 |
| CD45 | BUV395 | HI30 | BD | 563792 |
| CD38 | BV711 | HIT2 | BioLegend | 303528 |
| GZMK | AF647 | GM6C3 | SantaCruz | sc-56125 |
| KI67 | FITC | B56 | BD | 556026 |
| LEF1 | PE | C12A5 | Cell Signalling | BK14440S |
| **Intracellular staining (30 min, RT)** | | | | |
| CD3 | BUV496 | UCHT1 | BD | 564809 |
| FoxP3 | PE-Cy5.5 | PCH101 | eBioscience | 35-4776-42 |
| Eomes | PE-eFluor610 | WD1928 | eBioscience | 61-4877-42 |
| CXCL13 | APC | 53610 | ThermoFisher | MA5-23629 |
| GZMK | PE | GM6C3 | SantaCruz | sc-56125 |
| GZMB | AlexaFluor700 | GB11 | BD | 561016 |
| KI67 | BB780 | B56 | BD | 624269 |
| GNLY | AlexaFluor488 | RB1(RUO) | BD | 558254 |
| tbet | PE-Cy7 | 4-B10 | eBioscience | 25-5825-82 |
| Ki-67 | BV480 | B56 | BD Biosciences | 566109 |
| IRF4 | PE | | eBioscience | 12-9858-80 |
| CTLA-4 | PE-eF610 | 14D3 | eBioscience | 61-1529-41 |
| 4-1BB | PE | 4B4-1 | BioLegend | 309804 |
| KI67 | FITC | B56 | BD | 556026 |
| LEF1 | PE | C12A5 | Cell Signalling | BK14440S |
| GZMB | APCR700 | GB11 | BD | 560213 |

**Table 2: Fluorochrome-conjugated mAbs used for the study**

### 3.4.1 High-dimensional flow cytometry data analysis

Flow Cytometry Standard (FCS) 3.0 files were imported into FlowJo software version 9.4 correct for spillover of fluorochromes by applying compensation and analysed by standard gating to remove aggregates and dead cells. The subpopulation of interest (ie. $CD4^+$ cells) were subsequently imported in FlowJo version 10, bio-exponentially transformed and exported for further analysis in Python (version 3.7.3) by a custom-made script that makes use of PhenoGraph (scikit-learn package) and freely available in our GitHub repository: *https://github.com/luglilab/Cytophenograph*. All the parameters not providing information for separating cell subsets (ie. physical parameters, the "Time" parameter, viability staining as well as lineage markers (eg CD3) were exclude from the analysis. The different sample types (ie. Blood, adjacent lung tissue and tumor) were labelled with a unique computational barcode for further identification, converted in comma separated (CSV) files and concatenated in a single matrix by using the merge function of pandas package (Brummelman et al., 2019). The data were then re-organized and saved as new CSV files, one for each cluster, that were further analyzed in FlowJo to determine the frequency of positive cells for each marker and the corresponding median fluorescent intensity (MFI). These values were multiplied to derive the integrated MFI (iMFI, rescaled to values from 0 to 100) (Brummelman*; Mazza* et al., 2018).
Heatmaps and ballon plot, showing the iMFI of each marker per cluster, and the subsequent metaclustering was performed using the gplots R package. Hierarchical metaclustering of samples was performed in R according to the Ward minimum variance method. UMAPs were obtained by UMAP Python package and visualized in FlowJo 10.

## 3.5. In vitro assays

### 3.5.1. Treg cell transduction

Treg cells were enriched from buffy coats of healty donors using an EasySep Human CD4+ $CD127^{low}$ CD25+ Regulatory T cell Isolation kit. Purity was confirmed to be >90% by flow cytometry. Purified Treg cells were stimulated with Dynabeads human T-ACT CD3/CD28 at a 1:2 bead:cell ratio, in 96 U-bottomed well plates and in the presence of IL-2

(50 ng/mL; Peprotech). 24h and 48h after stimulation, cells were transduced with lentiviral particles harboring a custom human ORF for MEOX1 (Sigma-Aldrich, Mission TRC3) or empty backbone-vectors (mock), both expressing GFP as a reporter (Sigma-Aldrich). Cells were cultured for 5 additional days and then stained with fluorochrome-conjugated monoclonal antibodies (**Table 2**). GFP+ cells, pre-gated as CD3+CD8-CD4+Aqua-CD25+CD127- were isolated with a FACSAria cell sorter (BD Biosciences). To assess 4-1BB and CTLA4 expression (**Figure 30**)**,** GFP+ sorted cells were restimulated with CD3/28/2 for 16h and analyzed by flow cytometry.

### 3.5.2 Treg-mediated suppression of CD4+ Tconv proliferation

Results part 1 (**Figure 10**): Live (Aqua-) CD4+ CD25- Tconv responder cells (Tresp) were isolated from NSCLC patients' blood samples with FACSAria cell sorter and stained with CellTrace CFSE kit (final concentration: 2μM; ThermoFisher Scientific) according to the manufacturer's protocol. CCR8+ICOS+ and CCR8-ICOS- Tregs were FACS-sorted from NSCLC tumors and were added to autologous Tresp cell cultures at different ratios (Tconv:Treg ratio= 1:1, 2:1 and 4:1).
Results part 2 (**Figure 30**): Tresp were isolated from buffy coats using an EasySep Human CD4+CD25- Responder T cell enrichment kit (Stem Cell Technologies) and stained with a Cell Trace Violet (CTV) kit (final concentration: 2.5 μM; Thermo Fisher Scientific) according to the manufacturer's protocol. FACS-sorted transduced green fluorescent protein (GFP+) Tregs, obtained as abovementioned, were added to autologous Tconv cell cultures at different ratios (Tconv cells/Treg ratio = 2:1, 4:1, and 8:1).

Tresp cells were plated in R10 U-bottom 96-well plates (10,000 cells/well) and stimulated with human Treg Suppression Inspector beads (Miltenyi Biotec Ltd., UK) for 5 days at 37 °C. Tresp cultured alone, in the absence of bead stimulation, were used as non-proliferating, negative control. CFSE or CTV dilutions ware evaluated at day 5 by flow cytometry. Proliferation index (PI) was calculated as: MFI non-proliferating fraction / MFI proliferating fraction × % T conv cells with diluted proliferation dye.

## 3.6. Mouse procedures

Tak Mak originally provided *Irf4*$^{-/-}$ mice (Mittrücker et al., 1997). *Irf4*$^{-/-}$ mice were crossed to *Foxp3*$^{RFP}$ mice. Foxp3$^{eGFP\text{-}Cre\text{-}ERT2}$ (JAX #016961) (Rubtsov et al., 2010), were crossed to *Irf4* floxed mice (JAX stock #009380) (Klein et al., 2016) to allow for specific deletion of *Irf4* in Foxp3+ cells following Tamoxifen treatment.

MC38 cells were grown in DMEM with 10% FCS and 1% PenStrep (Gibco) in 37C, 5% $CO_2$ incubator and passaged every 2-3 days. For tumor inoculation, 1x10^6 cells were resuspended in 100ul PBS and injected sub-cutanously into the right flank of the mice. Tumor growth was assessed with a digital calliper every 2-3 days. Tamoxifen (2 mg/mouse) was administered in 200 uL Sunflower oil i.p. for five consecutive days. Upon the experimental endpoint, mice were euthanized with $CO_2$ and cervical dislocation and tumors were excised with forceps and scissors. Tumors were mechanically dissociated and digested in 1mg/ml Collagenase IV (Gibco) in RPMI medium for 45min at 37C, with constant agitation.

## 3.7. RNA sequencing and bioinformatic analysis

## 3.7.1. Single cell RNA sequencing (scRNAseq)

### 3.7.1.1. Library preparation

Frozen tumoral and peritumoral single-cell suspension were thawed, washed in PBS, stained with Live/dead Aqua Fluorescent Reactive Dye (Life Technologies) and mouse anti-human CD45 dye (30-F11, BD Biosciences) at 4°C for 20 minutes and sorted on a FACS Aria III (BD Biosciences) with a 100µm nozzle. FACS-purified CD45$^{+}$/CD45$^{-}$ cells were resuspended in 1ml PBS plus 0.04% BSA and washed two times by centrifugation at 450xg for 7min. After the second wash, cells were resuspended in 30 ml and counted with an automatic cell counter (Countess II, Thermo Fisher) to get a precise estimation of total number of cells recovered and of their concentration. Afterwards, CD45+ cells of each sample were loaded into one channel of the Single Cell Chip A using

the Single Cell 3' reagent kit v2 single cell reagent kit (10X Genomics) for Gel bead Emulsion generation into the Chromium system. Following capture and lysis, cDNA was synthesized and amplified for 14 cycles following the manufacturer's protocol (10X Genomics). 50 ng of the amplified cDNA were then used for each sample to construct Illumina sequencing libraries. Sequencing was performed on the NextSeq550 Illumina sequencing platform following 10x Genomics instruction for reads generation. A sequencing depth of at least ~ 30,000 reads/cell was obtained for each sample.

#### 3.7.1.2. Pre-processing of scRNA-seq data

Raw sequencing data was processed and aligned to the GRCh38 human reference genome with CellRanger (10X Genomics) v3.0.1. Resulting filtered count matrices were used as input for pre-processing with Seurat package v3.0.3 running under R v3.6.1 and Bioconductor v3.9 on a Debian GNU/Linux 9 operating system. First, ribosomial genes were removed from the count matrix. Then, in order to avoid dying/damaged cells or doublets, quality control was performed and cells having < 200 or > 3000 expressed genes or >20% mitochondrial counts were filtered out. Data normalization and log-transformation was performed by applying the NormalizeData Seurat function (method = LogNormalize).

In order to integrate sample datasets together, the "SCT" normalization (Hafemeister et al., 2019) was performed separately for each sample by running the SCTransform Seurat function where technical and cell-cycle effects were regressed out. The Seurat functions PrepSCTIntegration, FindIntegrationAnchors and IntegrateData were then applyed on the list of Seurat objects using 3,000 genes in the anchor finding process. A final integrated dataset consisting of 31,745 cells (14,824 from peritumoral and 16,921 from tumoral samples) was obtained. A principal component analysis (PCA) was performed on the top variable features by calling the RunPCA Seurat function and the first 20 principal components (PCs) were selected for downstream analysis. Imputation of missing count values was performed by applying the Adaptively-thresholded Low Rank Approximation (ALRA) method (Linderman et al., 2022) by calling the RunALRA Seurat function with default parameters.

### 3.7.1.3. Clustering and cell type identification

To identify cell clusters, the graph-based clustering approach implemented in the FindClusters Seurat function was used with a resolution value ranging from 0 to 1 by steps of 0.1. Clustering stability was assessed using clustree R package v.0.4.0. Marker genes were obtained for each cluster by running the FindAllMarkers Seurat function which performs a Wilcoxon Rank Sum test (adj.p-value < 0.05). The SingleR v1.0.6 (Aran et al., 2019) and AUCell v1.8.0 (Aibar et al., 2017) packages were used as an aid to manual clusters cell types annotation.

Reclustering of T cells was performed by repeating the analysis used for the whole dataset on the subsets of cells enriched for the “Main Immune Cell Expression Data’” CD8 and CD4 T cells reference signature after ALRA imputation (5,037 cells from peritumoral and 7,607 cells from tumoral samples). A clustering resolution of 0.8 was chosen, obtaining a total of 11 clusters. UMAP was obtained by running the RunUMAP Seurat function with default parameters for the whole dataset and with min.dist = 0.01 and n.neighbors = 20 for reclusterings of T cells. Cluster marker genes were obtained by running the FindAllMarkers Seurat function after imputation of missing count values with ALRA algorithm as previously described. For each cluster, genes having an adjusted p-value < 0.05 and absolute $\log_2$ of fold-change (FC) > 0.5 and detectable expression in > 50% of the cells in that cluster were selected and sorted in descending order by FC values. After data centering and scaling with ScaleData, the heatmap was generated using the DoHeatmap Seurat function with default parameters (**Figure 23**).

For each cluster, DEGs were obtained before ALRA imputation by comparing cells from peritumoral samples with cells from tumoral samples using the FindMarkers Seurat function (min.pct = 0.1, logfc.threshold = 0), which performs a Wilcoxon Rank Sum test. Genes having an adjusted p-value < 0.01 and an absolute FC > 1.5 were considered as statistically significant. Volcano plot was generated with EnhancedVolcano package v1.4.0 (https://github.com/kevinblighe/EnhancedVolcano).

### 3.7.1.4. Gene regulatory network analysis

The analysis of TF activity was performed by Single-Cell regulatory network Inference and Clustering (SCENIC, version 1.1.2) (Aibar et al., 2017) starting from ALRA imputed data. The genes with at least 3 UMIs in at least 10% of the cells and detected in at least 10% of samples were selected as the input genes. The co-expressed genes to each TF were calculated with GENIE3 (Huynh-Thu et al., 2010). The TF co-expression modules were then analyzed by RcisTarget Bioconductor package. The Normalized Enrichment Score (NES) of the transcription factor binding motifs (TFBMs) was calculated and NES > 3.0 were considered as significantly enriched. The filtered potential targets by RcisTarget mouse hg19 database (hg19-500bp-upstream-7species.mc9nr.feather; hg19-tss-centered-10kb-7species.mc9nr.feather) from the co-expression module were used to build the regulons. The regulon activity was analysed by AUCell and the active regulons were define by AUCell (Aibar et al., 2017) default threshold. The active regulons were then mapped to all cells by *t*-SNE in **Figure 25A**. Binary regulon activity active in at least 50% of cells was selected (**Figure 25B**).

#### 3.7.1.5. Trajectory analysis

Trajectory analysis was performed with SCORPIUS R package v1.0.7 (Saelens et al., 2019) on Regulon Activity Scores obtained by running SCENIC R package as described in the previous paragraph. Dimensionality reduction was obtained by applying the reduce_dimensionality function (dist = "spearman", ndim = 3) on the subset of cells belonging to C10 of T cells. Linear trajectory was inferred by using the infer_trajectory function with default parameters. The importance of each gene with respect to the trajectory was calculated by running the gene_importances function (num_permutations = 10, ntree = 10000, ntree_perm = 1000). Regulons having a false discovery rate (FDR)-adjusted p-values < 0.05 were considered significant.

### 3.7.2. Bulk RNA-sequencing and bioinformatic analysis

#### 3.7.2.1. Library preparation

RNA isolation from the FACS-purified CCR8+ICOS+, CCR8-ICOS- or GFP+ Treg cells was performed following the manufacturer's protocol using

the Quick-RNA Microprep kit (Zymo research). RNA quality control was performed with the Agilent 2200 Tape Station system and only RNAs having a RIN>8 were used for library preparation. Libraries for mRNA-sequencing were prepared starting from 10 ng tot RNA for each sample by using the SMART-Seq v4 Ultra Low Input RNA Kit (Clontech-Takara). All samples were sequenced on an Illumina NextSeq 500 at an average of 32.9 (**Figure 9**) or 17.5 (**Figure 29**) million 75-bp single-end reads.

#### 3.7.2.2. Bulk RNAseq analysis

After quality control, raw reads were aligned to the human genome (GRCh38.p12) using the STAR aligner with default parameters (version 2.7.0) (Dobin A et al., 2013). Gene-based read counts were then obtained using HTSeq count module (version 0.11) and GENCODE v29.gtf annotation (Frankish et al., 2019). The read counts were imported into R statistical software and differential gene expression analysis was performed using the edgeR package (version 3.22) (Robinson et al., 2010). For pair-wise comparisons, raw read counts were normalized using the TMM method (trimmed mean of log-ratio values) and genes that failed to achieve a counts per million (CPM) mapped reads value greater than 1 in at least two libraries were not considered. P-values were adjusted using the Benjamini-Hochberg method. Genes were considered differentially expressed when FDR< 0.05 and had an expression change of >1 $\log_2$ fold change. The heatmap representing the $\log_2$ of CPM (**Figure 9B**) was obtained using pheatmap R package (version 1.0.12) with the distance method "correlation" for both rows and columns. Volcano plot was generated with EnhancedVolcano package v1.4.0 (https://github.com/kevinblighe/EnhancedVolcano). Genes having an adjusted p-value < 0.05 and an absolute FC > 1.5 were considered as statistically significant.

#### 3.7.2.3. Gene Set Enrichment Analysis (GSEA)

GSEA was performed using GSEA software (Broad Institute, version 3.0 MIT) running the fgsea R package v1.12.0 (Korotkevich et. al, 2019). Ranking score was determined by a combination of fold-change and F-statistic. The gene set enrichment analysis was conducted in pre-ranked

mode with scoring scheme “classic” and 1,000 permutations. The maximum gene set size was fixed at 5,000 genes, and the minimum size fixed at 10 genes. The gene signature evaluated included: (*i*) the H collection (h.all.v6.2.symbols.gmt) of the Molecular Signatures Database (MSigDB v6.2); (*ii*) Treg vs Tconv activated_UP (GSE7460) gene set (Hill et al,. 2007); (*iii*) ICOS+CCR8+ vs ICOS-CCR8- intratumoral Treg_UP (GSE128822) gene set (Alvisi et al., 2020); (*iiii*) intratumoral Treg vs peritumoral Treg_UP (C10 of CD4+ Tregs from scRNA-seq, GSE171899).

#### 3.7.2.4 Motif enrichment analysis

The PScan software tool (version 1.5) was used to perform the in silico computational analysis of over-represented transcription factor binding sites (TFBS) within the 5′-promoter regions of differentially expressed genes (Zambelli et al., 2009). PScan was ran on [-950, +50] bp upstream regions onto the Homo Sapiens JASPAR 2018_NR database (Khan et al., 2018). Results were summarized with a scatter plot where p-values were plotted against Z-score on vertical axis by using Python Matplotlib package (version 3.0.3) (**Figure 9D**).

### 3.7.3. Re-analysis of publicly available datasets

#### 3.7.3.1. scRNaseq melanoma dataset

Normalized single-cell RNA sequencing (scRNA-seq) counts were extracted from GEO (dataset GSE72056). Analysis was focused on the cells previously labelled as “T cells” by Tirosh et al. (2016). In order to obtain a CD8 signature used in **Figure 15B**, differentially expressed genes in the pairwise comparison between CD8+ and CD4+ T cell subsets were determined by the “FindAllMarkers” function coded in the Seurat R package (version 2.3.4) with default parameters (Satija et al., 2015). In this way, we obtained 225 specific genes for the CD8+ subpopulation respect to the CD4+ T cells**.**

#### 3.7.3.2. scRNASeq lung and liver datasets

We took advantage of the webserver for investigation of NSCLC (http://lung.cancer-pku.cn; Guo et al., 2018) and of hepatocellular

carcinoma (http://hcc.cancer-pku.cn/; Zheng et al., 2017) single T cell RNA-seq data to assess the expression levels of markers of interest within the CD4+ intratumoral subpopulations. Lung and liver tumor infiltrating CD8+ signatures (**Figure 14** and **Figure 16**, respectively) were obtained by combining all the DEGs from the CD8+ tissue-specific clusters and by further excluding the circulating clusters labelled as CD8-C1-LEF1.

#### 3.7.3.3. Microarray mouse data

Microarray probe fluorescence signals downloaded from the GEO (GSE89656 and GSE61077) were converted to expression values using robust multiarray average procedure RMA (Irizzary et al., 2003) of Bioconductor Affy package. Fluorescence intensities were background-adjusted and normalized using quantile normalization, and expression values were calculated using median polish summarization and custom chip definition files for a total of 18,075 custom probe sets for Mouse Genome 430 2.0 Array based on Entrez genes (Mouse4302_Mm_ENTREZG version 21.0.0) and 12,426 custom probe sets for Mouse Genome 430A 2.0 Array based on Entrez genes (Mouse430A2_Mm_ENTREZG version 21.0.0). To identify genes that are differentially expressed, we compared the expression profiles of *Batf*$^{-/-}$ Treg and WT Treg cells, using limma algorithm coded in the same R package (Ritchie M et al., 2015). All data analyses were performed in R version 3.4.4 using Bioconductor libraries and R statistical packages.

## 3.8. Bioinformatic analysis of Chromatin Immunoprecipitation sequencing (ChIP) data

Raw data were retrieved from NCBI GEO (accession number GSE98264). Reads were aligned to mouse genome GRCm38.p6/mm10 using Bowtie2 (version 2.1.0) in local alignment mode. Afterwards, mitochondrial and ambiguously mapped reads were discarded with Samtools, further used for sorting and indexing mapping files. Bigwig files for IGV genome coverage visualization were generated with the multiBamSummary module from the deepTools suite (version 3.2.0). To call peaks, we used

MACS2 (version 2.1.2) with these parameters: callpeak gsize mm nomodel extsize 147 and Qvalue 1e-3. Peaks within 30 kb upstream and 10kb downstream of the TSS or within intragenic regions were annotated with the closest TSS using ChIPSeeker (version 1.18.0) (Yu G et al., 2015) and GENCODE M20.gtf gene annotation.

## 3.9 Assay for Transposase-Accessible Chromatin using sequencing (ATAC-seq)

### 3.9.1. Library preparation

Libraries were prepared using a protocol adapted from Buenrostro et al. (2015). 10,000 FACS-purified GFP+ Treg cells were washed in PBS without $Ca^{2+}$ and $Mg^{2+}$ and resuspended in 25µl lysis buffer (10 mM Tris-HCl pH 7.4, 10 mM MgCl2, 0.1% IPEGAL CA-630). Nuclei were pelleted by centrifugation for 10 min at 500g and resuspended in a final reaction volume of 25µl comprising 0.2µl of Tn5 transposase (made in-house), 5µl of 5×transposase buffer (50 mM Tris-HCl pH 8.4, 25 mM MgCl2) and 19.8µl of ultrapure water (Milli-Q). The reaction was incubated with mixing (300 r.p.m., 30 min, 37 °C), supplemented with 5 µl clean-up buffer (900 mM NaCl, 30 mM EDTA), 2.5µl of 20% SDS, 0.35µl of ultrapure water (Milli-Q) and 2.15µl of proteinase K (18.6 µg µl–1, ThermoFisher Scientific), and incubated for a further 30 min at 40 °C. Tagmented DNA was isolated using 2× SPRI Beads (Beckman Coulter) and amplified via PCR. Fragments smaller than 600 bp were isolated via negative size selection using 0.65× SPRI Beads (Beckman Coulter) and purified using 1.8× SPRI Beads (Beckman Coulter). Quality control was performed using a 4200 TapeStation System (Agilent) in conjunction with a Qubit 2.0 Fluorometer (Thermo Fisher Scientific). Libraries were then multiplexed in an equimolar pool and sequenced using a NextSeq 500/550 Platform (Illumina). At least 40 million single-end 75-bp reads were generated per sample.

### 3.9.2. ATAC-seq data analysis

After de-multiplexing with bcl2fastq v2.20 (Illumina, Inc.), quality control checks on raw sequencing data were performed with FastQC v0.11.8 (https://www.bioinformatics.babraham.ac.uk/projects/fastqc/). Adapters

removal and dynamic trimming of low-quality bases were performed using Trimmomatic v0.39. Single-end reads were mapped to the UCSC hg38 reference human genome using Bowtie2 v2.4.1. After alignment, several post-processing has been carried out. First, PCR duplicates, reads aligned to chrM and/or encode blacklisted regions v2 were filtered out using BEDTools v2.30. Second, only uniquely mapped reads were retained using SAMtools v1.9. Finally, reads aligning to the forward strand were offset by +4 bp, and reads aligning to the reverse strand were offset −5 bp. Non-shifted bam files were also kept for the differentially bound motif analysis. Peak calling was performed using MACS2 v2.2.6. In order to visualize the raw profiles with the Integrative Genomics Viewer (IGV) v2.9, RPM-normalized BedGraph files generated by MACS2 were converted to BigWig files v2.8 from UCSC tools. In order to obtain a set of unique genomic regions for the two conditions, MACS2 called peaks were processed with BEDTools v2.30. Each region was extended by 50bp at both ends and theirs overlapping mapped reads were counted with Rsubread v2.4. R package. The obtained count matrix was imported and processed by DeSeq2 v1.30.1 R package, and differential expression analysis was performed with a paired design. Differentially significant regions between the two conditions were selected by choosing a p-value cut-off of 0.05.

### 3.9.3. ATAC-seq footprint

Differentially bound motifs were obtained by applying the TOBIAS v0.12.10 pipeline (Bentsen et al., 2020) while the list of genomic regions that represents peaks merged across all conditions was obtained using BEDTools v2.30. First, to correct the Tn5 transposase insertion bias and to calculate a continuous footprinting score across regions, the ATACorrect and FootprintScores tools were runned for each condition with default parameters. Second, to make predictions on specific TF binding sites and to obtain the differential binding between conditions, the BINDetect tool was called with default parameters and by using the JASPAR 2020 core vertebrates non-redundant set of TF binding profiles (Fornes et al., 2019).

## 3.10. Survival analysis

Results part 1: Transcriptomic and clinical data of human lung adenocarcinoma, hepatocellular carcinoma and melanoma from the TCGA database (provisional cohorts) were obtained from the cBioPortal platform. Signatures of CCR8+ICOS+ Treg (DEGs from FACS-sorted CCR8+ICOS+ versus ICOS-CCR8- tumor-infiltrating Treg; FDR<0.05; log2FoldChange>1) and CD8+ T cells (see Methods 3.7.3.2. scRNASeq lung and liver datasets) were used to calculate patient-specific enrichment scores from specimens of lung adenocarcinoma (LUAD), hepatocellular carcinoma (LIHC) and melanoma (SKCM) datasets ("GSVA" R package, Hänzelmann et al., 2013). Survival curves were calculated between groups of patients subdivided according to the percentile rank (set at 0.8) of the resulting scores. The R packages "survival" (https://cran.rproject.org/web/packages/survival/index.html) and "survminer" (https://cran.r-project.org/web/packages/survminer/index.html) were used to assess statistics and obtain survival curves.

Results part 2: Bulk RNA-seq and clinical data of human iCCA were obtained from Dong et al. (2022). Patients with HBV positivity, elevated AFP, and liver fluke were excluded from the analysis; out of 244 reported patients, 147 were included in the analysis. RNA-seq profiles were used to calculate patient-specific enrichment scores for the following signatures: Tregs transduced with MEOX1 (DEGs: q-value< 0.05, |FC|> 1.5, n=3); **Figure 29**), CD8+ T cells (PTPRC, CD3E, CD3G, CD3D, CD8A, CD8B) and cDC2 (PTPRC, CDC1, FCER1A, CLEC10A). Scores were obtained by applying "GSVA" R package (Hänzelmann et al., 2013) Patients (n=147) were grouped by percentile rank (set at 0.7) according to the enrichment of the MEOX1 Treg signature as relative to the CD8+ T cell or cDC2 signature.

## 3.11. Statistical analysis

Statistical analyses were performed using GraphPad Prism version 7, unless specified otherwise. Data were first tested for normal distribution with D'Agostino-Pearson, Shapiro-Wilk, or Kolmogorov-Smirnov normality tests

and then analyzed with Wilcoxon rank test (paired non-parametric data) or Mann-Whitney (unpaired non-parametric data) when comparing 2 groups; Friedman test or two-way ANOVA with Bonferroni post-hoc test for multiple comparisons when comparing 3 groups (specific tests are specified in the figure legends).

## 3.12. Data availability

Raw data sets are available in the Gene Expression Omnibus (GEO) database (http://www.ncbi.nlm.nih.gov/geo) under accession number: GSE128822 (bulk RNA-seq data, **Figure 9**) and GSE171900, which comprises scRNA-seq data (GSE171899, **Figure 22**) and RNA-seq data (GSE171895, **Figure 29**).

## 3.13. Code availability

Scripts used to analyse the flow cytometry single-cell data are available at https://github.com/luglilab/Cytophenograph.

# 4. Results

## 4.1 Results part 1: "IRF4 instructs effector Treg differentiation and immune suppression in human cancer" (Alvisi et al., 2020)

### 4.1.1 Treg heterogeneity in the TME and its relation to IRF4.

To gain insight in CD4+ T cells phenotypes at the tumor site in NSCLC, we initially studied a cohort of 53 treatment-naïve patients (**Table 1**) by applying a 27-parameter polychromatic flow cytometry panel encompassing markers of memory and effector T cell differentiation, activation, metabolic activity, T cell exhaustion as well as Treg markers (**Table 2**). We profiled millions of single cells from tumor (n = 53), paired adjacent cancer-free lung tissues (n = 45), and peripheral blood (n = 22) samples. We used Uniform Manifold Approximation and Projection (UMAP) to visualize the multidimensional data and the extent of marker co-expression (**Figure 5, A** and **B**). UMAP is an algorithm for dimension reduction based on manifold learning technique that is competitive with t-distributed stochastic neighbor embedding (t-SNE) for visualization quality, but preserves more of the global structure with superior run time performance.

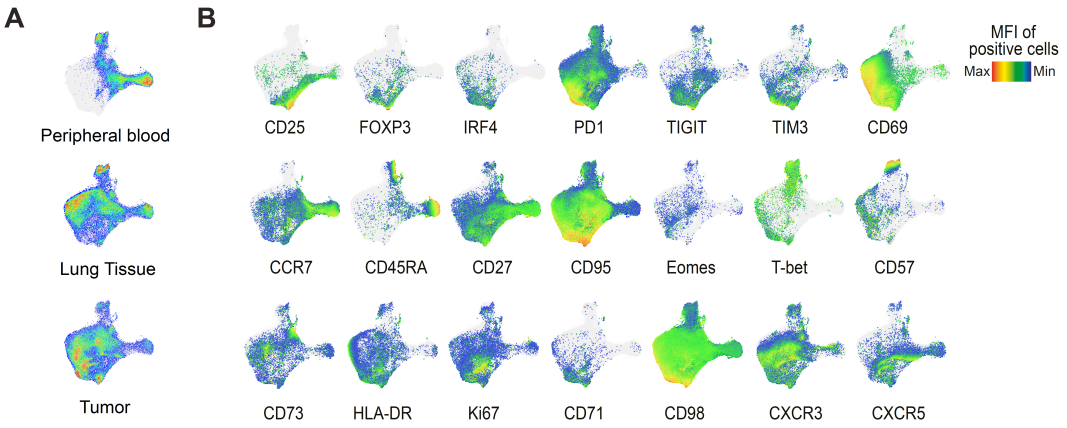


**Figure 5: High-dimensional single cell profiling of NSCLC-infiltrating CD4$^+$ T cells reveals tumor specific immune-phenotypes. A.** UMAP analysis of concatenated CD4+ T cells (1,500 cells/sample) from tumor (n = 53), adjacent lung tissue (n = 45), and blood (n = 22) samples from patients with NSCLC. **B.** UMAP of relative marker expression by concatenated CD4+ T cells from the same samples in **A.**

*Figure 5*

Overall, CD4+ T cells from the three body sites are highly distinct as far as their single cell profiles are concerned (**Figure 5A**). Lung tissues and tumors lacked CD45RA+, CCR7+ and CD27+ cells identifying naïve and

early memory T cells. Tumors also lacked CD4+ T cells with terminal effector/cytotoxic traits, i.e., CD57+ T-bet+ $T_{TE}$ cells but displayed highly expanded frequencies of a subset of CXCR5+ $T_{FH}$-like cells expressing PD1 and TIGIT, CXCR3+ $T_{H1}$-like cells as well as PD1+ TIM3+ TIGIT+ exhausted T cells featuring various activation and metabolic markers (HLA-DR, Ki-67, CD98, CD71). Remarkably, in tumors we distinguished cells with different intensities of CD25 and FOXP3 expression, hence classified as Tregs, featuring multiple activation markers (TIM3, HLA-DR, CD71 and CD98), high levels of CD27 and the transcription factor IRF4 (**Figure 5B**). Manual gating of flow cytometry data confirmed that in tumors around the 40% of CD25+FOXP3+ Tregs expresses IRF4, and that the majority of CD4+ Tconv cells is mostly IRF4- (**Figure 6, A** and **B**).

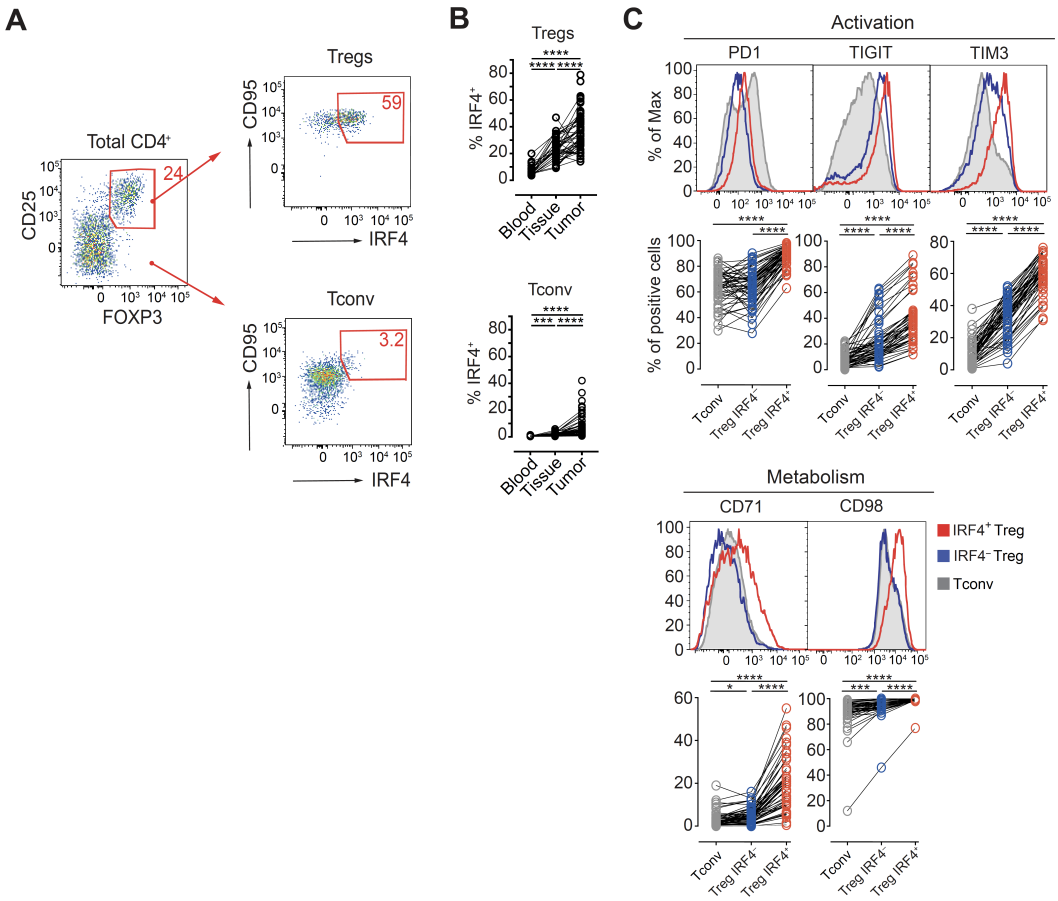


**Figure 6: Tumors are enriched in IRF4-expressing CD4+ T cells. A.** Manual flow cytometry analysis of CD4+CD25+FOXP3+ Tregs and FOXP3- Tconv cells expressing IRF4+. Numbers indicate the percentage of positive cells. **B.** Summary plot representing the IRF4 expression in CD4+ Tregs and Tconv from the same patients as in **Figure 5**. *** P value (P) <0.0005, ****; P < 0.0001; Kruskal-Wallis test. **C.** Representative distribution by flow cytometry (*top*) and summary of the percentage of expression (*bottom*) of selected markers in tumor-infiltrating IRF4+ and IRF4– Tregs and Tconv cells. *P < 0.01, ***P < 0.0005, ****P < 0.0001, nonparametric Friedman test.

*Figure 6*

IRF4+ Tregs were preferentially enriched in tumors while less frequent in adjacent lung tissues and virtually absent in the blood (**Figure 6B**). Moreover, as previously defined by computational analysis of flow cytometry data, they retained increased expression of activation markers such as PD1, TIGIT, TIM3, CD71 and CD98 compared to both IRF4– Tregs and Tconvs in tumors (**Figure 6C**).

The Treg identity of IRF4+ CD4+ T cells in the TME was confirmed by exploring published single cell RNAseq (scRNAseq) data of CD4+ TILs from NSCLC patients (Guo et al., 2018), according to which *IRF4*-expressing T cells were largely confined to a subpopulation of *CTLA*$^{high}$ T cells (subset 9-*CTLA4*; **Figure 7A**), previously defined as suppressive Tregs, and displaying an effector signature including *ICOS, CCR8, TNFRSF4* (encoding OX-40), *TNFRSF9* (encoding CD137/4-1BB) and the IRF4 transcriptional partner *BATF* (**Figure 7B**). Notably, *IRF4* expression was relatively lower in other cell subsets, including non-activated Tregs (subset 8-*FOXP3*).

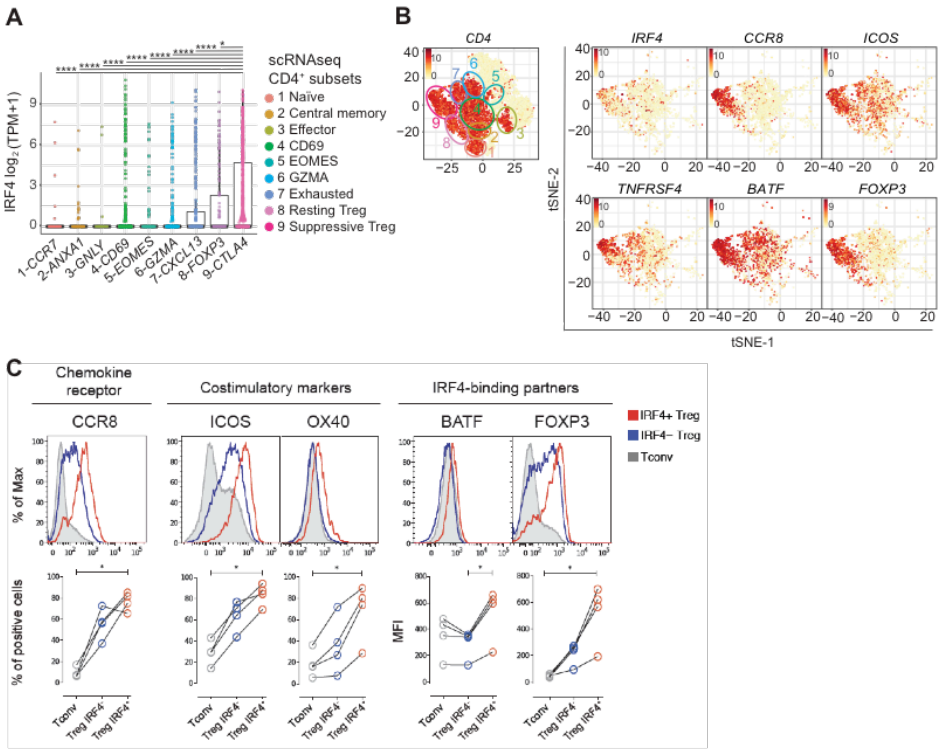


**Figure 7: Tregs heterogeneity in NSCLC. A.** Box plot showing the $\log_2$ (TPM+1) expression of *IRF4* transcript across 9 CD4+ T cells clusters as identified by single-cell RNA-seq (Guo et al., 2018). Each dot represents a single cell. *P ≤ 0.01, ****P ≤ 0.0001, Wilcoxon test. **B.** t-SNE plots illustrating the expression of selected genes in single CD4+ T cells from lung tumor lesions. Cell clusters, depicted on the left, were identified as in **A**. **C.** Representative distribution by flow cytometry (*top*) and summary of the percentage of expression (*bottom*) of selected

markers in tumor-infiltrating IRF4+ and IRF4– Tregs and Tconv cells. *P < 0.01, ***P < 0.0005, ****P < 0.0001, nonparametric Friedman test.

*Figure 7*

To confirm scRNAseq data at the protein level, we performed flow cytometric immunophenotyping in a subset of patients and indeed found that NSCLC-infiltrating IRF4+ Tregs also bear increased levels of CCR8, ICOS, OX40 and BATF compared to the IRF4– counterpart or Tconv (**Figure 7C**).

Overall, these data highlight the phenotypic complexity of the intratumoral CD4+ T cell compartment and further identifies Treg heterogeneity featuring IRF4– quiescent and IRF4+ activated/effector Tregs.

### 4.1.2 IRF4 expression defines effector Tregs with enhanced suppressive potential and capable of promoting tumor growth in vivo.

To gain more insights about the molecular features of intratumoral Treg, we further characterized IRF4+ and IRF4– Tregs by bulk RNA deep sequencing (RNAseq). As the intranuclear localization of transcription factors precluded the isolation of viable cells, we used surrogate surface staining strategies for FACS sorting, namely the combination of CD25 and CD127 to identify bulk Tregs (defined as $CD25^{high}$ $CD127^{low}$; **Figure 8, A** and **B)**, and of CCR8 and ICOS to additionally separate cells according to IRF4 expression (**Figure 8C**).

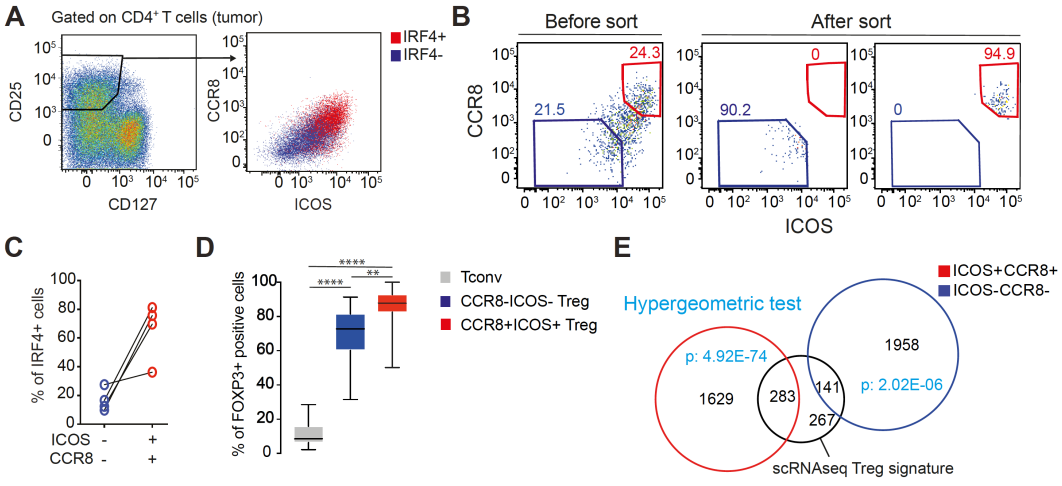


**Figure 8: Transcriptional profiling defines the effector and enhanced suppressive nature of IRF4+ Tregs. A.** Representative CCR8 and ICOS expression in tumor-infiltrating $CD25^{high}CD127^{low}$ Treg subsets defined by IRF4 expression. **B.** Representative dot plots depicting the purity after FACS purification. Numbers are percentages of positive cells. **C.** Percentage of IRF4 expression in tumor-infiltrating Tregs gated as CCR8–ICOS– or CCR8+ICOS+. **D.** Summary plot representing the frequency of FOXP3 expression in CD4+ Tregs

that are CCR8+ICOS+ and CCR8–ICOS–, and in Tconv cells from 48 NSCLC patients. Non parametric Friedman test, **** = P<0.0001. **E.** Venn diagram depicting the genes that are overlapping between FACS-sorted CCR8+ICOS+ (red) or CCR8–ICOS– (blue) Tregs (isolated as in **A**) and a gene expression of bulk Tregs isolated from lung tumors (Guo et al., 2018).
*Figure 8*

As expected, both of these subsets expressed higher levels of FOXP3 than Tconv cells (**Figure 8D**) and their gene expression significantly overlapped with a tumor-infiltrating Treg signature, as obtained from a NSCLC scRNA-seq data set (Guo et al., 2018), **Figure 8E**), confirming the Treg identity of these subsets. Multi-dimensional scaling plot of gene expression profiles showed that sorted intratumoral CCR8+ICOS+ (IRF4+) and CCR8–ICOS– (IRF4–) clustered separately, meaning that they are largely different at the transcriptional level (**Figure 9A**).

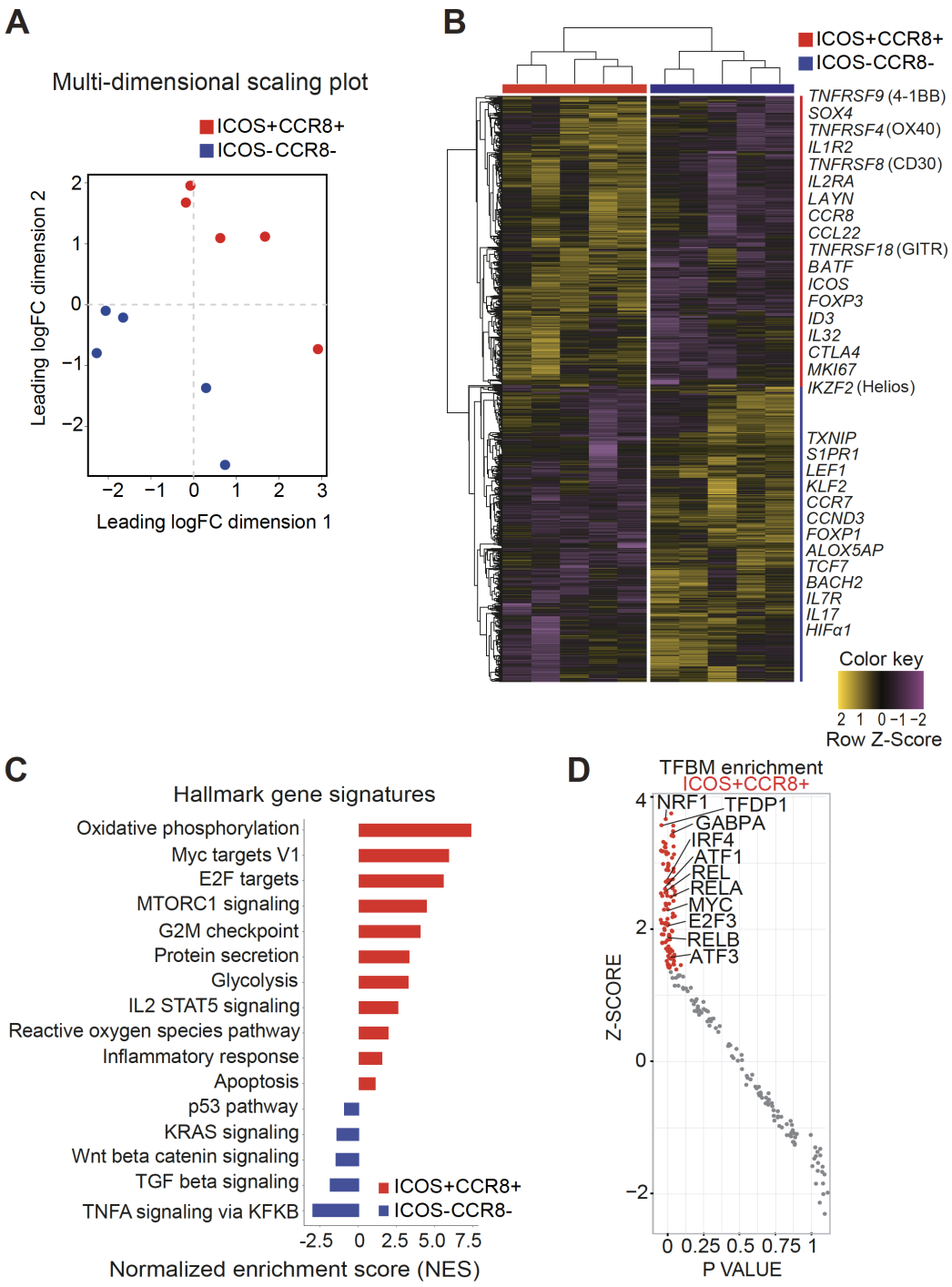


**Figure 9: Bulk RNAseq of CCR8+ICOS+ and CCR8-ICOS- tumor-infiltrating Treg subsets. A.** Multidimensional scaling plot of bulk RNAseq data from FACS-sorted CCR8+ICOS+ versus ICOS-CCR8- tumor-infiltrating Treg. **B.** Heatmap of differentially expressed genes (DEGs) (FDR<0.05; log2FoldChange>1). Selected DEGs are indicated. For some genes, protein names are indicated between brackets. **C.** "Hallmark" gene sets (MsigDB; as obtained by gene set enrichment analysis 'GSEA') **D.** TFBMs enrichment analysis by pScan. Colored dots indicate significant hits.

*Figure 9*

Overall, we identified 2,674 differentially expressed genes (DEGs; FDR<0.05; log2FoldChange>1). CCR8+ICOS+ Tregs overexpressed molecules involved in effector functions (e.g., *TNFRSF9, TNFRSF4,*

*TNFRSF18, BATF*, *IL2RA*), hyper-proliferation (*MKI67*), stability (*IKZF2*), co-stimulation (ICOS) and suppressive function (*CTLA4*). We also found novel transcripts previously not appreciated in Treg biology, such as cytokines (*IL32*), chemokines (*CCL22*) or their receptors (*CX3CR1*), suggesting their potential in Treg-mediated immunosuppression, tumor growth or recruitment to the tumor site. By contrast, CCR8-ICOS- Tregs overexpressed transcripts associated with early differentiation or quiescence including, among others, *CCR7, KLF2, LEF1, TCF7, BACH2* (the latter previously shown to represses effector programs to stabilize Treg-mediated immune homeostasis (Roychoudhuri R, et al., 2013)) and *TXNIP* (a negative regulator of AKT signaling and glycolytic metabolism through modulation of oxidative stress) (**Figure 9B**). Gene set enrichment analysis (GSEA) further revealed that, while CCR8-ICOS- Tregs were largely quiescent featuring transcriptional signatures of Wnt/Beta-catenin and TGFβ. On the other hand, CCR8+ICOS+ Tregs displayed enhanced metabolic activity, preferentially characterized by a signature of oxidative phosphorylation and glycolysis, mTORC1-dependent activity (previously shown to favour murine Treg-cell activation and prevention of autoimmunity (Chapman et al., 2018)) and reactive oxygen species metabolism (likely resulting from enhanced activation and/or mitochondrial respiration; Pilipow et al., 2018) **Figure 9C**).

With the aim of identifying transcriptional regulators at the basis of CCR8+ICOS+ (IRF4+) Treg hyperactivity in tumors, we performed computational analysis of TFBM enrichment in bulk RNAseq data. In this way, we defined that a different array of TFs that included IRF4 was predicted to be preferentially active in the CCR8+ICOS+ vs. the CCR8-ICOS- Treg subset (**Figure 9D**). We additionally identified NRF1, involved in antioxidant defense, lipid metabolism and mitochondrial respiratory function (Hirotsu et al., 2012), MYC, a master regulator of metabolic reprogramming in activated T cells (Wang et al., 2011) and the NF-*k*B family members RELA, previously shown to regulate effector Treg activity in nonlymphoid tissues downstream of TNFRSFs (Vasanthakumar A, et al., 2017). All in all, our transcriptional profiling further elucidates the activation status and enhanced suppressive potential of intratumoral IRF4+ vs. IRF4- Treg cells.

FACS-sorted CCR8+ICOS+ (IRF4+) and CCR8–ICOS– (IRF4–) intratumoral Tregs were further tested for their capacity to suppress

proliferation of autologous CD4+CD25– Tconv cells in vitro (**Figure 10A**). The two Treg subsets were endowed of similar suppressive capacity at a 1:1 Tconv cell/Treg ratio, while only CCR8+ICOS+ Tregs maintained substantial suppressive capacity at a 2:1 ratio (**Figure 10A**).

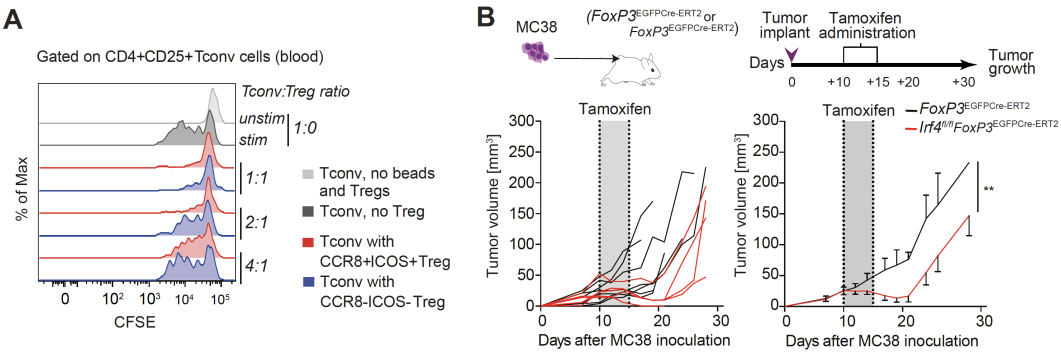


**Figure 10: Figure 10: Mechanistic evaluation of IRF4 function A.** CFSE-labeled CD4+CD25- Tconv cells dilution from a representative blood sample. Tconv cells were co-cultured with Suppression Inspector MACSiBead beads and different ratios of intratumoral Treg subsets for 5 days. Data are representative of 5 independent experiments. **B.** Tumor volumes in FoxP3$^{EGFP\text{-}cre\text{-}ERT2}$(control) (n=7) or Irf4$^{fl/fl}$FoxP3$^{EGFP\text{-}cre\text{-}ERT2}$ (n=5) mice following the administration of tamoxifen. Tumor curves in individual mice and mean ± SEM of the same cohort are shown. **P < 0.01, paired Student's t test.
*Figure 10*

IRF4 has been shown to boost effector Treg differentiation in peripheral tissues thus limiting autoimmunity (Cretney et al., 2013), but its role in the regulation of antitumor immunity remains completely unexplored. To test IRF4 relevance in suppressing the antitumor immune response, we used mice that allow tamoxifen-inducible deletion of IRF4 specifically in Tregs (Irf4$^{fl/fl}$Foxp3$^{EGFP\text{-}cre\text{-}ERT2}$) and controls (Foxp3$^{EGFP\text{-}cre\text{-}ERT2}$). Induced deletion of *Irf4* in FoxP3+ cells in MC38 tumor-bearing mice resulted in a significant delay in tumor growth (**Figure 10B**), meaning that IRF4+ Tregs suppress antitumor immunity.

### 4.1.3 IRF4 and its partner BATF control a molecular program of effector Treg differentiation and suppression in tumors.

We further investigated the relevance of IRF4 and its transcriptional partner BATF in determining the enhanced suppressive phenotype of tumor-infiltrating Tregs by integrating gene expression profiles with IRF4 binding in the genome from mouse models. As mouse vs. human gene regulation is difficult to be inferred due to species-specific differences in non-coding

regions, we first defined a conserved tumor-infiltrating Treg signature by integrating DEGs of CCR8+ICOS+ vs. CCR8– ICOS– Tregs and DEGs of Tregs infiltrating a murine colon carcinoma (dependent on the MC38 cell line) vs. those isolated from the spleen (Magnuson et al., 2018) (**Figure 11A**). Next, we defined the transcriptional program that is dependent on *Irf4* or *Batf* expression by analyzing gene expression profiles of splenic Tregs from wild-type vs. *Irf4*$^{-/-}$ and *Batf*$^{-/-}$ mice (Hayatsu et al., 2017; **Figure 11B**). Among the 382 genes shared between mouse and human Tregs, 61 genes were controlled only by *Irf4*, 10 only by *Batf* and 23 by both. We further used publicly available chromatin immunoprecipitation deep sequencing (ChIPseq) data to assess IRF4 occupancy at the loci of interest and thus define a direct role of this TF in directly controlling gene expression (**Figure 11C**). Genes dependent only on *Irf4* included several *Tnfr* family members involved in effector Treg differentiation such as *Tnfrsf1b*, *Tnfrsf8* (Vasanthakumar et al., 2017), chemokine receptors such as *Ccr8*, *Cxcr3* and *Ccr5*, likely involved in the localization of Tregs to tumors or to the lung, and *Zbtb32*, *Mki67*, *Map2k3, Kif23, Rrm2,* and *Aurkb*, previously linked to cell cycle in other cell types and likely contributing to Treg hyperproliferation. Instead, *Tnfrsf9, Icos*, *Ikzf2* (encoding Helios), and *Il1rl1* (also known as ST2 or IL-33 receptor), were dependent on both *Irf4* and *Batf*.

In conclusion, *Irf4* and *Batf* directly and indirectly control a program of effector Treg differentiation and immunosuppression in cancer.

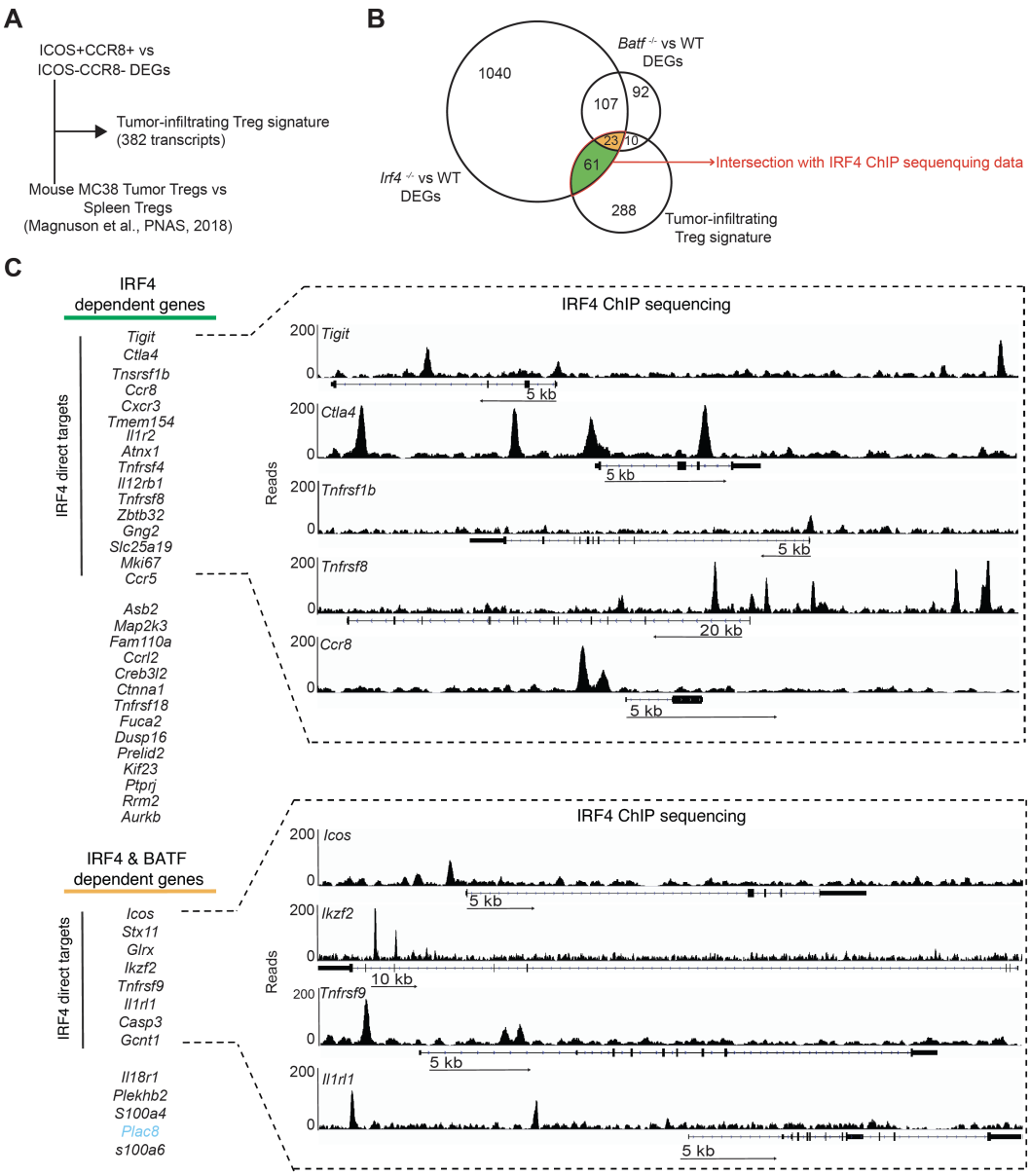


**Figure 11: IRF4 and its partner BATF directly and indirectly control a molecular program of effector Treg differentiation. A.** Identification of a shared gene expression signature between tumor-infiltrating human CCR8+ICOS+ vs CCR8–ICOS– Treg and murine Tregs (obtained from Magnuson et al., 2018). **B.** Venn diagram of the number of genes of the tumor-specific Treg signature obtained as in A that are differentially expressed in splenic Tregs from *Batf* $^{-/-}$ and *Irf4*$^{-/-}$ mice. **C.** List of tumor-infiltrating Treg genes that are dependent on the expression of *Irf4* or *Irf4* and *Batf*. All genes are induced, except for *Plac8* that is repressed (indicated in light blue). Those genes directly controlled by Irf4 binding to the genome as obtained from ChIPseq analysis of murine Tregs are in bold. Genomic binding of Irf4 to the DNA for selected genes is depicted.
*Figure 11*

### 4.1.4 scRNA-seq–guided high-dimensional flow cytometry profiling reveals that CCR8+ICOS+ (IRF4+) effector Tregs associate with multiple exhaustion traits of T cells.

To further characterize with high resolution the T cell phenotypic landscape associated with Treg subsets in patients with NSCLC, we

designed a second multi-parameter FACS panel (**Table 2**) exploiting the aforementioned transcriptomic results. We preferred markers identified by fluorochrome-conjugated antibodies providing a high signal-to-noise ratio (e.g., CCR8 and ICOS instead of IRF4) so as to enhance the identification of subsets by the clustering algorithm (Brummelman et al., 2019). We profiled tumors (n = 45), paired adjacent cancer-free lung tissues (n = 23), and peripheral blood samples (n = 23) from treatment-naive patients (**Table 1**). A workflow of the analysis is shown in **Figure 12A**. We next applied PhenoGraph, a computational algorithm capable to unbiasedly cluster single cells according to the relative expression of markers (Levine et al., 2015). With this approach, we identified 14 different CD4+ and 15 different CD8+ T cell clusters (**Figure 12B**). UMAP of single-cell distributions and principal component analysis (PCA) of cluster abundance clearly distinguished different T cells profiles from the peripheral blood, lung tissues and tumors (**Figure 12, C** and **D**).

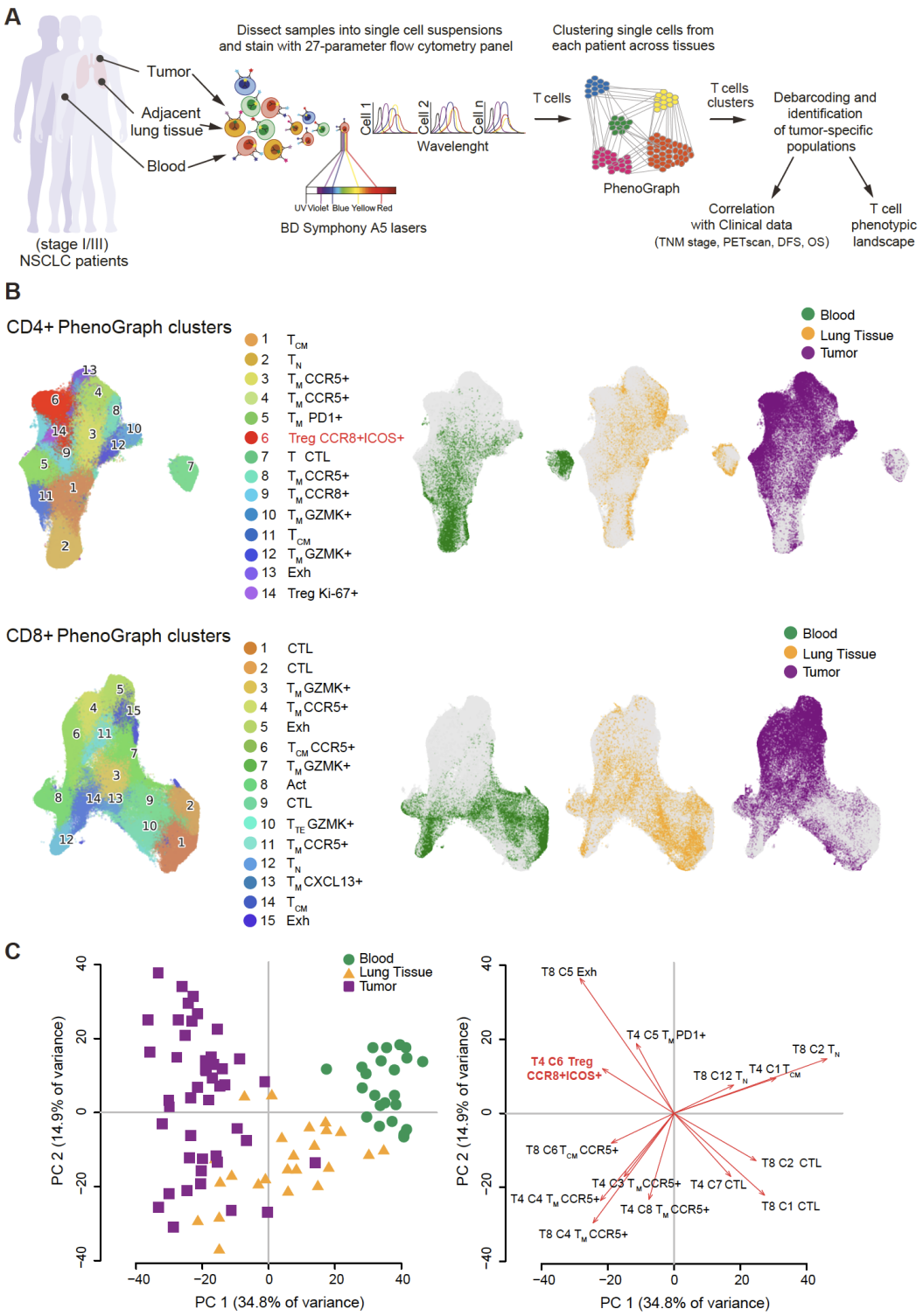


**Figure 12: Transcriptomic guided FACS panel design identifies tumor-specific T cell subpopulations. A.** Experimental workflow. **B.** UMAP analysis of concatenated CD4+ (*top*) and CD8+ (*bottom*) PhenoGraph clusters from peripheral blood (n = 23, green), normal lung tissue (n = 23, orange), and tumor (n = 45, purple) samples from NSCLC patients. **C.** *Left:* PCA plot showing the distribution of samples according to the frequency of CD4+ and CD8+ PhenoGraph clusters in each sample. The cohort was subdivided in three groups according to sample origin: Blood (green), Lung Tissue (orange), Tumor (purple). *Right:* PCA of PhenoGraph clusters. Those clusters most contributing to the PCA output in **B** are indicated.

*Figure 12*

We next calculated the integrated median fluorescence intensity (iMFI) values of each marker in each PhenoGraph cluster so as to gain indication on cluster identity (Brummelman*, Mazza* et al., 2018, **Figure 13A**)

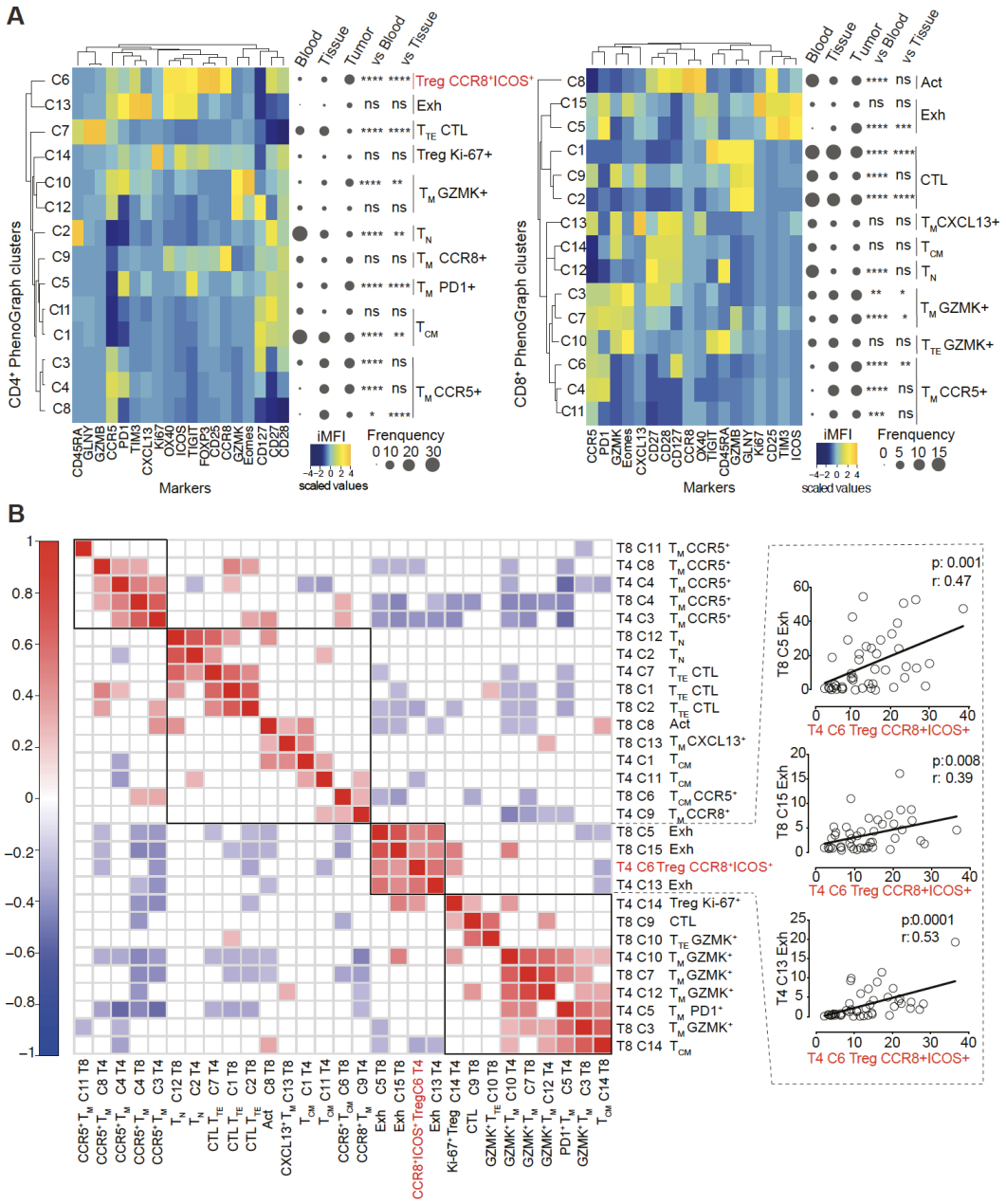


**Figure 13: Abundance of CCR8+ICOS+ intratumoral Tregs is associated with multiple features of T cell exhaustion. A.** Heatmaps of the relative expression, depicted as integrated MFI (iMFI: MFI x % antigen expression) of markers (columns) in discrete CD4+ (left panel) and CD8+ (right panel) Phenograph clusters (rows). Data are further metaclustered to group subpopulations with similar immunophenotypes. The median frequency of each PhenoGraph cluster in the different compartments is represented by Balloon plots. *p<0.05, **p<0.01, ***p<0.001, ****p<0.0001 tumor vs. blood or vs. normal tissue samples; two-way ANOVA with Bonferroni post-hoc test. **B.** Correlogram showing Pearson correlation between frequencies of CD4+ (T4) and CD8+ (T8) PhenoGraph clusters in tumor samples from 45 early stage (I-III) NSCLC patients. Not significant correlations (p-value > 0.05) are left blank.

*Figure 13*

Metaclustering of PhenoGraph clusters and markers grouped subpopulations with similar immunophenotypes. We documented the loss of subsets of naïve (CD4+, C2; CD8+, C12) and cytotoxic T cells (CD4+, C7; CD8+, C1, C9, C2) and the accumulation of exhausted T cells (CD8+, C5) in tumors compared with the blood or the adjacent lung tissue. As expected, we detected an increased presence of CCR8+ICOS+ (IRF4+) activated Tregs (CD4+, C6) in tumors. We further investigated the association of these cells with specific T cell subsets in the TME by performing a Pearson correlation analysis of the abundance of all T cell clusters identified by PhenoGraph in 45 patients (**Figure 13B**). Notably, intratumoral CCR8+ICOS+ Tregs correlated with CD4+ (C13) and CD8+ (C5 and C15) T cells with features of exhaustion (i.e., expressing PD1, TIM3, and TIGIT). At the same time, CCR8+ICOS+ Tregs negatively correlated with cytotoxic CD8+ T cells (C2, coexpressing GZMB and GNLY and thus endowed of effector functions) and with clusters of central memory T cells (CD4+, C11 and CD8+, C14). In summary, high-dimensional single-cell profiling identifies a T cell signature with increased frequencies of CCR8+ICOS+ effector Tregs associated with T cell exhaustion.

### 4.1.5 Prevalence of IRF4+ (CCR8+ICOS+) Tregs is positively correlated with worse prognosis in NSCLC.

We finally tested whether patients with different prognosis might be characterized by differential abundance of CCR8+ICOS+ effector Tregs. To this end, we subdived a sub-cohort of patients (n=26) in two groups according to the median distribution of the maximum standardized value of fluorodeoxyglucose uptake (SUVmax), a positron emission tomography (PET) indicator of tumor glycolysis and aggressiveness (Lopci et al., 2016). PCA revealed a bimodal separation of the $SUVmax^{low}$ and $SUVmax^{high}$ groups of patients according to the relative frequencies of CD4+ and CD8+ PhenoGraph clusters (**Figure 14A**, *left panel*), indicating that they display a different T cell profile as a whole. Analysis of PCA loadings identified clusters contributing the most to such distribution (**Figure 14A**, *right panel*). Indeed loadings are from a numerical point of view, equal to the coefficients of the variables, and provide information about which independent variables (clusters in our case) give the largest contribution to the components.

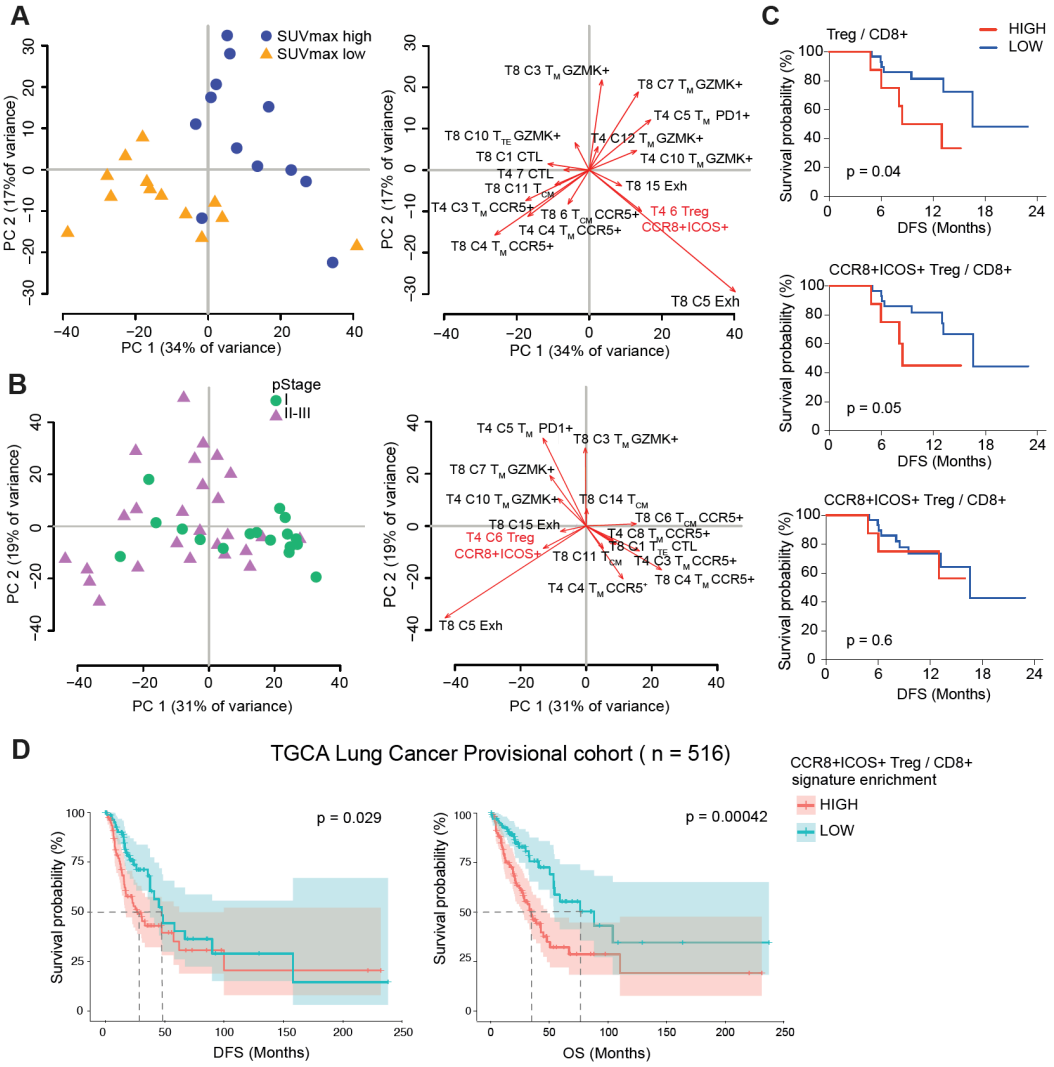


**Figure 14: Impact of the immune landscape at surgery on the prognosis of NSCLC patients**. **A.** *Left:* PCA plot showing the distribution of patients (*n* = 26) according to the frequency of CD4+ and CD8+ PhenoGraph clusters in each patient. The cohort was subdivided in 2 groups according to the median distribution of maximum standardized uptake value (SUVmax). *Right*: PCA loading plot of PhenoGraph clusters most contributing to the PCA output on the left. **B.** *Left:* Principal component analysis (PCA) plot showing the distribution of patients (*n* = 48) according to the frequency of CD4+ and CD8+ PhenoGraph clusters in each patient. Patients were classified according to pathological stage (pStage) I, II, or III of the International TNM classification. *Right:* PCA loading plot as in **A**. **C**. Kaplan-Meier progression-free survival curves according to the intratumoral frequencies of Tregs subsets over CD8+ T cells in each patient (*n* = 38). The cohort was subdivided in 2 groups according to the percentile rank (set at 0.8). The *P* value was calculated by Gehan Breslow-Wilcoxon test. **D.** Kaplan-Meier disease-free survival (DFS) and overall survival (OS) curves in the TCGA lung adenocarcinoma (LUAD) lung cancer cohort (*n* = 516). Patients were grouped by percentile rank (set at 0.8) according to the enrichment of the CCR8+ICOS+ bulk Treg signature (as obtained in **Figure 8** and **9**) as relative to the CD8+ T cell signature. + indicates censored observations. *P* values were calculated by Cox regression. Dotted lines indicate the time at which 50% of the cohort was still free of the event.

*Figure 14*

In particular, SUVmax$^{high}$ patients harbored increased frequencies of CCR8+ICOS+ Tregs (C6), subsets of CD8+ (C5 and C15) and CD4+ (C5) exhausted T cells as well as memory T ($T_M$) cells expressing GZMK, PD1 (CD8$^+$: C3, C7) and EOMES (associated with T cell dysfunction in humans41) and. By contrast, SUVmax$^{low}$ patients harbored increased frequencies of CCR5+ clusters (CD8+: C4, C6 and CD4+: C3, C4) or terminal effector, cytotoxic T cells (CD8+ C1 and CD4+ C7). We observed similar results when we considered a parameter of disease progression, *i.e.* the international TNM classification. Indeed, CCR8+ICOS+ Tregs (CD4+ C6) as well as T cells featuring exhaustion/activation markers (CD8+: C5 and C15) were more abundant in patients with advanced pathological stage (pStage) II and III (**Figure 14B**).

Infiltration of CD8+ T cells is a well-known predictor of good prognosis in cancer (Galon et al., 2013). We thus investigated disease free survival (DFS) of our patients according to the frequency among CD3+ of Treg/CD8+ T cell ratios in tumor lesions. We found that a higher ratio is significantly associated with early tumor relapse **(Figure 14C)**. As predicted by their superior suppressive activity, this was due to the contribution of CCR8+ICOS+, but not of CCR8- ICOS- Tregs. We next validated our findings exploiting the larger cohorts of individuals available from the cancer genome atlas (TCGA). In this case, the degree of infiltration of specific subpopulations was determined by enrichment of transcriptional signatures. Similar to results from our NSCLC cohort, we found that a higher CCR8+ICOS+ Treg/CD8+ T cell signature in bulk RNAseq data from primary biopsies was associated both with worse DFS as well as overall survival (OS) in lung adenocarcinoma (**Figure 14D**; Cancer Genome Atlas Research Network, 2014).

### 4.1.6 CCR8+ICOS+ effector Treg infiltration relative to CD8+ defines a signature of disease progression in different cancer types.

We finally investigate wheatear IRF4 overexpression by effector Tregs is a generalized phenomenon in human cancer by re-analyzing public available datasets. Specifically, we retrieved normalized scRNA-seq counts from the Gene Expression Omnibus (GEO GSE72056) melanoma dataset. The analysis was restricted to the cells labeled as “T cells,” as previously defined by (Tirosh et al., 2016) T cells were divided into CD4+

and CD8+, based on the normalized expression levels (E) of CD4 (E>4) and CD8 (average of CD8A and CD8B, E>4). Among all samples composing the data set, 466 were identified as CD4+. To asses which genes have the expression profile most correlated with that of IRF4, a Pearson correlation coefficient, indicated as score in **Figure 15A**, and a corresponding P value were computed between each gene expression profile in the matrix (consisting of 23,686 genes) and IRF4.

**A**

| Rank | Gene | Score | P-Value |
|---|---|---|---|
| 1 | *IRF4* | 1 | -- |
| 2 | *BATF* | 0.251 | <0.0001 |
| 4 | *PRDM1* | 0.231 | <0.0001 |
| 8 | *CTLA4* | 0.216 | <0.0001 |
| 9 | *HLA-DRB5* | 0.215 | <0.0001 |
| 23 | *IL1R2* | 0.202 | <0.0001 |
| 39 | *GATA1* | 0.192 | <0.0001 |
| 56 | *FOXP3* | 0.187 | <0.0001 |
| 90 | *CCR8* | 0.169 | 0.0002 |
| 123 | *CD59* | 0.161 | 0.0004 |
| 187 | *IL2RA* | 0.152 | 0.001 |
| 358 | *CXCR6* | 0.140 | 0.003 |
| 383 | *CD177* | 0.13 | 0.003 |
| 402 | *ICOS* | 0.13 | 0.004 |
| 991 | *RORC* | 0.104 | 0.025 |
| 3099 | *GATA3* | 0.059 | 0.204 |
| 3445 | *TBX21* | 0.054 | 0.247 |

**B**

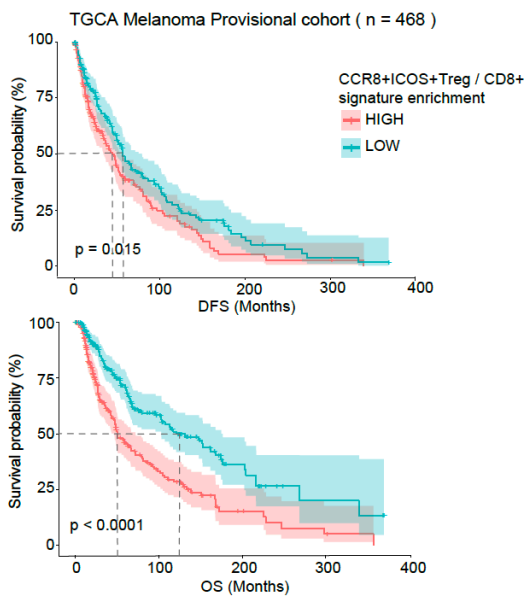


**Figure 15: Figure 15: IRF4 expression in Tregs is associated with worse clinical outcome in melanoma. A.** Pearson analysis of IRF4-correlated genes in melanoma (Tirosh. et al., 2016) **B.** Kaplan–Meier survival curves of TCGA melanoma patients (n=468) grouped by percentile rank (0.8) according to the CCR8+ICOS+ Treg bulk/CD8+ T cell signature enrichment. + represents censored observations, and p value was calculated by Cox regression.
*Figure 15*

Similarly to Tregs in NSCLC, *IRF4* expression correlated with effector Treg markers such as *CTLA4*, *FOXP3*, *PRDM1* (a downstream transcriptional target of IRF4), *BATF* or *IL1R2* (**Figure 15A**). In attempt to correlate our finding with clinical outcome of melanoma patients we took advantage of 468 bulk RNAseq samples from TGCA repository. We found that a higher CCR8+ICOS+Treg/CD8+ T cell signature was associated both with worse DFS and overall survival.

Moreover, we identified a similar subset of IRF4-expressing Tregs by scRNA-seq analysis of CD45+ cells infiltrating hepatocellular carcinoma (**Figure 16A**).

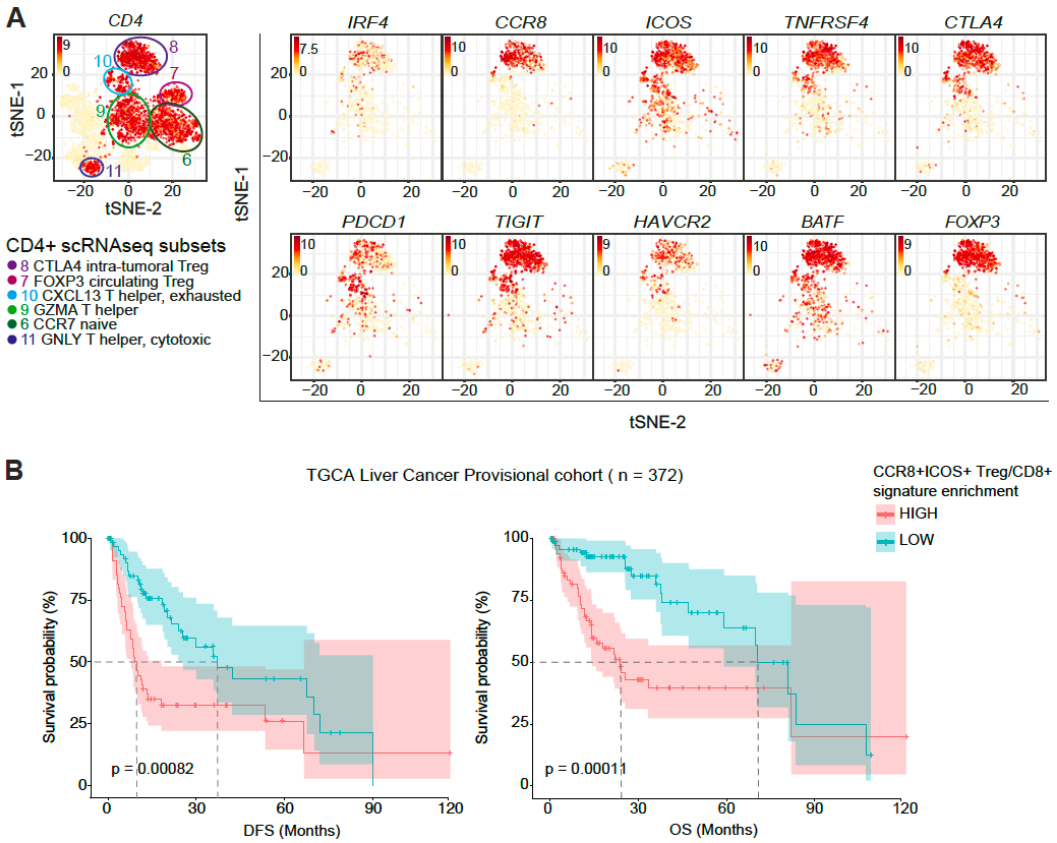


**Figure 16: CCR8+ICOS+ effector Treg infiltration relative to CD8+ defines a signature of disease progression in hepatocellular carcinoma. A.** t-SNE plots illustrating the expression level of selected genes across single CD4+ T cells from hepatocellular carcinoma lesions (Zheng et al., 2017). The 6 CD4+ subsets identified in the study are labelled in the plot on the left. **B.** Kaplan–Meier DFS (*left*) and OS (*right*) curves of TCGA LIHC liver cancer patients (n=372) grouped by percentile rank (0.8) according to the enrichment of the CCR8+ICOS+ bulk Treg signature (as obtained in **Figure 8** and **9**) as relative to the CD8+ T cell signature. + represents censored observations, and p value was calculated by multivariate Cox regression.

*Figure 16*

We further obtained the tumor-infiltrating CD8+ signatures by combining all the DEGs from the CD8+ tissue-specific clusters and by excluding the circulating clusters labeled as CD8-C1-LEF1. Even in this case, the enrichment of the IRF4 Treg over CD8 showed significant worst outcome in TGCA survival analysis (**Figure 16B**).

We conclude that IRF4 instructs effector Treg differentiation and immune suppression in multiple human cancers.

## 4.2 Results part 2: *"*Multimodal single-cell profiling of intrahepatic cholangiocarcinoma (iCCA) defines hyperactivated Tregs as a potential therapeutic target*"*

### 4.2.1. High-dimensional flow cytometry defines the T cell and myeloid cell composition of human iCCA.

iCCA is a deadly bile duct cancer. It is commonly asymptomatic in the early stages and no molecular clinical markers for early diagnosis are known (Banales et al., 2020). Late diagnosis highly compromises surgery, the only current potentially curative option, and even among the 10-30% patients eligible for resection at diagnosis, 50% recur within the first year (Tariq N. et al., 2019). Conventional chemotherapy and pharmacological therapies have limited efficacy (with 5-year survival rate below 10%), prompting interest in immunotherapy approaches. Knowledge regarding the architecture of the immune system in iCCA is still limited. Overall, iCCA is generally referred as a "cold" tumor because of the absence of pro-inflammatory myeloid cells and failure of T cell priming (Malenica et al., 2020). To identify cell-specific alterations associated with this disease we studied a cohort of 20 chemotherapy-naïve patients who were eligible for surgery shortly after diagnosis (**Table 1**). Specifically, we generated single-cell suspensions from the tumor, adjacent tumor-free tissue (hereafter referred to as peritumor), peripheral blood mononuclear cells (PBMCs) and circulating immune cells perfused from the liver parenchyma (hereafter referred to as perfusate). We next profiled millions of single cells with 2 high-dimensional flow cytometry panels encompassing markers of T cell memory and effector differentiation, activation, cytotoxicity and exhaustion, CD4+ Treg markers as well as markers capable to define subsets of myeloid cells (**Figure 17A**).

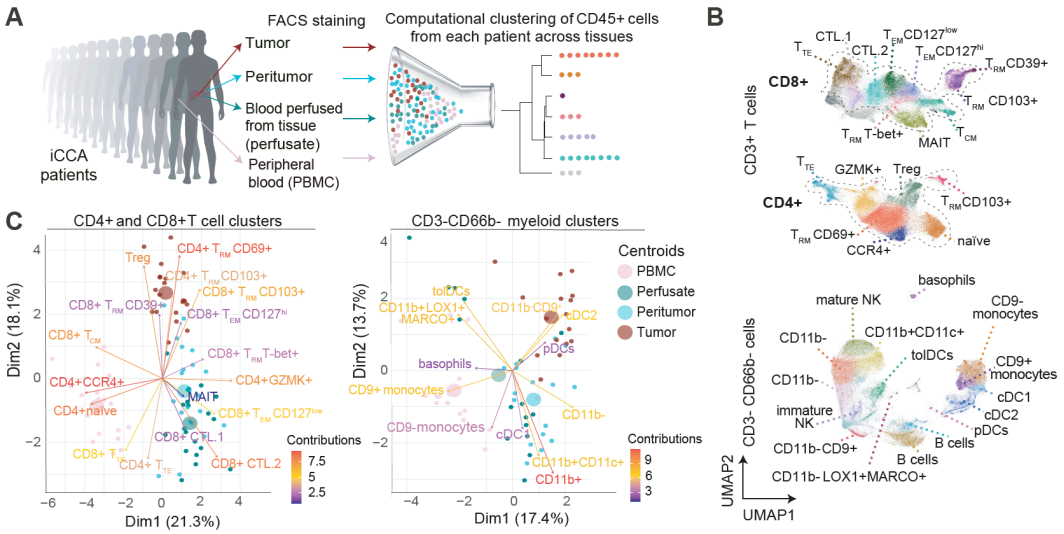


**Figure 17: High-dimensional single-cell profiling of CD45+ cells infiltrating human iCCA. A.** Experimental workflow. **B.** UMAP representation of concatenated CD3+ T cell and CD3-CD66b- myeloid cell PhenoGraph clusters resulting from the flow cytometric analysis of paired tissue sites of iCCA patients (n=20 for T cell data; n=16 for myeloid data). **C.** PCA plots showing the distribution of samples according to the frequency of CD3+ T cell (left) and CD3-CD66b- myeloid cell (right) PhenoGraph clusters as in **B**. Small circles identify single samples, while big circles the mean of the distribution. Colors of the arrows and the cluster labels reflect the relative contribution to the PCA distribution.
*Figure 17*

CD3+ cells, identifying the bulk of T cells, and CD3-CD66b- cells, enriched mainly in myeloid cells, were further clustered by PhenoGraph (Materials and Methods; Brummelman et al., 2019). In this way, we identified 7, 10 and 12 CD4+, CD8+ and myeloid clusters, respectively (**Figure 17B**). Principal Component Analysis (PCA) of PhenoGraph cluster abundance revealed that the four tissue sites had a different T-cell and myeloid composition as a whole, although perfusate and the peritumor tended to share a similar immunophenotypic landscape (**Figure 17C**).

As far as T cells are concerned, PBMCs were characterized by the presence of CD4+ naïve and memory T cells expressing C-C chemokine receptor 4 (labelled as CD4+CCR4+)) as well as CD45RO+CCR7+ central memory CD8+ T cells (CD8+ $T_{CM}$); perfusate and peritumor by CD4+GZMK+CCR2$^{dull}$ (CD4+GZMK+) and, to a lesser extent, CD4+GZMB+2B4+ terminal effector T cells (CD4+ $T_{TE}$), by CD8+ T cells with a CD45RO-CCR7-GZMK+GZMB+ phenotype (CD8+ CTL.2) or with a CD127$^{low}$CD45RO+CCR7–GZMK+GZMB+ effector memory T cell phenotype (CD8+ $T_{EM}$ CD127$^{low}$), by CD8+ T cells with a CD127$^{low}$GZMK+CD161+ phenotype, labelled as MAIT cells (Dusseaux et al., 2011); tumors by subsets of CD4+ and CD8+ memory T cells

expressing different combinations of the markers CD69 and CD103, collectively labelled as tissue-resident memory T cells ($T_{RM}$) (**Figure 18**).

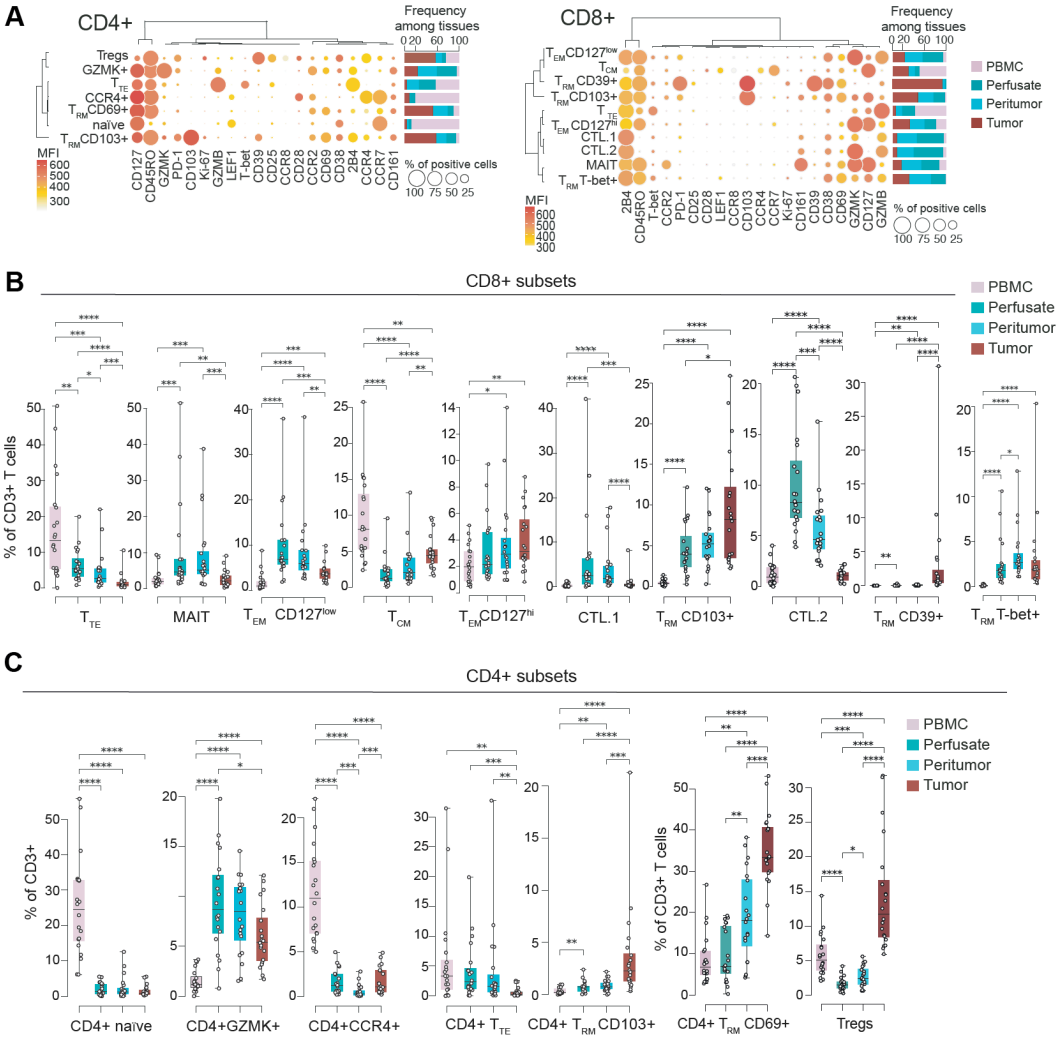


**Figure 18: T cell landscapes of intrahepatic cholangiocarcinoma. A.** Balloon plot maps showing the percent expression and the mean fluorescent intensity (MFI) of specific markers (columns) in discrete PhenoGraph clusters (rows) of CD4+ and CD8+ T cells. Hierarchical meta-clustering grouped markers and clusters with similar immunophenotypes. Bar plots show the percent frequency of each cluster among different tissues. **B.** Box plots showing the median and the IQR of PhenoGraph cluster frequency at different tissue sites. Bars indicated the SD. Dots depict single patient values. *=P<0.05, **=P<0.01, ***=P<0.001, ****=P<0.0001, two-sided Mann-Whitney test.

*Figure 18*

In the case of CD8+ T cells, a subset of CD69+ CD103+ $T_{RM}$ also expressed high levels of CD39 (CD8 $T_{RM}$ CD39+), a marker recently associated with CD8+ T cell reactivity to tumor antigens (**Figure 18A**) (Duhen et al., 2018; Simoni et al., 2018). In line with their putative chronic stimulation by tumor antigens, these cells also expressed increased levels of the inhibitory receptor PD-1 and the activation marker CD38 compared to other iCCA-infiltrating CD8+ T cell clusters. Albeit present almost

exclusively in tumors, the relative abundance of CD8+ CD39+ $T_{RM}$ among total CD3+ was low (median=0.68, IQR: 0.41 and 3.32; **Figure 18B**), possibly suggesting the poor immunogenicity of human cholangiocarcinoma or suppression of T cell responses against them (Losurdo et al., 2021).

Notably, tumors were highly infiltrated by CD4+CD127-CD25+ Tregs (**Figure 18A** and **Figure 19A**) overexpressing PD1, CD39, CCR8, CD69, CD38 and the TF T-bet compared to Tregs from other tissue sites or the circulation (**Figure 19B and C**), thereby indicating acquisition of a hyperactivated phenotype similar to that previously described in NSCLC, melanoma and HCC (Results, Part 1).

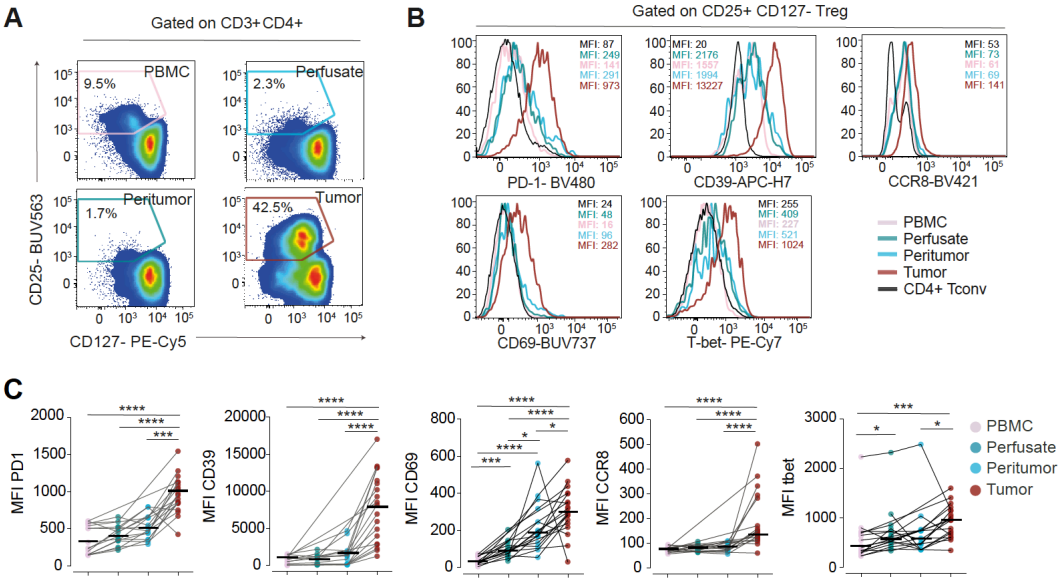


**Figure 19: Phenotypic analysis of Treg cells across different tissue sites A.** Representative flow cytometric analysis of CD25+CD127- Tregs from the different tissue sites. Numbers indicate the percentage of cells **B.** Median fluorescence intensities (MFI) of Tregs identified as in A. Conventional CD4+ CD25- CD127+ T cells (Tconv) are depicted as a control. **C.** Summary of the data in B (n=20). Bars indicate the median. Mann-Whitney-Wilcoxon test, two-sided. *P<0.05; ****, P<0.001.

*Figure 19*

We further profiled a subset of iCCA samples (n=5) with a Treg-specific panel of markers. We identified two major subclusters of Tregs by PhenoGraph analysis (**Figure 20A**), according to which “activated” Tregs express high levels of effector Treg-related markers 41BB, ICOS, CCR8, GITR and, to a lesser extent, PD-L1 compared to “quiescent” Tregs (**Figure 20B**). Overall, these data confirm that iCCA-infiltrating Tregs show a heterogeneous pattern and activated phenotype similar to those we previously found in other solid tumors.

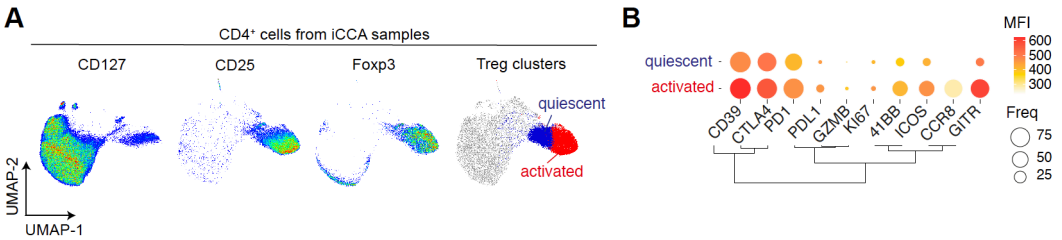


**Figure 20: Intratumoral Treg heterogeneity. A**. UMAP-based analysis of concatenated CD4+ T cells from iCCA samples (n=5). Among Tregs (CD25+CD127-FOXP3+), Phenograph identifies a quiescent (blue) and an activated (red) cluster. **B.** Balloon plot maps showing the percent expression and MFI of specific markers (columns) in discrete Phenograph clusters of intratumoral Tregs identified as in **A**.

*Figure 20*

### 4.2.2. scRNA-seq reveals tumor-specific differences in gene expression by specific T cell subpopulations.

We next performed scRNA-seq of CD45+ immune cells isolated from 6 cholangiocarcinomas and paired peritumoral tissues to gain more insights on the molecular characteristics of the tumor specific immune infiltrate (**Figure 21A**).

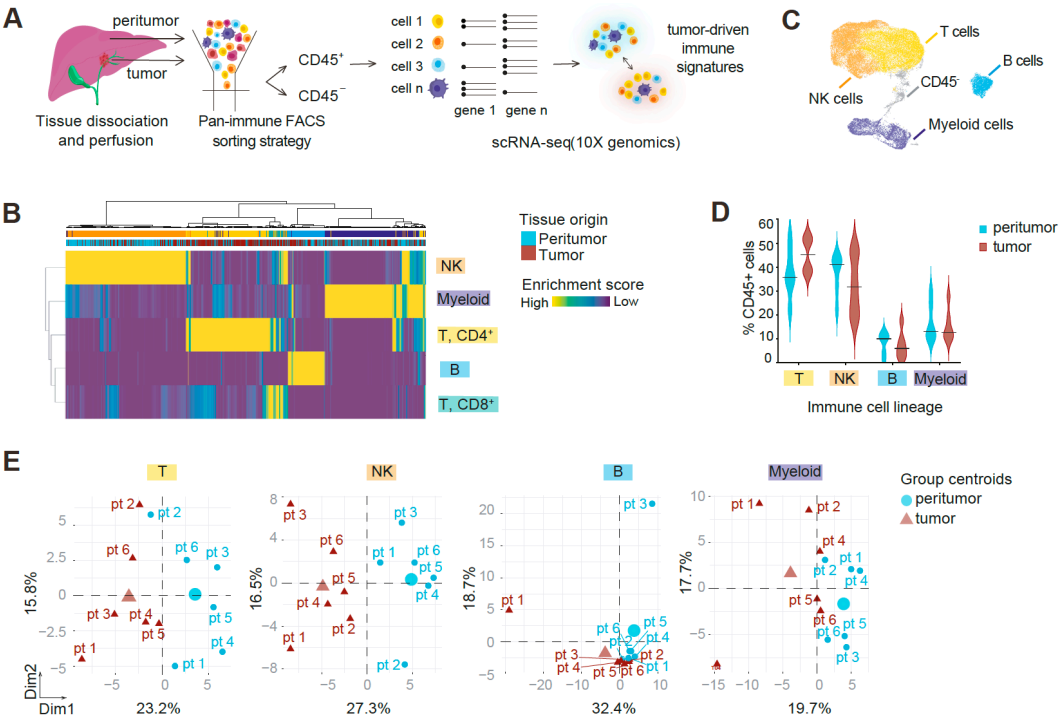


**Figure 21: The landscape of immune infiltrates in human iCCA revealed by scRNA-seq. A.** Experimental workflow. **B.** Heatmap of SingleR enrichment scores of single CD45+ cells (*column*) to each "Main Immune Cell Expression Data'" reference signature (*row*) after ALRA imputation. Cells were further meta-clustered based on SingleR enrichment scores. **B.** UMAP of all cells (n = 31,745). CD45+ SingleR clusters are color-coded. **D.** Violin plots showing the relative frequency of immune cell types identified in **A**. Lines represent median frequencies (n=6 patients). **E.** PCA plots showing the distribution of peritumoral (light blue circles) and tumoral (dark red triangles) samples from 6 patients (pt) according the gene expression profile of each sample. Symbols of bigger size indicate the centroid of the distribution.

*Figure 21*

Cluster analysis of scRNA-seq data and subsequent enrichment of defined main immune signatures revealed cells identity (**Figure 21, B** and **C**). CD45– stromal/tumor cells from 2 patients, spiked in at known concentration as a control, separated from these subsets of immune cells. Among CD45+ cells, tumors tended to harbor increased frequencies of T cells, reduced frequencies of NK and B cells, and similar frequency of myeloid cells compared to adjacent peritumoral tissue (**Figure 21D**). Overall, tumoral and peritumoral tissues could be clearly distinguished on the basis of T and NK cell gene expression profiles, and less so by B cell and myeloid profiles, indicating that T cells and NK cells undergo specific transcriptional changes in the tumors (**Figure 21E**).

We focused our subsequent investigation on T cells and subclustered these populations of cells. We identified 11 clusters, reflecting those subpopulations that were previously identified by flow cytometry (**Figure 22A**).

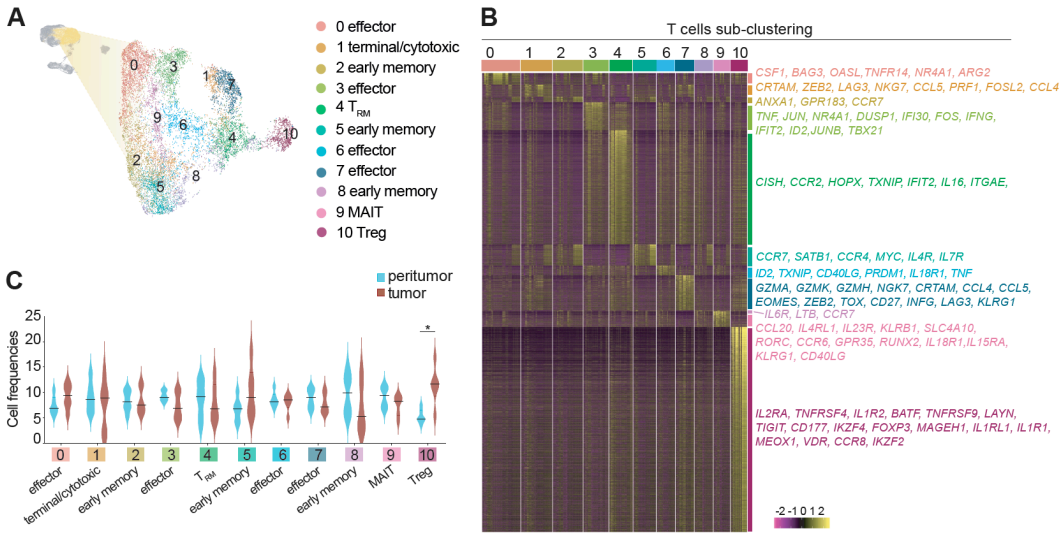


**Figure 22: T cell landscape in iCCA revealed by scRNA-seq. A.** Coloured clusters of T cells (n = 12,644) visualized by UMAP. **B.** Heatmap of marker genes in scRNA-seq clusters. *Columns*: single cells. *Rows*: cluster marker genes. Manually selected representative genes are on the right. **C.** Violin plots showing the relative distribution of each T cell cluster between tumoral and peritumoral samples. Lines: median frequencies. 2-way ANOVA test,*P<0.05.

*Figure 22*

We identified subsets of early differentiated memory T cells (C2, C5 and C8), expressing different combinations of genes previously related to stem-like memory cell differentiation such as *CCR7*, *GPR183*, *IL6R*, *SATB1*, *CCR4* and *IL7R* (Galletti et al., 2020) subsets of effector cells (C0,

C3, C6 and C7), expressing different combinations of genes previously related to effector memory differentiation, such as *CSF1* (encoding M-CSF), *TNF*, *IFNG*, *TBX21* [encoding the TF T-bet], *ID2*, *PRDM1* (encoding the TF BLIMP-1), *GZMA*, *GZMK* and the C-C chemokines *CCL4* and *CCL5*, among others; a terminally differentiated/cytotoxic subset (C1), expressing the cytotoxicity-related genes *CRTAM*, *NKG7* and *PRF1* (encoding perforin) and the terminal differentiation-related TF *ZEB2*; a $T_{RM}$ cell subset (C4), expressing *ITGAE* (encoding CD103 integrin), *CISH*, *CCR2*, *HOPX* as well as detectable levels of *ENTPD1* (encoding CD39), suggesting potential tumor reactivity (Simoni et al., 2018; Duhen et al., 2018); and a subset expressing several CD4+ Treg-related genes (C10), including *IL2RA*, *FOXP3*, *BATF*, *TIGIT*, *CD177*, *IL1R2*, among others (**Figure 22B**). An additional subset, C9, was found to express *CCL20*, *IL23R*, *RORC* and *KLRB1* (encoding CD161), suggesting the identification of CD8+ MAIT cells or, alternatively, CD4+ $T_H17$. Overall, scRNA-seq revealed significant increased abundance of CD4+ Tregs in tumoral compared to peritumoral tissues (**Figure 22C**), in line with results obtained by flow cytometry. We further identified differences in T-cell gene expression between these two tissue sites. Notably, C4 $T_{RM}$ and C7 effector subsets from tumors upregulated exhaustion markers such as *HAVCR2* and *CTLA4* (only C7) and downregulated effector/killer molecules compared to those from peritumor (**Figure 23A**), suggesting T cell dysfunction at the tumor site.

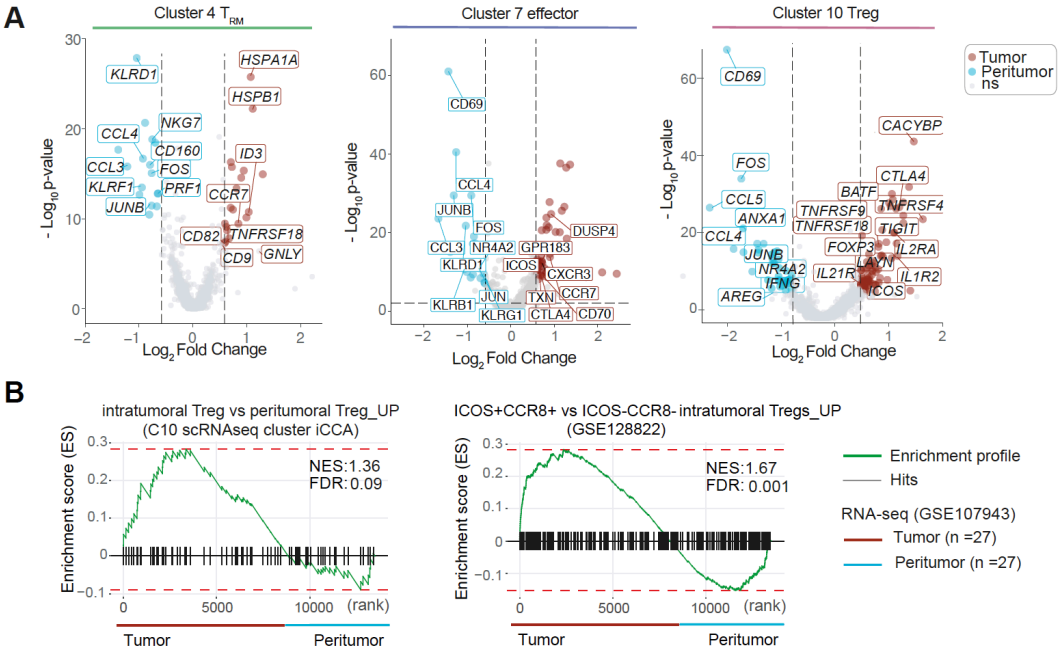

**Figure 23: Tumor driven expression patterns. A.** Volcano plot showing differentially expressed genes between tumoral (dark red) and peritumoral (light blue) cells from scRNA-seq C4 ($T_{RM}$), C7 (effector) and C10 (Tregs); (q-value<0.01; |FC|>1.5) **B.** GSEA of different gene set in bulk RNAseq (GSE107943) consisting of 27 paired iCCA and peritumoral samples.

*Figure 23*

Concerning Tregs, those from tumors upregulated activation markers such as *TNFRSF9*, *TNFRSF4, TIGIT*, *LAYN, ICOS* and *ENTPD1*, among others (**Figure 23A**). This iCCA-infiltrating Treg gene signature was significantly enriched in an independent dataset of bulk RNA-seq consisting of 27 paired iCCA and peritumoral samples (**Figure 23B**; Sia et al., 2013). Similar data were obtained with our abovementioned (Results part 1) gene signature obtained by comparing highly immunosuppressive ICOS+ CCR8+ Tregs vs. more quiescent ICOS-CCR8- Tregs infiltrating NSCLC.
Overall, these data suggest functional modulation of the iCCA T-cell infiltrate, with increased activation of Tregs and reduced functional capacity of putative tumor-specific *ENTPD1*$^{high}$ $T_{RM}$ cells and effector T cells.

### 4.2.3. Transcriptional network inference to understand the molecular basis of diminished effector T cell activation and enhanced Treg activation in iCCA.

In order to identify master transcriptional regulators that are critical for cell identity in tumors, we applied SCENIC, a computational pipeline able to predict TF activity by the analysis of TF motifs that are enriched at the promoters of expressed genes in our scRNA-seq data (Aibar et al., 2017). SCENIC analysis clearly separated tumoral and peritumoral T cells (**Figure 24A**), thus indicating that tissue-derived T-cell states can be described by their inferred TF activity.

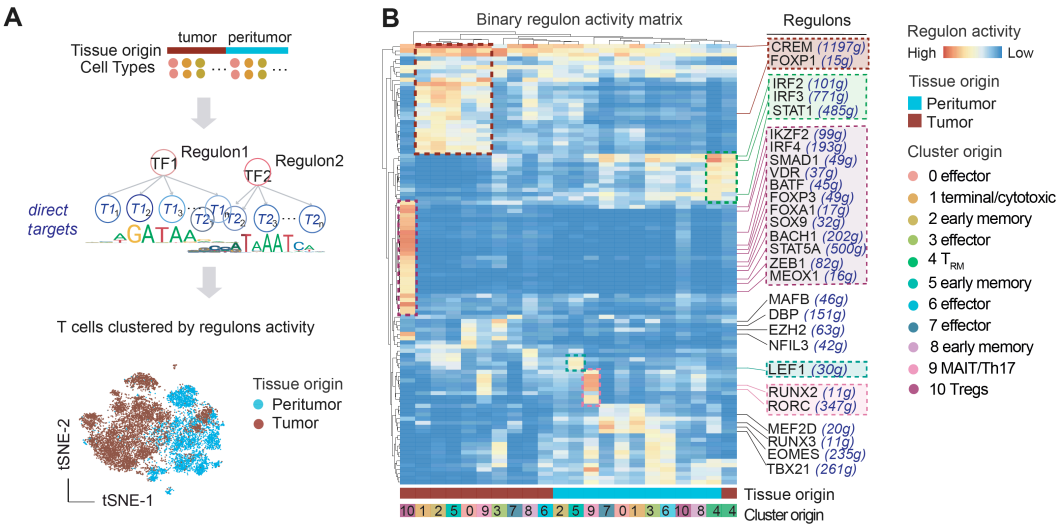


**Figure 24: Transcriptional network inference of iCCA-infiltrating T cells. A.** *Top:* Schematic overview of the single-cell regulatory network inference and clustering (SCENIC) pipeline: *Bottom:* t-SNE map for all T cells based on regulon activity scores. Each T cell is color-coded based on tissue origin: tumor (darkred) and peritumor (light blue). **B.** Heatmap of binary (threshold = 0.5) TF activity by scRNAseq T cell clusters related to peritumoral (light blue) and tumoral (darkred) tissues. TF of interest are indicated. The putative number of genes regulated by TF and expressed by the specific cluster is indicated between brackets (blue).
*Figure 24*

Among others, we found that IRF2, IRF3 and STAT1-mediated transcriptional activities, possibly dependent on type I interferon signaling and involved in promoting effector functional capacity (Huber et al., 2011) were reduced in tumoral vs. peritumoral T cell clusters, especially in C3, C6 and C7 of effector cells and, at a lesser extent, in C4 of $T_{RM}$ cells (**Figure 24B**). C7 along with C1 of terminal/cytotoxic T cells from tumors vs. peritumors also showed reduced transcriptional activities of RUNX3, EOMES and TBX21 TFs, which mediate the expression of effector and cytotoxic molecules (Cruz et al., 2009). Altogether, these data suggest loss of $T_{RM}$ and effector T-cell functionality in iCCA. By contrast, tumor-infiltrating Tregs displayed increased activity of several TFs compared to those infiltrating the peritumor, including IRF4 and its transcriptional partner BATF, that we previoulsy reported to play a pivotal role in Treg enhanced immunosuppressive capacity in tumors (Results part 1). We also found FOXP3, the lineage-specification factor for Treg cells, IKZF2, linked to stability of the Treg lineage (Getnet et al., 2010) STAT5A and SMAD1, possibly reflecting IL-2 and TGFβ signaling, respectively, FOXA1, linked to enhanced suppressive function (Liu et al., 2014), and several others, such as VDR, SOX9, ZEB1 and Mesenchyme Homeobox 1 (MEOX1), whose functions in Treg biology remain unknown.

We further ordered TF activities in pseudotime by using a dedicated algorithm, i.e., SCORPIUS (Saelens et al. 2019), so to possibly identify specific patterns of their activation or repression during Treg adaptation from peritumor to tumor. In line with data at the level of single genes, SCORPIUS was able to clearly separate Tregs from the two different sites (**Figure 25A**), and identified domains of activity, suggesting that different TFs might be involved at different steps of effector Treg differentiation and activation in iCCA.

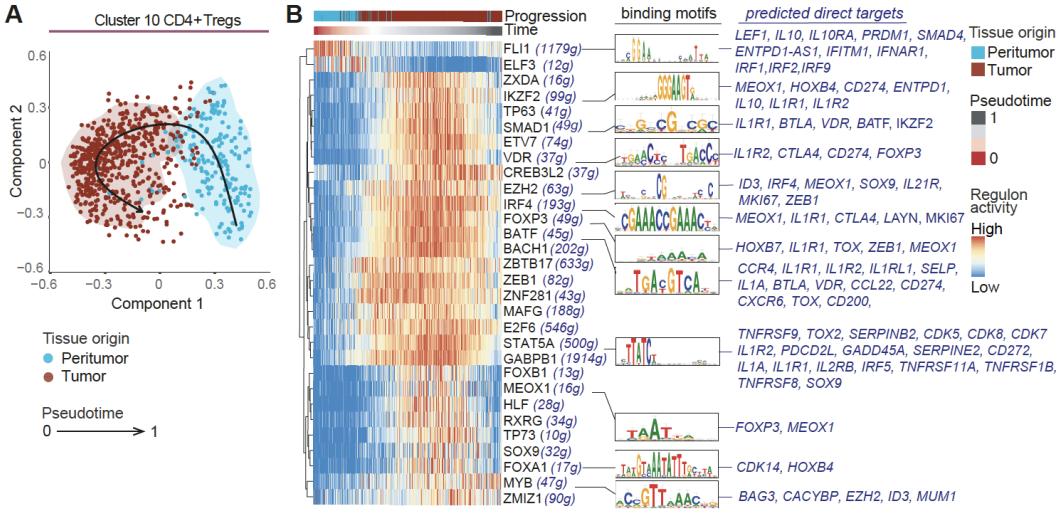


**Figure 25: Treg heterogeneity and tissue adaptation. A.** Zoom-in view of the cluster 10 ($CD4^+$ Treg). Treg cells are distributed in a trajectory map by SCORPIUS according to regulon activity scores and color-coded based on tissue origin: tumor (darkred) and peritumor (light blue). **B.** Pseudo-time alignment of Treg cells determined by SCORPIUS trajectory analysis based on regulons activity. The top 30 TF leading the time line are represented along with their corresponding binding motifs and their (manually selected) predicted targets (dark blue).
*Figure 25*

Specifically, loss of activity of FLI1, recently shown to inhibit effector CD8+ T cell differentiation in murine models of chronic infection and cancer (Chen et al., 2021) was accompanied by increased activity of several TFs simultaneously, *e.g.*, of IKZF2, SMAD1, VDR, IRF4, FOXP3 and BATF, during transition from peritumors to tumors (**Figure 25B**). Several of these TFs are known to be upregulated, or to play a direct role in the enhanced immunosuppression of Tregs in solid tumors. We also revealed increased activity related to enhancer of zeste homolog 2 (EZH2), a histone $H_3K_{27}$ methyltransferase elevated in tumor-infiltrating Tregs and whose pharmacological inhibition results in proinflammatory Treg reprogramming and enhanced anti-tumor immunity (Goswami et al., 2018; Wang et al., 2018). A second group of TFs, including MEOX1, TP73 (encoding p73),

SOX9 and FOXA1, among others, was activated in Tregs in iCCA, and was later followed by enhanced ZMIZ1 and MYB activities, the latter reported to regulate effector Treg differentiation in murine peripheral organs (Dias et al., 2017). Collectively, our analysis identified novel TF activities possibly related to effector Treg differentiation and activation in iCCA.

### 4.2.4. MEOX1 transcriptionally and epigenetically reprograms circulating Tregs to a tumor-infiltrating phenotype.

We next focused on one hit from SCENIC analysis of intratumoral Tregs, *i.e.*, MEOX1, whose role in the immune system in undetermined. MEOX1 encodes a mesodermal TF that plays a key role in somitogenesis and sclerotome development and whose mutation in humans results in the incomplete development of bones in the neck (also known as Klippel-Feil syndrome; Mohamed et al. 2013). In our scRNA-seq dataset, MEOX1 expression could be detected only in tumor-infiltrating Tregs, and not in other T cells (**Figure 26 A** and **B**).

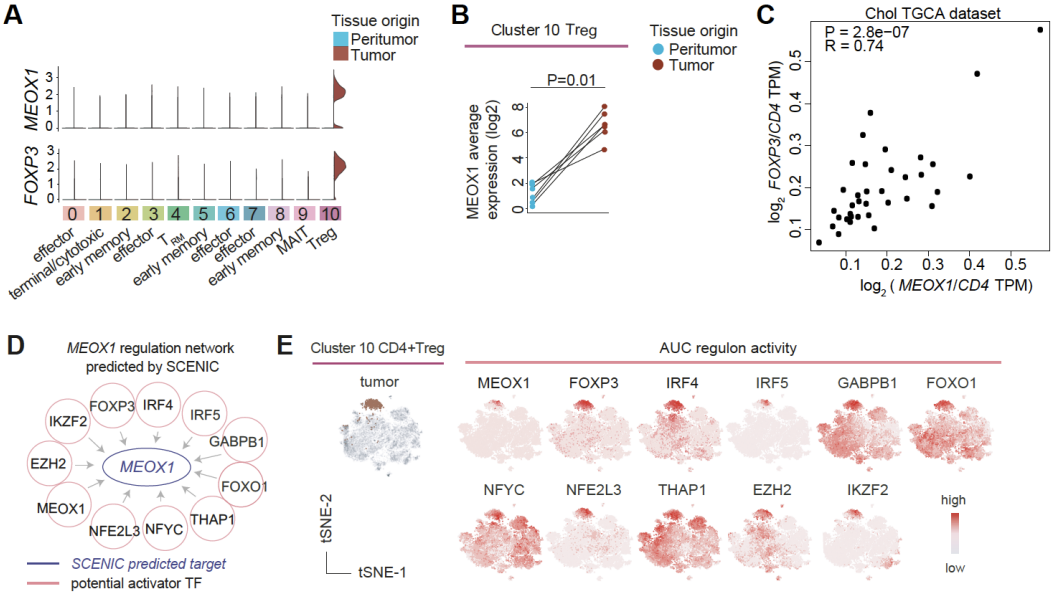


**Figure 26: Tregs infiltrating iCCA upregulate MEOX1. A.** Imputed expression levels of MEOX1 and FOXP3 among single-cell RNA-seq T cell clusters. Violin plot's colours denote tissue of origin: tumoral and peritumoral. **B.** Dot plot depicting the average expression level of MEOX1 among tumoral and peritumoral Tregs samples. Dots depict values of single patients. **C.** Pair-wise correlation between MEOX1 and FOXP3 expression in the The Cancer Genoma Atlas (TGCA) cholangiocarcinoma (Chol) dataset (n=36), as from Gene Expression Profiling Interactive Analysis (GEPIA2). MEOX1 and FOXP3 expression have been normalized by CD4 expression. P: p-value; R: Pearson correlation coefficient. **D.** MEOX1 regulation network predicted by SCENIC. **E.** t-SNE map of all T cells depicting Tregs from tumors (scRNAseq cluster 10) and regulons predicted to activate MEOX1.

*Figure 26*

Moreover, *MEOX1* mRNA levels strongly correlated with those of *FOXP3* in a larger cholangiocarcinoma dataset from the cancer genome atlas (TCGA; **Figure 26 C**), confirming a relationship with Tregs in tumors. By analyzing the MEOX1 promoter, we found binding motifs of FOXP3, IRF4, FOXO1, EZH2 and IKZF2 TFs, among others (**Figure 26 D**). Moreover, the predicted activity of these TFs was co-regulated with that of MEOX1 in a subset of hyperactivated iCCA-infiltrating Tregs (**Figure 26 D**), collectively suggesting a role in the regulation of MEOX1 expression.

To investigate the functional relevance of MEOX1 in specifying the molecular characteristics of tumor-infiltrating Tregs, we isolated peripheral blood CD4+ Tregs from healthy donors, activated them for 24 hours with anti-CD3/CD28 + IL-2 and transduced them with a lentivirus capable of overexpressing the full-length MEOX1 cDNA, or with a mock lentivirus control. (**Figure 27A**). Transduced cells, identified by GFP reporter, were further purified as CD127–CD25+ by fluorescence-activated cell sorting (FACS) and analysed at the transcriptomic and chromatin accessibility level by bulk RNA-seq and assay for transposase-accessible chromatin using sequencing (ATAC-seq), respectively (**Figure 27B**).

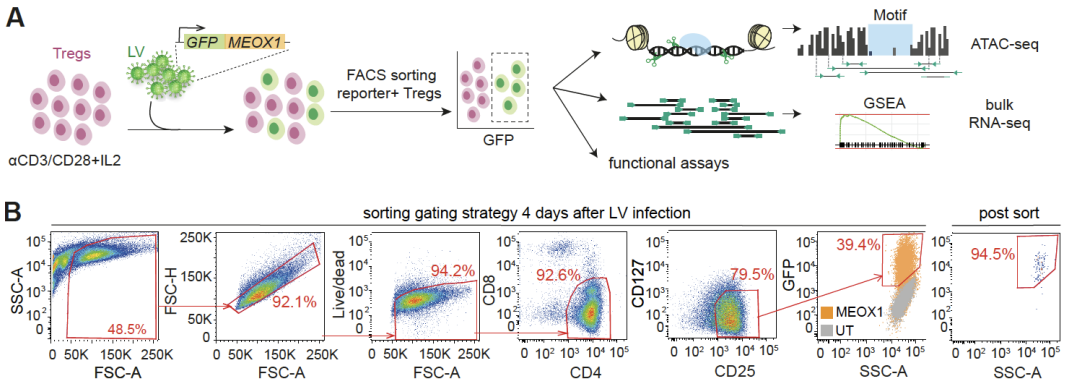


**Figure 27. Mechanistic evaluation of MEOX1 function A.** Schematic view of the MEOX1 overexpression (OE) approach by Lentiviral (LV) vector in Tregs isolated from the peripheral blood of healthy donors (n=3). ATAC-seq: Assay for Transposase-Accessible Chromatin using sequencing; bulk RNA-seq: bulk transcriptome sequencing. GSEA: Gene Set Enrichment Analysis. **B.** Representative gating strategy applied to isolate live Tregs (CD4+ CD25+ CD127low GFP+) 4 days after lentiviral infection. Untransduced cells (UT) were use as a fluorescence minus one (FMO) control. Numbers indicate percentages of cells in the drawn gates.

*Figure 27*

At the chromatin level, we found that genes previously shown to be overexpressed by Tregs in tumors and associated with effector

differentiation (*TNFRSF9*, *IL1RN*) and with disease progression in multiple cancers (*LAYN*) (De Simone et al., 2016) or responsible for IL-10 production by Tregs (*PRDM1*) (Cretney et al., 2011) among others, were more accessible at multiple genomic sites in MEOX1-transduced vs. mock-transduced Tregs (**Figure 28A**).

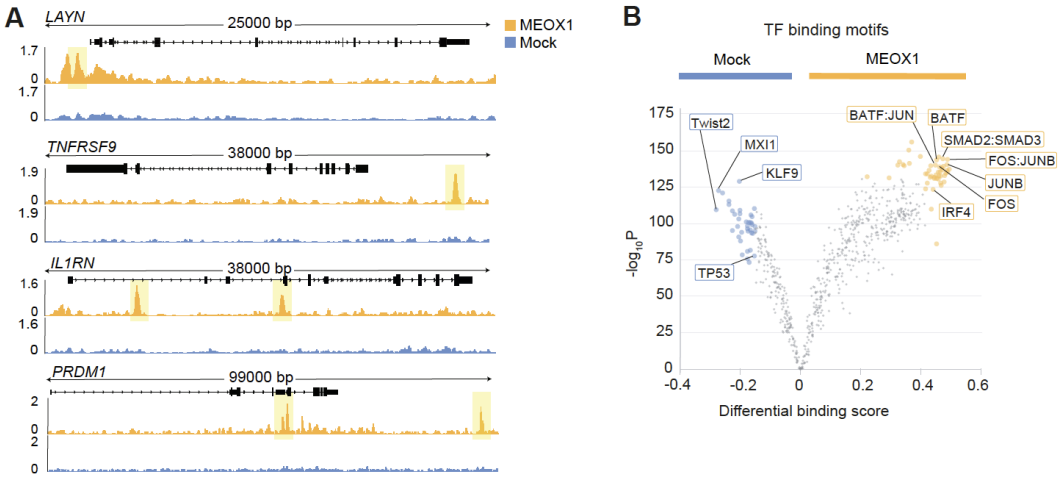


**Figure 28: Epigenetic analysis of MEOX1-overexpressing Treg cells. A.** Representative accessible genomic regions in ATAC-seq data from mock- (CTRL, cornflower blue) or MEOX1-transduced (orange) Treg cells (n=3) from A. Significant differentially accessible regions (DARs) are highlighted in yellow. **B.** TFBM enrichment analysis by TOBIAS (Transcription factor Occupancy prediction By Investigation of ATAC-seq Signal). Each coloured dot represents one significant motif. TF of interest are labelled.
*Figure 28*

Computational analysis of differentially accessible regions in the whole ATAC-seq dataset further identified differentially accessible TFBMs. Motifs attributable to AP-1 (FOS, JUNB and the combined FOS:JUNB motif), to AP-1 transcriptional partners (BATF, IRF4 and the combined BATF:JUN motifs, mechanistically linked to hyperactivated Tregs in tumors; Results part 1) and the SMAD2:SMAD3 combined motif, reflecting increased accessibility of genes possibly controlled by TGFβ signaling, were enriched in MEOX1-transduced Tregs, whereas motifs attributable to TWIST2, MXI1, KLF9 and TP53 were enriched in mock-transduced Tregs (**Figure 28 B**).

In agreement with ATAC-seq results, overexpression of MEOX1 upregulated the effector Treg-related genes *TNFRSF9*, *IL1RN*, *LAYN*, *CD70*, *MAGEH1, ICOS, NRP1* (encoding Neuropilin-1), *IL10* and *CTLA4* (**Figure 29A**).

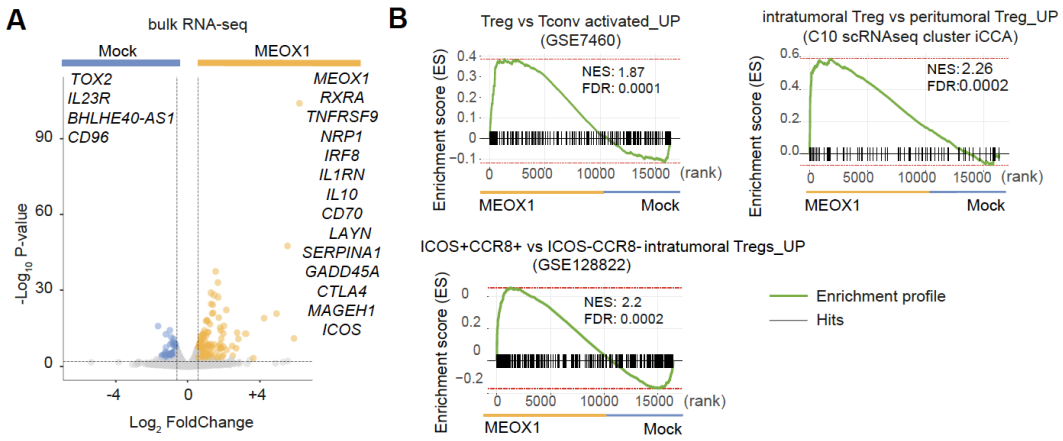


**Figure 29: MEOX1 promotes a tumor-specific Treg signature. A.** Volcano plot of DEGs in bulk RNA-seq from MEOX1-transduced (orange) Treg cells compared to mock-transduced (CTRL, cornflower blue) Treg cells from A (q-value< 0.05, |FC|> 1.5, n=3). Relevant genes are indicated. E. GSEA of different gene set in bulk RNA-seq data obtained as in A.
*Figure 29*

By gene set enrichment analysis (**Figure 29B**), MEOX1-overexpressing Tregs were strongly enriched in specific transcriptomic signatures of Treg vs. CD4+ Tconv (public available data GSE7460), of iCCA vs. peritumor-infiltrating Tregs (data from **Figure 24A**), or of ICOS+CCR8+ vs. ICOS-CCR8- Tregs (data from **Figure 9B,** results part 1). Thus, MEOX1 promotes the acquisition of a tumor-infiltrating Treg phenotype by reprogramming the transcriptional and epigenetic landscape of circulating Tregs.

### 4.2.5. Suppressive potential and prognostic significance of MEOX1-expressing Tregs.

We next investigated the functional role of MEOX1 in Tregs. Circulating Tregs overexpressing MEOX1 tended to be more efficient than mock-transduced Tregs at inhibiting proliferation (assessed by CTV dilution) and activation (CD25 expression) of CD4+ Tconv activated with anti-CD3/28 in vitro, especially at a Tconv:Treg ratio of 4:1 (**Figure 30**, **A** and **B**).

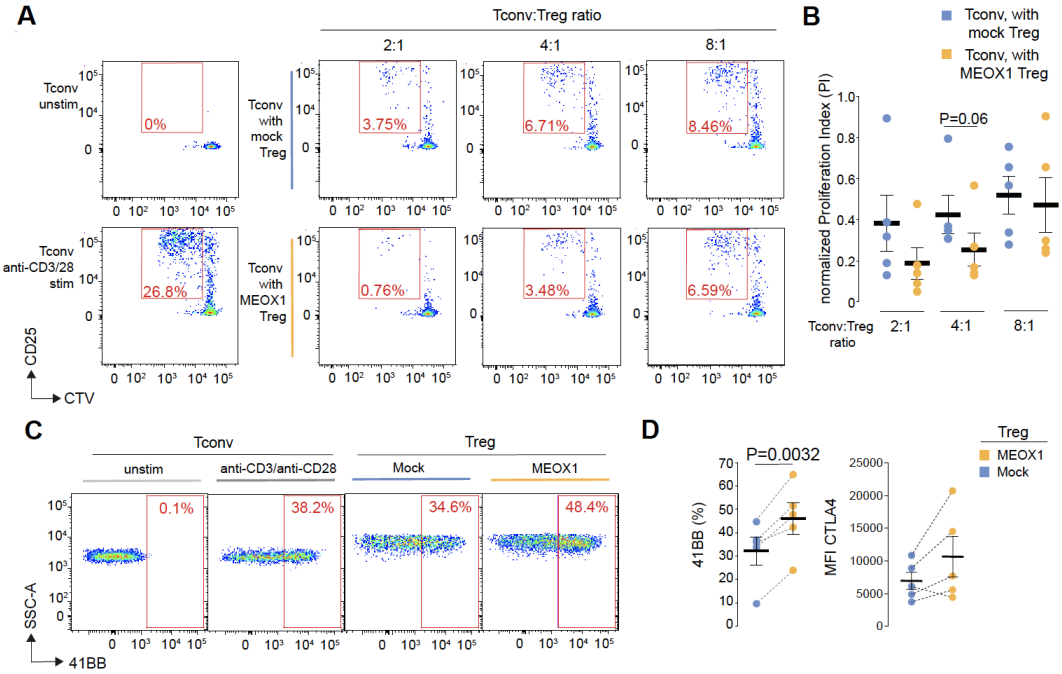


**Figure 30: MEOX1 mediate enhanced suppressive activity and 41BB upregulation in Tregs. A.** Suppressive capacity of MEOX1 and mock-transduced Tregs on Tconv. Numbers: percentage of proliferating cells. **B.** Summary of the proliferation index (PI; mean ± SEM, n=5), normalized by the PI of Tconv without Tregs. Representative 41BB expression after 16h stimulation with Dynabeads. Unstimulated Tconv: staining control. **C.** Summary of 41BB and CTLA4 expression (mean ± SEM; n=5 independent experiments) by MEOX1 and mock-transduced Tregs. Paired t-test.

*Figure 30*

MEOX1 overexpression also resulted in increased surface levels of 41BB and, at a lesser extent, CTLA4 following TCR re-stimulation of Tregs at day 4 after transduction (**Figure 30**, **C** and **D**). These data confirmed at the protein level our previous transcriptomic data showing *TNFRSF9* and *CTLA4* as MEOX1 targets.

Considering the negative prognostic impact of these and other Treg related genes in multiple cancers (De Simone et al., 2016; Plitas et al., 2016; Alvisi et al., 2020), we tested whether the gene program induced by MEOX1 in Tregs could specifically influence iCCA disease progression as determined by signature enrichment in 147 treatment-naïve tumors previously characterized by bulk RNA-seq (Dong et al., 2022).

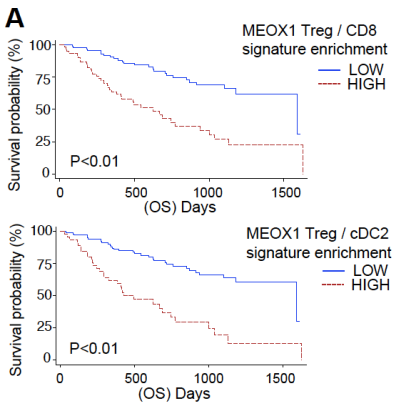


**B**

| Multivariate analysis | Haz. Ratio | Std. Err | z | P>\|z\| | [95% Conf. | Interval] |
|---|---|---|---|---|---|---|
| intrahepatic metastasis | 1.88 | 0.51 | 2.32 | 0.021* | 1.1 | 3.21 |
| tumor size diameter (cm) | 0.67 | 0.21 | -1.3 | 0.194 | 0.37 | 1.22 |
| vascular invasion | 1.56 | 0.48 | 1.44 | 0.15 | 0.85 | 2.86 |
| regional lymph node metastasis | 2.75 | 0.83 | 3.35 | 0.001* | 1.52 | 4.99 |
| distal metastasis | 2.5 | 1.07 | 2.16 | 0.031 | 1.08 | 5.80 |
| perineural invasion | 1.18 | 0.37 | 0.53 | 0.59 | 0.63 | 2.21 |
| carbohydrate antigen19-9 (Ca 19-9, U/ml) | 2.25 | 0.76 | 2.40 | 0.016 | 1.16 | 4.37 |
| MEOX1 Treg /CD8 signature enrichment | 2.14 | 0.71 | 2.3 | 0.022* | 1.12 | 4.11 |
| MEOX1 Treg/cDC2 signature enrichment | 1.97 | 0.67 | 2.01 | 0.045* | 1.01 | 3.82 |

**Figure 31: Prognostic significance of MEOX1-expressing Tregs. A.** Kaplan-Meier OS curves (n=147). **B.** Multivariate cox-regression analysis considering clinicopathological factors that were associated with OS in univariate analysis.
*Figure 31*

When related to the content of CD8+ T cells, which is generally associated with favorable prognosis, a higher MEOX1-dependent gene program was significantly associated with worse OS, both in univariate (**Figure 31A**) and in multivariate analysis after correction for co-varying factors such as the presence of intrahepatic metastasis, regional lymph node metastasis and vascular invasion (**Figure 31B**). We obtained very similar results when relating the MEOX1-dependent gene program to a conventional type 2 dendritic cell (cDC2) signature, in accordance with recent data showing Treg-dependent inhibition of cDC2 activity and tumor immunosuppression in other cancers (Binnewies et al., 2019). Of note, MEOX1 per se was not predictive of disease progression, probably because of its expression by adipocytes and endothelial cells, as assed by in silico analysis with the Human Protein Atlas (data not shown).

Overall, our data identify MEOX1-dependent Treg signature in the iCCA microenvironment whose perturbation might favor anti-tumor immune responses.

# 5. Discussion

Human tumors are abundantly infiltrated by CD4+ Tregs that display an activated phenotype and enhanced suppressive capacity compared to those present in the peripheral blood and in the adjacent tumor-free tissues (De Simone et al., 2016; Plitas et al., 2016). Our study shows that the TF IRF4 drives the transcriptional program associated with such activation and suppression in the TME.

IRF4 was previously linked to effector Treg differentiation in murine tissues in physiology (Cretney et al., 2011). Our study deepens what is known about IRF4 biology in human Tregs by describing IRF4 expression in the tumor, cancer-free tissue and peripheral blood samples from a broad population of patients with cancer and by providing a comprehensive examination of the suppressive program of IRF4-expressing Tregs.

IRF4 controls gene expression of tumor-infiltrating Tregs both directly, by binding gene promoters or distal regulatory regions, and indirectly, by inducing the expression of additional transcriptional regulators such as *IKZF2* (Helios), required for Treg stability (Kim et al., 2015). IRF4 binding to DNA is increased when it is part of a macromolecular complex involving AP-1 family members BATF, JUN, JUNB or JUND, recognizing AICEs DNA motifs. In relation to this, *Junb* has recently been shown to control murine effector Treg differentiation in lung and colon (Koizumi et al., 2018) while additional TFs, such as STAT3, may physically interact with c-JUN (Schaefer et al., 1993). *STAT3* mRNA is upregulated and the STAT3 binding motif is enriched in IRF4+ vs. IRF4- Tregs, indicating that complex molecular interactions cooperate to shape the effector differentiation and enhanced suppressive activity of Tregs residing in the TME. By studying iCCA infiltrating Tregs, we found increased activity of different TFs compared to Tregs infiltrating the peritumor, including IRF4/BATF and AP1 family members, but also other TFs whose functional role in Treg biology remains to be established. Among these, we found MEOX1, whose overexpression was sufficient to reprogram circulating Tregs to acquire a transcriptional and epigenetic landscape that is highly reminiscent of tumor-infiltrating Tregs, and to induce 4-1BB and CTLA4 expression, which previously associated with worse survival outcomes in patients with multiple tumor types. The employment in our study of circulating Tregs activated in

vitro to assess MEOX1 function for feasibility reasons could represent a limitation, as these cells might reflect only in part the molecular landscape of tumor-infiltrating Tregs. This experimental strategy could explain the only modest increase in the ability to suppress Tconv proliferation when MEOX1 is ectopically overexpressed. Nevertheless, the gene program downstream of MEOX1 strongly correlated with worse OS specifically in iCCA, suggesting that additional signals in the tumor microenvironment are required to shape and further sustain the inhibitory potential of Tregs. The mechanism by which MEOX1 is induced and operates in hyperactivated Tregs is still undefined. MEOX1 is triggered by TGFβ signaling in non-immune cells such as cardiac fibroblasts (Alexanian et al., 2021), and mediates cell differentiation by direct binding to DNA. Although these aspects were not tested directly on intratumoral Tregs, pseudotemporal ordering of TF activities suggests a model according to which IRF4 and BATF precede MEOX1 activity, which in turn sustains hyperactivated Treg gene expression by favoring chromatin accessibility at AP-1/IRF4/BATF consensus sites. The current study lacks a proper investigation on the possible physical interaction between MEOX1 and AP-1/IRF4/BATF element. Rapid immunoprecipitation mass spectrometry of endogenous protein (RIME; Mohammed et al., 2016) would be applied to address this point. Additionally, the definition of MEOX1 and IRF4 consensus sequence on the DNA by Motif Analysis of Large Nucleotide Datasets (MEME)-ChIP would determine the presence of sequences known to be bound by other TFs and thus find alternative DNA-binding partners.

Our study reveals a futher important aspect, namely that effector differentiation is not a feature of all intratumoral Tregs (**Figure 32**). Rather, a subset of these cells defined by IRF4 and MEOX1 expression is characterized by high amounts of molecules associated with enhanced immunosuppression, have increased metabolic demand and are phenotypically and transcriptionally distinct when compared to the more quiescent IRF4-/MEOX1- Tregs.

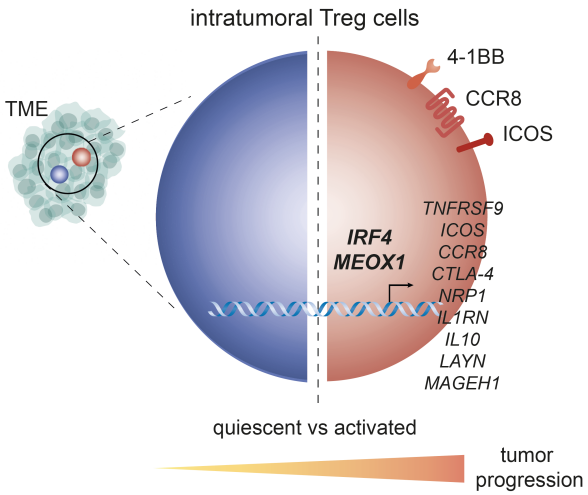


**Figure 32. IRF4 and MEOX1 define a subset of hyperactivated intratumoral Treg cells.** High-dimensional single-cell profiling of T cells from chemotherapy-naive cancer patients identified the TF IRF4 as specifically expressed by a subset of intratumoral eTregs with superior suppressive activity. In contrast to the IRF4- (CCR8-ICOS-) counterparts, IRF4+ (CCR8+ICOS+) Tregs expressed a vast array of suppressive molecules (ie. *TNFRSF9*, *CTLA-4*, *IL10* etc), and their presence correlated with poor prognosis. By gene set enrichment analysis, MEOX1-overexpressing Tregs were strongly enriched in the transcriptomic signature of ICOS+ CCR8+ vs. ICOS– CCR8– Tregs, suggesting functional cooperation between IRF4 and MEOX1.

The abundance of the IRF4+, but not of the IRF4- Tregs correlated with multiple exhausted T cell clusters and disease progression when dividing patients according to the pathological stage of the disease (pStage; I vs. II/III). Moreover, patients with highly glycolytic tumors (those with high SUVmax values as obtained from PET scan of lesions at diagnosis) had a different T cell profile as a whole, featuring increase in IRF4+ Tregs and activated, exhausted T cells, and decrease in Th1-like effectors and Tfh cells. This is consistent with the fact that tumor prefers quick yet less efficient energy supply from glycolysis over OXPHOS and puts effector T cells in a hyporesponsive state (MacIver NJ et al., 2013). While effector T cells suffer in this harsh landscape, Tregs grow largely due to their adaptations for utilizing fatty acids and lactate. Indeed, Foxp3 suppresses c-Myc expression, thus limits glucose uptake and glycolysis of Tregs while promoting OXPHOS (Angelin A. et al., 2017). Accordingly, our bulk RNAseq on intratumoral Tregs reveals that ICOS+CCR8+ displayed enhanced metabolic activity, preferentially characterized by a signature of oxidative phosphorylation and glycolysis, Myc targets and reactive oxygen species metabolism (likely resulting from enhanced activation and/or mitochondrial respiration; Pilipow et al., 2018).

Although the present study was focused on tumor infiltrating T cells, we also characterized the heterogeneity of myeloid compartment in the iCCA tumor microenvironment and its possible relationship with hyperactivated

Treg. Specifically, we profiled iCCA samples, peritumoral and blood samples with with 2 high-dimensional flow cytometry panels encompassing markers of T-cell differentiation, as well as markers related to subsets of myeloid cells. As far as myeloid cells were concerned, tumors were preferentially infiltrated compared to other tissues by CD11b+ CD11c+ HLA-DR CD1c+ cDC2 cells and by CD11b– CD9+ cells. scRNA-seq further informed on the characteristics of the different immune cell types, recapitulating what we found with facs analysis although at a different level of resolution. When we investigated whether a different immune landscape could influence disease progression we found that the relative abundance of single clusters alone was not informative in this regard (data now shown). Combinatorial analysis of cluster abundance defined that the enrichment of Tregs as relative to that of cDC2 were highly associated with overall survival. Specifically, worse prognosis was associated with high MEOX1+ Tregs infiltration over low cDC2 infiltration, as defined by signature enrichment in treatment-naïve iCCA samples previously characterized by bulk RNA-seq (Dong et al., 2022). Interestingly, a recent report mechanistically related Treg-dependent inhibition of cDC2 activity with tumor immunosuppression using preclinical models (Binnewies et al., 2019). Accordingly, the relative abundance of these two cell types was associated with disease progression of head and neck squamous cell carcinoma and response of melanoma to checkpoint blockade (Binnewies et al., 2019), thus suggesting that a common axis might regulate anti-tumor immunity in different cancer types. This hypothesis is further corroborated by the fact that Tregs from lung, ovarian and breast tumors significantly overexpressed MEOX1 compared to conventional CD4+ T cells (Alvisi et al., 2022). Further spatial transcriptomic analyses are warranted to comprehensively characterize tissue organization and architecture at the single-cell and thus inform about the spatial co-locatization of Tregs subsets and possible myeloid interactors. Our results indicate that tumor infiltrating Tregs are characterized by extensive remodeling of the expression of receptor-ligand pairs required for cell-cell communication, suggestive of enhanced Treg-mediated immunosuppression in the iCCA microenvironment. Tregs are predicted to engage multiple inhibitory pathways on T and myeloid cells in the tumor microenvironment, while

receiving signals that in turn may support their hyperactivated phenotype, thereby offering novel, more specific targets for cancer immunotherapy. In agreement with the Treg-mediated inhibition, in several iCCA-infiltrating Tcell subsets we observed reduced activity of TFs promoting the cytotoxic program and effector function of T cells, including RUNX3, EOMES and TBX21 (encoding T-bet) activities.

Overall, our results indicate that combined analysis involving flow cytometry and next-generation sequencing can identify those subsets specifically associated with tumor growth and anti-tumor responses with enhanced precision. The simple addition of an effector Treg marker (*e.g.*, IRF4, ICOS or CCR8 or a TNFR superfamily member) to FoxP3 staining, as done by immunohistochemistry in immunoscore approaches (Cavalleri et al., 2019), may improve the definition of patients with improved prognosis. Moreover, the identification of a molecular program leading the differentiation of those Tregs with enhanced suppressive capacity offers novel opportunities to reverse immunosuppression while favoring anti-tumor immune responses. Depletion of Tregs has been tested in a number of preclinical approaches to promote anti-tumor response (Wei et al. 2005; Dannull et al., 2005; Colombo et al., 2007; Luo et al., 2016), however novel strategies interfering selectively with the activated, effector Treg state are emerging as a promising tool to boost effective anti-tumor immunity without resulting in overt autoimmunity due to the loss of peripheral tolerance. Targeting those signals leading to IRF4 activation, or downstream IRF4-dependent Treg activation seems an attractive approach to consider in this regard. As a proof of concept, Kidani et al. (2022), recently proved that administration of cell-depleting anti-CCR8 mAb selectively depletes tumor Treg, leading to tumor regression in mice. The treatment induced expansion of activated but not exhausted CD8+ and CD4+ Tconvs, as well as the up-regulation of CD80/CD86 expression on APC, leading to the development of tumor-antigen specific effector/memory CD8+ T cells. Despite induction of such potent antitumor-immunity, the treatment elicited minimal autoimmunity in mice, even when combined with anti PD-1 mAb treatment. These results suggest that the combination of CCR8-targeted selective Treg depletion and immune checkpoint blockade would prevent Treg dependent HPD occasionally observed in the course of anti-PD1 treatment (S.Champiat et al., 2018;

C.Tay et al., 2020). This approach may be widely applicable, as our data show that IRF4-driven effector Treg differentiation is common to different tumor types, *i.e.*, lung cancer, melanoma, hepatocellular carcinoma and cholagiocarcinoma. Although differences that are yet to be identified might be present according to the specific tumor type, our data suggest that intratumoral Tregs share a core transcriptional and functional program, characterized by the increased expression of inhibitory molecules, chronic immune activation and enhanced suppressive capacity, compared to those from the circulation or the peritumoral area. Accordingly, Mair et al. (2022) recently identified an intratumoral clonally expanded Treg population reminiscent of our IRF4+ (CCR8+ICOS+) Treg population by profiing the immune landscape of human head and squamous cell carcinoma (HNSCC) and matched, non malignant, inflamed oral mucosal tissue. This population is defined by the expression of two direct targets of IRF4, namely IL-1R1 and ICOS, and is characterized by a transcriptional signature consistent with recent TCR engagement.

To conclude, our results provide a detailed and comprehensive molecular characterization of the tumor-infiltrating Tregs with enhanced suppressive activity and reveal those molecular patterns that could be targeted by novel cancer immunotherapy approaches, thus are of immediate translational impact. Although focusing on lung cancer and cholangiocarcinoma, we also show that IRF4 and MEOX1 driven effector Treg differentiation is common to different cancers. Thus, interfering with the IRF4/MEOX1 pathway or their downstream targets is an interesting therapeutic strategy that is widely applicable and can specifically target the most suppressive Tregs in the TME.

# 6. References


Abbas, A. K., Benoist, C., Bluestone, J. A., Campbell, D. J., Ghosh, S., Hori, S., Jiang, S., Kuchroo, V. K., Mathis, D., Roncarolo, M. G., Rudensky, A., Sakaguchi, S., Shevach, E. M., Vignali, D. A. A., & Ziegler, S. F. (2013). Regulatory T cells: recommendations to simplify the nomenclature. Nature Immunology, 14(4), 307–308. https://doi.org/10.1038/ni.2554

Ahmadzadeh, M., Pasetto, A., Jia, L., Deniger, D. C., Stevanović, S., Robbins, P. F., & Rosenberg, S. A. (2019). Tumor-infiltrating human CD4 + regulatory T cells display a distinct TCR repertoire and exhibit tumor and neoantigen reactivity. Science Immunology, 4(31). https://doi.org/10.1126/sciimmunol.aao4310

Aibar, S., González-Blas, C. B., Moerman, T., Huynh-Thu, V. A., Imrichova, H., Hulselmans, G., Rambow, F., Marine, J.-C., Geurts, P., Aerts, J., van den Oord, J., Atak, Z. K., Wouters, J., & Aerts, S. (2017a). SCENIC: single-cell regulatory network inference and clustering. Nature Methods, 14(11), 1083–1086. https://doi.org/10.1038/nmeth.4463

Alexanian, M., Przytycki, P. F., Micheletti, R., Padmanabhan, A., Ye, L., Travers, J. G., Gonzalez-Teran, B., Silva, A. C., Duan, Q., Ranade, S. S., Felix, F., Linares-Saldana, R., Li, L., Lee, C. Y., Sadagopan, N., Pelonero, A., Huang, Y., Andreoletti, G., Jain, R., … Srivastava, D. (2021). A transcriptional switch governs fibroblast activation in heart disease. Nature, 595(7867), 438–443. https://doi.org/10.1038/s41586-021-03674-1

Alvisi, G., Brummelman, J., Puccio, S., Mazza, E. M. C., Tomada, E. P., Losurdo, A., Zanon, V., Peano, C., Colombo, F. S., Scarpa, A., Alloisio, M., Vasanthakumar, A., Roychoudhuri, R., Kallikourdis, M., Pagani, M., Lopci, E., Novellis, P., Blume, J., Kallies, A., … Lugli, E. (2020). IRF4 instructs effector Treg differentiation and immune suppression in human cancer. The Journal of Clinical Investigation, 130(6), 3137–3150. https://doi.org/10.1172/JCI130426

Angelin, A., Gil-de-Gómez, L., Dahiya, S., Jiao, J., Guo, L., Levine, M. H., Wang, Z., Quinn, W. J., Kopinski, P. K., Wang, L., Akimova, T., Liu, Y., Bhatti, T. R., Han, R., Laskin, B. L., Baur, J. A., Blair, I. A., Wallace, D. C., Hancock, W. W., & Beier, U. H. (2017). Foxp3 Reprograms T Cell Metabolism to Function in Low-Glucose, High-Lactate Environments. *Cell Metabolism*, *25*(6), 1282-1293.e7. https://doi.org/10.1016/j.cmet.2016.12.018

Aran, D., Looney, A. P., Liu, L., Wu, E., Fong, V., Hsu, A., Chak, S., Naikawadi, R. P., Wolters, P. J., Abate, A. R., Butte, A. J., & Bhattacharya, M. (2019). Reference-based analysis of lung single-cell sequencing reveals a transitional profibrotic macrophage. Nature Immunology, 20(2), 163–172. https://doi.org/10.1038/s41590-018-0276-y

Attia, P., Maker, A. v, Haworth, L. R., Rogers-Freezer, L., & Rosenberg, S. A. (2005). Inability of a Fusion Protein of IL-2 and Diphtheria Toxin (Denileukin Diftitox, DAB389IL-2, ONTAK) to Eliminate Regulatory T Lymphocytes in Patients With Melanoma. Journal of Immunotherapy, 28(6), 582–592. https://doi.org/10.1097/01.cji.0000175468.19742.10

Banales, J. M., Marin, J. J. G., Lamarca, A., Rodrigues, P. M., Khan, S. A., Roberts, L. R., Cardinale, V., Carpino, G., Andersen, J. B., Braconi, C.,

Calvisi, D. F., Perugorria, M. J., Fabris, L., Boulter, L., Macias, R. I. R., Gaudio, E., Alvaro, D., Gradilone, S. A., Strazzabosco, M., … Gores, G. J. (2020). Cholangiocarcinoma 2020: the next horizon in mechanisms and management. Nature Reviews Gastroenterology & Hepatology, 17(9), 557–588. https://doi.org/10.1038/s41575-020-0310-z

Bennett, C. L., Christie, J., Ramsdell, F., Brunkow, M. E., Ferguson, P. J., Whitesell, L., Kelly, T. E., Saulsbury, F. T., Chance, P. F., & Ochs, H. D. (2001). The immune dysregulation, polyendocrinopathy, enteropathy, X-linked syndrome (IPEX) is caused by mutations of FOXP3. Nature Genetics, 27(1), 20–21. https://doi.org/10.1038/83713

Bentsen, M., Goymann, P., Schultheis, H., Klee, K., Petrova, A., Wiegandt, R., Fust, A., Preussner, J., Kuenne, C., Braun, T., Kim, J., & Looso, M. (2020). ATAC-seq footprinting unravels kinetics of transcription factor binding during zygotic genome activation. Nature Communications, 11(1), 4267. https://doi.org/10.1038/s41467-020-18035-1

Binnewies, M., Mujal, A. M., Pollack, J. L., Combes, A. J., Hardison, E. A., Barry, K. C., Tsui, J., Ruhland, M. K., Kersten, K., Abushawish, M. A., Spasic, M., Giurintano, J. P., Chan, V., Daud, A. I., Ha, P., Ye, C. J., Roberts, E. W., & Krummel, M. F. (2019). Unleashing Type-2 Dendritic Cells to Drive Protective Antitumor CD4+ T Cell Immunity. Cell, 177(3), 556-571.e16. https://doi.org/10.1016/j.cell.2019.02.005

Bonnal, R. J. P., Rossetti, G., Lugli, E., de Simone, M., Gruarin, P., Brummelman, J., Drufuca, L., Passaro, M., Bason, R., Gervasoni, F., della Chiara, G., D'Oria, C., Martinovic, M., Curti, S., Ranzani, V., Cordiglieri, C., Alvisi, G., Mazza, E. M. C., Oliveto, S., … Pagani, M. (2021). Clonally expanded EOMES+ Tr1-like cells in primary and metastatic tumors are associated with disease progression. Nature Immunology, 22(6), 735–745. https://doi.org/10.1038/s41590-021-00930-4

Bouneaud, C., Kourilsky, P., & Bousso, P. (2000). Impact of Negative Selection on the T Cell Repertoire Reactive to a Self-Peptide. Immunity, 13(6), 829–840. https://doi.org/10.1016/S1074-7613(00)00080-7

Brummelman, J., Haftmann, C., Núñez, N. G., Alvisi, G., Mazza, E. M. C., Becher, B., & Lugli, E. (2019). Development, application and computational analysis of high-dimensional fluorescent antibody panels for single-cell flow cytometry. Nature Protocols, 14(7), 1946–1969. https://doi.org/10.1038/s41596-019-0166-2

Brummelman, J., Mazza, E. M. C., Alvisi, G., Colombo, F. S., Grilli, A., Mikulak, J., Mavilio, D., Alloisio, M., Ferrari, F., Lopci, E., Novellis, P., Veronesi, G., & Lugli, E. (2018). High-dimensional single cell analysis identifies stem-like cytotoxic CD8+ T cells infiltrating human tumors. Journal of Experimental Medicine, 215(10), 2520–2535. https://doi.org/10.1084/jem.20180684

Brummelman, J., Pilipow, K., & Lugli, E. (2018). The Single-Cell Phenotypic Identity of Human CD8+ and CD4+ T Cells (pp. 63–124). https://doi.org/10.1016/bs.ircmb.2018.05.007

Brunkow, M. E., Jeffery, E. W., Hjerrild, K. A., Paeper, B., Clark, L. B., Yasayko, S.-A., Wilkinson, J. E., Galas, D., Ziegler, S. F., & Ramsdell, F. (2001). Disruption of a new forkhead/winged-helix protein, scurfin, results in the

fatal lymphoproliferative disorder of the scurfy mouse. Nature Genetics, 27(1), 68–73. https://doi.org/10.1038/83784

Buenrostro, J. D., Wu, B., Litzenburger, U. M., Ruff, D., Gonzales, M. L., Snyder, M. P., Chang, H. Y., & Greenleaf, W. J. (2015). Single-cell chromatin accessibility reveals principles of regulatory variation. Nature, 523(7561), 486–490. https://doi.org/10.1038/nature14590

Bulliard, Y., Jolicoeur, R., Windman, M., Rue, S. M., Ettenberg, S., Knee, D. A., Wilson, N. S., Dranoff, G., & Brogdon, J. L. (2013). Activating Fc γ receptors contribute to the antitumor activities of immunoregulatory receptor-targeting antibodies. Journal of Experimental Medicine, 210(9), 1685–1693. https://doi.org/10.1084/jem.20130573

Burzyn, D., Kuswanto, W., Kolodin, D., Shadrach, J. L., Cerletti, M., Jang, Y., Sefik, E., Tan, T. G., Wagers, A. J., Benoist, C., & Mathis, D. (2013). A Special Population of Regulatory T Cells Potentiates Muscle Repair. Cell, 155(6), 1282–1295. https://doi.org/10.1016/j.cell.2013.10.054

Cancer Genome Atlas Research Network. (2014). Comprehensive molecular profiling of lung adenocarcinoma. Nature, 511(7511), 543–550. https://doi.org/10.1038/nature13385

Cavalleri, T., Bianchi, P., Basso, G., Celesti, G., Grizzi, F., Bossi, P., Greco, L., Pitrone, C., Valtorta, E., Mauri, G., Truini, M., Dall'Olio, F. G., Brandi, G., Sartore-Bianchi, A., Ricciardiello, L., Torri, V., Rimassa, L., Siena, S., Mantovani, A., … Laghi, L. (2019). Combined Low Densities of FoxP3+ and CD3+ Tumor-Infiltrating Lymphocytes Identify Stage II Colorectal Cancer at High Risk of Progression. Cancer Immunology Research, 7(5), 751–758. https://doi.org/10.1158/2326-6066.CIR-18-0661

Champiat, S., Ferrara, R., Massard, C., Besse, B., Marabelle, A., Soria, J.-C., & Ferté, C. (2018). Hyperprogressive disease: recognizing a novel pattern to improve patient management. Nature Reviews Clinical Oncology, 15(12), 748–762. https://doi.org/10.1038/s41571-018-0111-2

Chapman, N. M., Zeng, H., Nguyen, T.-L. M., Wang, Y., Vogel, P., Dhungana, Y., Liu, X., Neale, G., Locasale, J. W., & Chi, H. (2018). mTOR coordinates transcriptional programs and mitochondrial metabolism of activated Treg subsets to protect tissue homeostasis. Nature Communications, 9(1), 2095. https://doi.org/10.1038/s41467-018-04392-5

Chen, M.-L., Pittet, M. J., Gorelik, L., Flavell, R. A., Weissleder, R., von Boehmer, H., & Khazaie, K. (2005). Regulatory T cells suppress tumor-specific CD8 T cell cytotoxicity through TGF-β signals in vivo. Proceedings of the National Academy of Sciences, 102(2), 419–424. https://doi.org/10.1073/pnas.0408197102

Chen, Z., Arai, E., Khan, O., Zhang, Z., Ngiow, S. F., He, Y., Huang, H., Manne, S., Cao, Z., Baxter, A. E., Cai, Z., Freilich, E., Ali, M. A., Giles, J. R., Wu, J. E., Greenplate, A. R., Hakeem, M. A., Chen, Q., Kurachi, M., … Shi, J. (2021). In vivo CD8+ T cell CRISPR screening reveals control by Fli1 in infection and cancer. Cell, 184(5), 1262-1280.e22. https://doi.org/10.1016/j.cell.2021.02.019

Chinen, T., Kannan, A. K., Levine, A. G., Fan, X., Klein, U., Zheng, Y., Gasteiger, G., Feng, Y., Fontenot, J. D., & Rudensky, A. Y. (2016). An essential role for the IL-2 receptor in Treg cell function. Nature Immunology, 17(11), 1322–1333. https://doi.org/10.1038/ni.3540

Cipolletta, D., Feuerer, M., Li, A., Kamei, N., Lee, J., Shoelson, S. E., Benoist, C., & Mathis, D. (2012). PPAR-γ is a major driver of the accumulation and phenotype of adipose tissue Treg cells. Nature, 486(7404), 549–553. https://doi.org/10.1038/nature11132

Collison, L. W., Workman, C. J., Kuo, T. T., Boyd, K., Wang, Y., Vignali, K. M., Cross, R., Sehy, D., Blumberg, R. S., & Vignali, D. A. A. (2007). The inhibitory cytokine IL-35 contributes to regulatory T-cell function. Nature, 450(7169), 566–569. https://doi.org/10.1038/nature06306

Colombo, M. P., & Piconese, S. (2007). Regulatory T-cell inhibition versus depletion: the right choice in cancer immunotherapy. Nature Reviews Cancer, 7(11), 880–887. https://doi.org/10.1038/nrc2250

Cretney, E., Kallies, A., & Nutt, S. L. (2013). Differentiation and function of Foxp3+ effector regulatory T cells. Trends in Immunology, 34(2), 74–80. https://doi.org/10.1016/j.it.2012.11.002

Cretney, E., Xin, A., Shi, W., Minnich, M., Masson, F., Miasari, M., Belz, G. T., Smyth, G. K., Busslinger, M., Nutt, S. L., & Kallies, A. (2011). The transcription factors Blimp-1 and IRF4 jointly control the differentiation and function of effector regulatory T cells. Nature Immunology, 12(4), 304–311. https://doi.org/10.1038/ni.2006

Cruz-Guilloty, F., Pipkin, M. E., Djuretic, I. M., Levanon, D., Lotem, J., Lichtenheld, M. G., Groner, Y., & Rao, A. (2009). Runx3 and T-box proteins cooperate to establish the transcriptional program of effector CTLs. Journal of Experimental Medicine, 206(1), 51–59. https://doi.org/10.1084/jem.20081242

Curti, B. D., Kovacsovics-Bankowski, M., Morris, N., Walker, E., Chisholm, L., Floyd, K., Walker, J., Gonzalez, I., Meeuwsen, T., Fox, B. A., Moudgil, T., Miller, W., Haley, D., Coffey, T., Fisher, B., Delanty-Miller, L., Rymarchyk, N., Kelly, T., Crocenzi, T., … Weinberg, A. D. (2013). OX40 Is a Potent Immune-Stimulating Target in Late-Stage Cancer Patients. *Cancer Research*, *73*(24), 7189–7198. https://doi.org/10.1158/0008-5472.CAN-12-4174

Curiel, T. J., Coukos, G., Zou, L., Alvarez, X., Cheng, P., Mottram, P., Evdemon-Hogan, M., Conejo-Garcia, J. R., Zhang, L., Burow, M., Zhu, Y., Wei, S., Kryczek, I., Daniel, B., Gordon, A., Myers, L., Lackner, A., Disis, M. L., Knutson, K. L., … Zou, W. (2004). Specific recruitment of regulatory T cells in ovarian carcinoma fosters immune privilege and predicts reduced survival. Nature Medicine, 10(9), 942–949. https://doi.org/10.1038/nm1093

Dannull, J. (2005). Enhancement of vaccine-mediated antitumor immunity in cancer patients after depletion of regulatory T cells. Journal of Clinical Investigation, 115(12), 3623–3633. https://doi.org/10.1172/JCI25947

Deaglio, S., Dwyer, K. M., Gao, W., Friedman, D., Usheva, A., Erat, A., Chen, J.-F., Enjyoji, K., Linden, J., Oukka, M., Kuchroo, V. K., Strom, T. B., & Robson, S. C. (2007). Adenosine generation catalyzed by CD39 and CD73 expressed on regulatory T cells mediates immune suppression. Journal of Experimental Medicine, 204(6), 1257–1265. https://doi.org/10.1084/jem.20062512

De Simone, M., Arrigoni, A., Rossetti, G., Gruarin, P., Ranzani, V., Politano, C., Bonnal, R. J. P., Provasi, E., Sarnicola, M. L., Panzeri, I., Moro, M.,

Crosti, M., Mazzara, S., Vaira, V., Bosari, S., Palleschi, A., Santambrogio, L., Bovo, G., Zucchini, N., … Pagani, M. (2016). Transcriptional Landscape of Human Tissue Lymphocytes Unveils Uniqueness of Tumor-Infiltrating T Regulatory Cells. Immunity, 45(5), 1135–1147. https://doi.org/10.1016/j.immuni.2016.10.021

Dias, S., D'Amico, A., Cretney, E., Liao, Y., Tellier, J., Bruggeman, C., Almeida, F. F., Leahy, J., Belz, G. T., Smyth, G. K., Shi, W., & Nutt, S. L. (2017). Effector Regulatory T Cell Differentiation and Immune Homeostasis Depend on the Transcription Factor Myb. Immunity, 46(1), 78–91. https://doi.org/10.1016/j.immuni.2016.12.017

Dobin, A., Davis, C. A., Schlesinger, F., Drenkow, J., Zaleski, C., Jha, S., Batut, P., Chaisson, M., & Gingeras, T. R. (2013). STAR: ultrafast universal RNA-seq aligner. Bioinformatics, 29(1), 15–21. https://doi.org/10.1093/bioinformatics/bts635

Dong, H., Strome, S. E., Salomao, D. R., Tamura, H., Hirano, F., Flies, D. B., Roche, P. C., Lu, J., Zhu, G., Tamada, K., Lennon, V. A., Celis, E., & Chen, L. (2002). Tumor-associated B7-H1 promotes T-cell apoptosis: A potential mechanism of immune evasion. Nature Medicine, 8(8), 793–800. https://doi.org/10.1038/nm730

Dong, L., Lu, D., Chen, R., Lin, Y., Zhu, H., Zhang, Z., Cai, S., Cui, P., Song, G., Rao, D., Yi, X., Wu, Y., Song, N., Liu, F., Zou, Y., Zhang, S., Zhang, X., Wang, X., Qiu, S., … Fan, J. (2022). Proteogenomic characterization identifies clinically relevant subgroups of intrahepatic cholangiocarcinoma. Cancer Cell, 40(1), 70-87.e15. https://doi.org/10.1016/j.ccell.2021.12.006

Duhen, T., Duhen, R., Montler, R., Moses, J., Moudgil, T., de Miranda, N. F., Goodall, C. P., Blair, T. C., Fox, B. A., McDermott, J. E., Chang, S.-C., Grunkemeier, G., Leidner, R., Bell, R. B., & Weinberg, A. D. (2018). Co-expression of CD39 and CD103 identifies tumor-reactive CD8 T cells in human solid tumors. Nature Communications, 9(1), 2724. https://doi.org/10.1038/s41467-018-05072-0

Dusseaux, M., Martin, E., Serriari, N., Péguillet, I., Premel, V., Louis, D., Milder, M., le Bourhis, L., Soudais, C., Treiner, E., & Lantz, O. (2011). Human MAIT cells are xenobiotic-resistant, tissue-targeted, CD161hi IL-17–secreting T cells. Blood, 117(4), 1250–1259. https://doi.org/10.1182/blood-2010-08-303339

Fontenot, J. D., Gavin, M. A., & Rudensky, A. Y. (2003). Foxp3 programs the development and function of CD4+CD25+ regulatory T cells. Nature Immunology, 4(4), 330–336. https://doi.org/10.1038/ni904

Fornes, O., Castro-Mondragon, J. A., Khan, A., van der Lee, R., Zhang, X., Richmond, P. A., Modi, B. P., Correard, S., Gheorghe, M., Baranašić, D., Santana-Garcia, W., Tan, G., Chèneby, J., Ballester, B., Parcy, F., Sandelin, A., Lenhard, B., Wasserman, W. W., & Mathelier, A. (2019). JASPAR 2020: update of the open-access database of transcription factor binding profiles. Nucleic Acids Research. https://doi.org/10.1093/nar/gkz1001

Frankish, A., Diekhans, M., Ferreira, A.-M., Johnson, R., Jungreis, I., Loveland, J., Mudge, J. M., Sisu, C., Wright, J., Armstrong, J., Barnes, I., Berry, A., Bignell, A., Carbonell Sala, S., Chrast, J., Cunningham, F., Di Domenico, T., Donaldson, S., Fiddes, I. T., … Flicek, P. (2019). GENCODE

reference annotation for the human and mouse genomes. Nucleic Acids Research, 47(D1), D766–D773. https://doi.org/10.1093/nar/gky955

Freeman, G. J., Long, A. J., Iwai, Y., Bourque, K., Chernova, T., Nishimura, H., Fitz, L. J., Malenkovich, N., Okazaki, T., Byrne, M. C., Horton, H. F., Fouser, L., Carter, L., Ling, V., Bowman, M. R., Carreno, B. M., Collins, M., Wood, C. R., & Honjo, T. (2000). Engagement of the Pd-1 Immunoinhibitory Receptor by a Novel B7 Family Member Leads to Negative Regulation of Lymphocyte Activation. Journal of Experimental Medicine, 192(7), 1027–1034. https://doi.org/10.1084/jem.192.7.1027

Galletti, G., de Simone, G., Mazza, E. M. C., Puccio, S., Mezzanotte, C., Bi, T. M., Davydov, A. N., Metsger, M., Scamardella, E., Alvisi, G., de Paoli, F., Zanon, V., Scarpa, A., Camisa, B., Colombo, F. S., Anselmo, A., Peano, C., Polletti, S., Mavilio, D., … Lugli, E. (2020). Two subsets of stem-like CD8+ memory T cell progenitors with distinct fate commitments in humans. Nature Immunology, 21(12), 1552–1562. https://doi.org/10.1038/s41590-020-0791-5

Gallimore, A., Quezada, S. A., & Roychoudhuri, R. (2019). Regulatory T cells in cancer: where are we now? *Immunology*, *157*(3), 187–189. https://doi.org/10.1111/imm.13088

Galon, J., Angell, H. K., Bedognetti, D., & Marincola, F. M. (2013). The Continuum of Cancer Immunosurveillance: Prognostic, Predictive, and Mechanistic Signatures. Immunity, 39(1), 11–26. https://doi.org/10.1016/j.immuni.2013.07.008

Getnet, D., Grosso, J. F., Goldberg, M. v., Harris, T. J., Yen, H.-R., Bruno, T. C., Durham, N. M., Hipkiss, E. L., Pyle, K. J., & Wada, S. (2010). A role for the transcription factor Helios in human CD4+CD25+ regulatory T cells. Molecular Immunology, 47(7–8), 1595–1600. https://doi.org/10.1016/j.molimm.2010.02.001

Geva, R., Voskoboynik, M., Dobrenkov, K., Mayawala, K., Gwo, J., Wnek, R., Chartash, E., & Long, G. v. (2020). First-in-human phase 1 study of MK-1248, an anti–glucocorticoid-induced tumor necrosis factor receptor agonist monoclonal antibody, as monotherapy or with pembrolizumab in patients with advanced solid tumors. *Cancer*, *126*(22), 4926–4935. https://doi.org/10.1002/cncr.33133

Ghiringhelli, F., Puig, P. E., Roux, S., Parcellier, A., Schmitt, E., Solary, E., Kroemer, G., Martin, F., Chauffert, B., & Zitvogel, L. (2005). Tumor cells convert immature myeloid dendritic cells into TGF-beta-secreting cells inducing CD4+CD25+ regulatory T cell proliferation. The Journal of Experimental Medicine, 202(7), 919–929. https://doi.org/10.1084/jem.20050463

Goswami, S., Apostolou, I., Zhang, J., Skepner, J., Anandhan, S., Zhang, X., Xiong, L., Trojer, P., Aparicio, A., Subudhi, S. K., Allison, J. P., Zhao, H., & Sharma, P. (2018). Modulation of EZH2 expression in T cells improves efficacy of anti–CTLA-4 therapy. Journal of Clinical Investigation, 128(9), 3813–3818. https://doi.org/10.1172/JCI99760

Grossman, W. J., Verbsky, J. W., Barchet, W., Colonna, M., Atkinson, J. P., & Ley, T. J. (2004). Human T Regulatory Cells Can Use the Perforin Pathway to Cause Autologous Target Cell Death. Immunity, 21(4), 589–601. https://doi.org/10.1016/j.immuni.2004.09.002

Guo, X., Zhang, Y., Zheng, L., Zheng, C., Song, J., Zhang, Q., Kang, B., Liu, Z., Jin, L., Xing, R., Gao, R., Zhang, L., Dong, M., Hu, X., Ren, X., Kirchhoff, D., Roider, H. G., Yan, T., & Zhang, Z. (2018). Global characterization of T cells in non-small-cell lung cancer by single-cell sequencing. Nature Medicine, 24(7), 978–985. https://doi.org/10.1038/s41591-018-0045-3

Hafemeister, C., & Satija, R. (2019). Normalization and variance stabilization of single-cell RNA-seq data using regularized negative binomial regression. Genome Biology, 20(1), 296. https://doi.org/10.1186/s13059-019-1874-1

Hänzelmann, S., Castelo, R., & Guinney, J. (2013a). GSVA: gene set variation analysis for microarray and RNA-Seq data. BMC Bioinformatics, 14(1), 7. https://doi.org/10.1186/1471-2105-14-7

Hänzelmann, S., Castelo, R., & Guinney, J. (2013b). GSVA: gene set variation analysis for microarray and RNA-Seq data. BMC Bioinformatics, 14(1), 7. https://doi.org/10.1186/1471-2105-14-7

Hayatsu, N., Miyao, T., Tachibana, M., Murakami, R., Kimura, A., Kato, T., Kawakami, E., Endo, T. A., Setoguchi, R., Watarai, H., Nishikawa, T., Yasuda, T., Yoshida, H., & Hori, S. (2017a). Analyses of a Mutant Foxp3 Allele Reveal BATF as a Critical Transcription Factor in the Differentiation and Accumulation of Tissue Regulatory T Cells. Immunity, 47(2), 268-283.e9. https://doi.org/10.1016/j.immuni.2017.07.008

Hayatsu, N., Miyao, T., Tachibana, M., Murakami, R., Kimura, A., Kato, T., Kawakami, E., Endo, T. A., Setoguchi, R., Watarai, H., Nishikawa, T., Yasuda, T., Yoshida, H., & Hori, S. (2017b). Analyses of a Mutant Foxp3 Allele Reveal BATF as a Critical Transcription Factor in the Differentiation and Accumulation of Tissue Regulatory T Cells. Immunity, 47(2), 268-283.e9. https://doi.org/10.1016/j.immuni.2017.07.008

Hill, J. A., Feuerer, M., Tash, K., Haxhinasto, S., Perez, J., Melamed, R., Mathis, D., & Benoist, C. (2007). Foxp3 Transcription-Factor-Dependent and -Independent Regulation of the Regulatory T Cell Transcriptional Signature. Immunity, 27(5), 786–800. https://doi.org/10.1016/j.immuni.2007.09.010

Hindley, J. P., Ferreira, C., Jones, E., Lauder, S. N., Ladell, K., Wynn, K. K., Betts, G. J., Singh, Y., Price, D. A., Godkin, A. J., Dyson, J., & Gallimore, A. (2011). Analysis of the T-cell receptor repertoires of tumor-infiltrating conventional and regulatory T cells reveals no evidence for conversion in carcinogen-induced tumors. *Cancer Research*, *71*(3), 736–746. https://doi.org/10.1158/0008-5472.CAN-10-1797

Hirotsu, Y., Hataya, N., Katsuoka, F., & Yamamoto, M. (2012). NF-E2-Related Factor 1 (Nrf1) Serves as a Novel Regulator of Hepatic Lipid Metabolism through Regulation of the Lipin1 and PGC-1 β Genes. Molecular and Cellular Biology, 32(14), 2760–2770. https://doi.org/10.1128/MCB.06706-11

Hoelzinger, D. B., Smith, S. E., Mirza, N., Dominguez, A. L., Manrique, S. Z., & Lustgarten, J. (2010). Blockade of CCL1 Inhibits T Regulatory Cell Suppressive Function Enhancing Tumor Immunity without Affecting T Effector Responses. The Journal of Immunology, 184(12), 6833–6842. https://doi.org/10.4049/jimmunol.0904084

Hori, S., Nomura, T., & Sakaguchi, S. (2003). Control of Regulatory T Cell Development by the Transcription Factor Foxp3. Science, 299(5609), 1057–1061. https://doi.org/10.1126/science.1079490

Huber, J. P., & David Farrar, J. (2011). Regulation of effector and memory T-cell functions by type I interferon. Immunology, 132(4), 466–474. https://doi.org/10.1111/j.1365-2567.2011.03412.x

Huynh-Thu, V. A., Irrthum, A., Wehenkel, L., & Geurts, P. (2010). Inferring Regulatory Networks from Expression Data Using Tree-Based Methods. PLoS ONE, 5(9), e12776. https://doi.org/10.1371/journal.pone.0012776

Irizarry, R. A. (2003). Exploration, normalization, and summaries of high density oligonucleotide array probe level data. Biostatistics, 4(2), 249–264. https://doi.org/10.1093/biostatistics/4.2.249

Jacobs, J. F. M., Punt, C. J. A., Lesterhuis, W. J., Sutmuller, R. P. M., Brouwer, H. M. H., Scharenborg, N. M., Klasen, I. S., Hilbrands, L. B., Figdor, C. G., de Vries, I. J. M., & Adema, G. J. (2010). Dendritic Cell Vaccination in Combination with Anti-CD25 Monoclonal Antibody Treatment: A Phase I/II Study in Metastatic Melanoma Patients. Clinical Cancer Research, 16(20), 5067–5078. https://doi.org/10.1158/1078-0432.CCR-10-1757

Jaime-Sanchez, P., Uranga-Murillo, I., Aguilo, N., Khouili, S. C., Arias, M. A., Sancho, D., & Pardo, J. (2020). Cell death induced by cytotoxic CD8 + T cells is immunogenic and primes caspase-3–dependent spread immunity against endogenous tumor antigens. Journal for ImmunoTherapy of Cancer, 8(1), e000528. https://doi.org/10.1136/jitc-2020-000528

Josefowicz, S. Z., Lu, L.-F., & Rudensky, A. Y. (2012). Regulatory T Cells: Mechanisms of Differentiation and Function. Annual Review of Immunology, 30(1), 531–564. https://doi.org/10.1146/annurev.immunol.25.022106.141623

Khan, A., Fornes, O., Stigliani, A., Gheorghe, M., Castro-Mondragon, J. A., van der Lee, R., Bessy, A., Chèneby, J., Kulkarni, S. R., Tan, G., Baranasic, D., Arenillas, D. J., Sandelin, A., Vandepoele, K., Lenhard, B., Ballester, B., Wasserman, W. W., Parcy, F., & Mathelier, A. (2018). JASPAR 2018: update of the open-access database of transcription factor binding profiles and its web framework. Nucleic Acids Research, 46(D1), D260–D266. https://doi.org/10.1093/nar/gkx1126

Kidani, Y., Nogami, W., Yasumizu, Y., Kawashima, A., Tanaka, A., Sonoda, Y., Tona, Y., Nashiki, K., Matsumoto, R., Hagiwara, M., Osaki, M., Dohi, K., Kanazawa, T., Ueyama, A., Yoshikawa, M., Yoshida, T., Matsumoto, M., Hojo, K., Shinonome, S., … Sakaguchi, S. (2022). CCR8-targeted specific depletion of clonally expanded Treg cells in tumor tissues evokes potent tumor immunity with long-lasting memory. Proceedings of the National Academy of Sciences, 119(7). https://doi.org/10.1073/pnas.2114282119

Kim, H.-J., Barnitz, R. A., Kreslavsky, T., Brown, F. D., Moffett, H., Lemieux, M. E., Kaygusuz, Y., Meissner, T., Holderried, T. A. W., Chan, S., Kastner, P., Haining, W. N., & Cantor, H. (2015). Stable inhibitory activity of regulatory T cells requires the transcription factor Helios. Science, 350(6258), 334–339. https://doi.org/10.1126/science.aad0616

Klein, U., Casola, S., Cattoretti, G., Shen, Q., Lia, M., Mo, T., Ludwig, T., Rajewsky, K., & Dalla-Favera, R. (2006). Transcription factor IRF4

controls plasma cell differentiation and class-switch recombination. Nature Immunology, 7(7), 773–782. https://doi.org/10.1038/ni1357

Koch, M. A., Tucker-Heard, G., Perdue, N. R., Killebrew, J. R., Urdahl, K. B., & Campbell, D. J. (2009). The transcription factor T-bet controls regulatory T cell homeostasis and function during type 1 inflammation. Nature Immunology, 10(6), 595–602. https://doi.org/10.1038/ni.1731

Koizumi, S., Sasaki, D., Hsieh, T.-H., Taira, N., Arakaki, N., Yamasaki, S., Wang, K., Sarkar, S., Shirahata, H., Miyagi, M., & Ishikawa, H. (2018). JunB regulates homeostasis and suppressive functions of effector regulatory T cells. Nature Communications, 9(1), 5344. https://doi.org/10.1038/s41467-018-07735-4

Kuehn, H. S., Ouyang, W., Lo, B., Deenick, E. K., Niemela, J. E., Avery, D. T., Schickel, J.-N., Tran, D. Q., Stoddard, J., Zhang, Y., Frucht, D. M., Dumitriu, B., Scheinberg, P., Folio, L. R., Frein, C. A., Price, S., Koh, C., Heller, T., Seroogy, C. M., … Uzel, G. (2014). Immune dysregulation in human subjects with heterozygous germline mutations in CTLA4. Science, 345(6204), 1623–1627. https://doi.org/10.1126/science.1255904

Kumagai, S., Togashi, Y., Kamada, T., Sugiyama, E., Nishinakamura, H., Takeuchi, Y., Vitaly, K., Itahashi, K., Maeda, Y., Matsui, S., Shibahara, T., Yamashita, Y., Irie, T., Tsuge, A., Fukuoka, S., Kawazoe, A., Udagawa, H., Kirita, K., Aokage, K., … Nishikawa, H. (2020). The PD-1 expression balance between effector and regulatory T cells predicts the clinical efficacy of PD-1 blockade therapies. Nature Immunology, 21(11), 1346–1358. https://doi.org/10.1038/s41590-020-0769-3

Lainé, A., Labiad, O., Hernandez-Vargas, H., This, S., Sanlaville, A., Léon, S., Dalle, S., Sheppard, D., Travis, M. A., Paidassi, H., & Marie, J. C. (2021). Regulatory T cells promote cancer immune-escape through integrin αvβ8-mediated TGF-β activation. Nature Communications, 12(1), 6228. https://doi.org/10.1038/s41467-021-26352-2

Larmonier, N., Marron, M., Zeng, Y., Cantrell, J., Romanoski, A., Sepassi, M., Thompson, S., Chen, X., Andreansky, S., & Katsanis, E. (2006). Tumor-derived CD4+CD25+ regulatory T cell suppression of dendritic cell function involves TGF-β and IL-10. Cancer Immunology, Immunotherapy, 56(1), 48–59. https://doi.org/10.1007/s00262-006-0160-8

Levine, J. H., Simonds, E. F., Bendall, S. C., Davis, K. L., Amir, E. D., Tadmor, M. D., Litvin, O., Fienberg, H. G., Jager, A., Zunder, E. R., Finck, R., Gedman, A. L., Radtke, I., Downing, J. R., Pe'er, D., & Nolan, G. P. (2015). Data-Driven Phenotypic Dissection of AML Reveals Progenitor-like Cells that Correlate with Prognosis. Cell, 162(1), 184–197. https://doi.org/10.1016/j.cell.2015.05.047

Li, J., He, Y., Hao, J., Ni, L., & Dong, C. (2018). High Levels of Eomes Promote Exhaustion of Anti-tumor CD8+ T Cells. Frontiers in Immunology, 9. https://doi.org/10.3389/fimmu.2018.02981

Li, P., Spolski, R., Liao, W., Wang, L., Murphy, T. L., Murphy, K. M., & Leonard, W. J. (2012). BATF–JUN is critical for IRF4-mediated transcription in T cells. Nature, 490(7421), 543–546. https://doi.org/10.1038/nature11530

Linderman, G. C., Zhao, J., Roulis, M., Bielecki, P., Flavell, R. A., Nadler, B., & Kluger, Y. (2022). Zero-preserving imputation of single-cell RNA-seq

data. Nature Communications, 13(1), 192. https://doi.org/10.1038/s41467-021-27729-z

Liu, W., Putnam, A. L., Xu-yu, Z., Szot, G. L., Lee, M. R., Zhu, S., Gottlieb, P. A., Kapranov, P., Gingeras, T. R., de St. Groth, B. F., Clayberger, C., Soper, D. M., Ziegler, S. F., & Bluestone, J. A. (2006). CD127 expression inversely correlates with FoxP3 and suppressive function of human CD4+ T reg cells. Journal of Experimental Medicine, 203(7), 1701–1711. https://doi.org/10.1084/jem.20060772

Liu, Y., Carlsson, R., Comabella, M., Wang, J., Kosicki, M., Carrion, B., Hasan, M., Wu, X., Montalban, X., Dziegiel, M. H., Sellebjerg, F., Sørensen, P. S., Helin, K., & Issazadeh-Navikas, S. (2014). FoxA1 directs the lineage and immunosuppressive properties of a novel regulatory T cell population in EAE and MS. Nature Medicine, 20(3), 272–282. https://doi.org/10.1038/nm.3485

Lopci, E., Toschi, L., Grizzi, F., Rahal, D., Olivari, L., Castino, G. F., Marchetti, S., Cortese, N., Qehajaj, D., Pistillo, D., Alloisio, M., Roncalli, M., Allavena, P., Santoro, A., Marchesi, F., & Chiti, A. (2016). Correlation of metabolic information on FDG-PET with tissue expression of immune markers in patients with non-small cell lung cancer (NSCLC) who are candidates for upfront surgery. European Journal of Nuclear Medicine and Molecular Imaging, 43(11), 1954–1961. https://doi.org/10.1007/s00259-016-3425-2

Losurdo A, Scirgolea C, Alvisi G, Brummelman J, Errico V, Di Tommaso L, Pilipow K, Colombo FS, Bethania Fernandes B, Peano C, Testori A, Tinterri C, Roncalli M, Santoro A, Mazza EMC, Lugli E. *Single-cell profiling defines the prognostic benefit of CD39high tissue resident memory T cells in luminal-like breast cancer.* Communication Biology. Commun Biol. 2021

Lugli, E., Zanon, V., Mavilio, D., & Roberto, A. (2017). FACS Analysis of Memory T Lymphocytes (pp. 31–47). https://doi.org/10.1007/978-1-4939-6548-9_3

Luo, C. T., Liao, W., Dadi, S., Toure, A., & Li, M. O. (2016). Graded Foxo1 activity in Treg cells differentiates tumour immunity from spontaneous autoimmunity. Nature, 529(7587), 532–536. https://doi.org/10.1038/nature16486

MacIver, N. J., Michalek, R. D., & Rathmell, J. C. (2013). Metabolic Regulation of T Lymphocytes. *Annual Review of Immunology*, *31*(1), 259–283. https://doi.org/10.1146/annurev-immunol-032712-095956

Magnuson, A. M., Kiner, E., Ergun, A., Park, J. S., Asinovski, N., Ortiz-Lopez, A., Kilcoyne, A., Paoluzzi-Tomada, E., Weissleder, R., Mathis, D., & Benoist, C. (2018). Identification and validation of a tumor-infiltrating Treg transcriptional signature conserved across species and tumor types. Proceedings of the National Academy of Sciences, 115(45). https://doi.org/10.1073/pnas.1810580115

Mahnke, K., Schönfeld, K., Fondel, S., Ring, S., Karakhanova, S., Wiedemeyer, K., Bedke, T., Johnson, T. S., Storn, V., Schallenberg, S., & Enk, A. H. (2007). Depletion of CD4+CD25+ human regulatory T cellsin vivo: Kinetics of Treg depletion and alterations in immune functionsin vivo andin vitro. International Journal of Cancer, 120(12), 2723–2733. https://doi.org/10.1002/ijc.22617

Mair, F., Erickson, J. R., Frutoso, M., Konecny, A. J., Greene, E., Voillet, V., Maurice, N. J., Rongvaux, A., Dixon, D., Barber, B., Gottardo, R., & Prlic, M. (2022). Extricating human tumour immune alterations from tissue inflammation. Nature, 605(7911), 728–735. https://doi.org/10.1038/s41586-022-04718-w

Malenica, I., Donadon, M., & Lleo, A. (2020). Molecular and Immunological Characterization of Biliary Tract Cancers: A Paradigm Shift Towards a Personalized Medicine. Cancers, 12(8), 2190. https://doi.org/10.3390/cancers12082190

Mannie, M. D. (1991). A unified model for T cell antigen recognition and thymic selection of the T cell repertoire. Journal of Theoretical Biology, 151(2), 169–192. https://doi.org/10.1016/S0022-5193(05)80360-1

McHugh, R. S., & Shevach, E. M. (2002). Cutting Edge: Depletion of CD4 + CD25 + Regulatory T Cells Is Necessary, But Not Sufficient, for Induction of Organ-Specific Autoimmune Disease. The Journal of Immunology, 168(12), 5979–5983. https://doi.org/10.4049/jimmunol.168.12.5979

Mittrücker, H.-W., Matsuyama, T., Grossman, A., Kündig, T. M., Potter, J., Shahinian, A., Wakeham, A., Patterson, B., Ohashi, P. S., & Mak, T. W. (1997). Requirement for the Transcription Factor LSIRF/IRF4 for Mature B and T Lymphocyte Function. Science, 275(5299), 540–543. https://doi.org/10.1126/science.275.5299.540

Miyara, M., Chader, D., Sage, E., Sugiyama, D., Nishikawa, H., Bouvry, D., Claër, L., Hingorani, R., Balderas, R., Rohrer, J., Warner, N., Chapelier, A., Valeyre, D., Kannagi, R., Sakaguchi, S., Amoura, Z., & Gorochov, G. (2015). Sialyl Lewis x (CD15s) identifies highly differentiated and most suppressive FOXP3 high regulatory T cells in humans. Proceedings of the National Academy of Sciences, 112(23), 7225–7230. https://doi.org/10.1073/pnas.1508224112

Miyara, M., Yoshioka, Y., Kitoh, A., Shima, T., Wing, K., Niwa, A., Parizot, C., Taflin, C., Heike, T., Valeyre, D., Mathian, A., Nakahata, T., Yamaguchi, T., Nomura, T., Ono, M., Amoura, Z., Gorochov, G., & Sakaguchi, S. (2009). Functional Delineation and Differentiation Dynamics of Human CD4+ T Cells Expressing the FoxP3 Transcription Factor. Immunity, 30(6), 899–911. https://doi.org/10.1016/j.immuni.2009.03.019

Miyazaki, M., Miyazaki, K., Chen, S., Itoi, M., Miller, M., Lu, L.-F., Varki, N., Chang, A. N., Broide, D. H., & Murre, C. (2014). Id2 and Id3 maintain the regulatory T cell pool to suppress inflammatory disease. Nature Immunology, 15(8), 767–776. https://doi.org/10.1038/ni.2928

Mohamed, J. Y., Faqeih, E., Alsiddiky, A., Alshammari, M. J., Ibrahim, N. A., & Alkuraya, F. S. (2013). Mutations in MEOX1, Encoding Mesenchyme Homeobox 1, Cause Klippel-Feil Anomaly. The American Journal of Human Genetics, 92(1), 157–161. https://doi.org/10.1016/j.ajhg.2012.11.016

Mohammed, H., Taylor, C., Brown, G. D., Papachristou, E. K., Carroll, J. S., & D'Santos, C. S. (2016). Rapid immunoprecipitation mass spectrometry of endogenous proteins (RIME) for analysis of chromatin complexes. *Nature Protocols*, *11*(2), 316–326. https://doi.org/10.1038/nprot.2016.020

Morris, G. P., & Allen, P. M. (2012). How the TCR balances sensitivity and specificity for the recognition of self and pathogens. Nature Immunology, 13(2), 121–128. https://doi.org/10.1038/ni.2190

Nishikawa, H., Kato, T., Tawara, I., Saito, K., Ikeda, H., Kuribayashi, K., Allen, P. M., Schreiber, R. D., Sakaguchi, S., Old, L. J., & Shiku, H. (2005). Definition of target antigens for naturally occurring CD4+ CD25+ regulatory T cells. Journal of Experimental Medicine, 201(5), 681–686. https://doi.org/10.1084/jem.20041959

Ohkura, N., Hamaguchi, M., Morikawa, H., Sugimura, K., Tanaka, A., Ito, Y., Osaki, M., Tanaka, Y., Yamashita, R., Nakano, N., Huehn, J., Fehling, H. J., Sparwasser, T., Nakai, K., & Sakaguchi, S. (2012). T Cell Receptor Stimulation-Induced Epigenetic Changes and Foxp3 Expression Are Independent and Complementary Events Required for Treg Cell Development. Immunity, 37(5), 785–799. https://doi.org/10.1016/j.immuni.2012.09.010

Ohkura, N., Kitagawa, Y., & Sakaguchi, S. (2013). Development and Maintenance of Regulatory T cells. Immunity, 38(3), 414–423. https://doi.org/10.1016/j.immuni.2013.03.002

Oliveira, G., Stromhaug, K., Cieri, N., Iorgulescu, J. B., Klaeger, S., Wolff, J. O., Rachimi, S., Chea, V., Krause, K., Freeman, S. S., Zhang, W., Li, S., Braun, D. A., Neuberg, D., Carr, S. A., Livak, K. J., Frederick, D. T., Fritsch, E. F., Wind-Rotolo, M., … Wu, C. J. (2022). Landscape of helper and regulatory antitumour CD4+ T cells in melanoma. *Nature*, *605*(7910), 532–538. https://doi.org/10.1038/s41586-022-04682-5

Ouyang, W., Liao, W., Luo, C. T., Yin, N., Huse, M., Kim, M. v., Peng, M., Chan, P., Ma, Q., Mo, Y., Meijer, D., Zhao, K., Rudensky, A. Y., Atwal, G., Zhang, M. Q., & Li, M. O. (2012). Novel Foxo1-dependent transcriptional programs control Treg cell function. Nature, 491(7425), 554–559. https://doi.org/10.1038/nature11581

Park, Y. M., & Bochner, B. S. (2010). Eosinophil Survival and Apoptosis in Health and Disease. *Allergy, Asthma and Immunology Research*, *2*(2), 87. https://doi.org/10.4168/aair.2010.2.2.87

Piconese, S., Valzasina, B., & Colombo, M. P. (2008). OX40 triggering blocks suppression by regulatory T cells and facilitates tumor rejection. *Journal of Experimental Medicine*, *205*(4), 825–839. https://doi.org/10.1084/jem.20071341

Pilipow, K., Scamardella, E., Puccio, S., Gautam, S., de Paoli, F., Mazza, E. M. C., de Simone, G., Polletti, S., Buccilli, M., Zanon, V., di Lucia, P., Iannacone, M., Gattinoni, L., & Lugli, E. (2018). Antioxidant metabolism regulates CD8+ T memory stem cell formation and antitumor immunity. JCI Insight, 3(18). https://doi.org/10.1172/jci.insight.122299

Pircher, H., Rohrer, U. H., Moskophidis, D., Zinkernagel, R. M., & Hengartner, H. (1991). Lower receptor avidity required for thymic clonal deletion than for effector T-cell function. Nature, 351(6326), 482–485. https://doi.org/10.1038/351482a0

Plitas, G., Konopacki, C., Wu, K., Bos, P. D., Morrow, M., Putintseva, E. V., Chudakov, D. M., & Rudensky, A. Y. (2016). Regulatory T Cells Exhibit

Distinct Features in Human Breast Cancer. Immunity, 45(5), 1122–1134. https://doi.org/10.1016/j.immuni.2016.10.032

Rech, A. J., Mick, R., Martin, S., Recio, A., Aqui, N. A., Powell, D. J., Colligon, T. A., Trosko, J. A., Leinbach, L. I., Pletcher, C. H., Tweed, C. K., DeMichele, A., Fox, K. R., Domchek, S. M., Riley, J. L., & Vonderheide, R. H. (2012). CD25 Blockade Depletes and Selectively Reprograms Regulatory T Cells in Concert with Immunotherapy in Cancer Patients. Science Translational Medicine, 4(134). https://doi.org/10.1126/scitranslmed.3003330

Redmond, W. L., & Sherman, L. A. (2005). Peripheral Tolerance of CD8 T Lymphocytes. Immunity, 22(3), 275–284. https://doi.org/10.1016/j.immuni.2005.01.010

Reinhardt, R. L., Khoruts, A., Merica, R., Zell, T., & Jenkins, M. K. (2001). Visualizing the generation of memory CD4 T cells in the whole body. Nature, 410(6824), 101–105. https://doi.org/10.1038/35065111

Ritchie, M. E., Phipson, B., Wu, D., Hu, Y., Law, C. W., Shi, W., & Smyth, G. K. (2015). limma powers differential expression analyses for RNA-sequencing and microarray studies. Nucleic Acids Research, 43(7), e47–e47. https://doi.org/10.1093/nar/gkv007

Robey, E., & Fowlkes, B. J. (1994). Selective Events in T Cell Development. Annual Review of Immunology, 12(1), 675–705. https://doi.org/10.1146/annurev.iy.12.040194.003331

Robins, H. S., Campregher, P. v., Srivastava, S. K., Wacher, A., Turtle, C. J., Kahsai, O., Riddell, S. R., Warren, E. H., & Carlson, C. S. (2009). Comprehensive assessment of T-cell receptor β-chain diversity in αβ T cells. Blood, 114(19), 4099–4107. https://doi.org/10.1182/blood-2009-04-217604

Robinson, M. D., McCarthy, D. J., & Smyth, G. K. (2010). edgeR: a Bioconductor package for differential expression analysis of digital gene expression data. Bioinformatics, 26(1), 139–140. https://doi.org/10.1093/bioinformatics/btp616

Roychoudhuri, R., Eil, R. L., & Restifo, N. P. (2015). The interplay of effector and regulatory T cells in cancer. Current Opinion in Immunology, 33, 101–111. https://doi.org/10.1016/j.coi.2015.02.003

Roychoudhuri, R., Hirahara, K., Mousavi, K., Clever, D., Klebanoff, C. A., Bonelli, M., Sciumè, G., Zare, H., Vahedi, G., Dema, B., Yu, Z., Liu, H., Takahashi, H., Rao, M., Muranski, P., Crompton, J. G., Punkosdy, G., Bedognetti, D., Wang, E., … Restifo, N. P. (2013). BACH2 represses effector programs to stabilize Treg-mediated immune homeostasis. Nature, 498(7455), 506–510. https://doi.org/10.1038/nature12199

Rubtsov, Y. P., Niec, R. E., Josefowicz, S., Li, L., Darce, J., Mathis, D., Benoist, C., & Rudensky, A. Y. (2010). Stability of the Regulatory T Cell Lineage in Vivo. Science, 329(5999), 1667–1671. https://doi.org/10.1126/science.1191996

Rudensky, A. Y. (2011). Regulatory T cells and Foxp3. Immunological Reviews, 241(1), 260–268. https://doi.org/10.1111/j.1600-065X.2011.01018.x

Saelens, W., Cannoodt, R., Todorov, H., & Saeys, Y. (2019a). A comparison of single-cell trajectory inference methods. Nature Biotechnology, 37(5), 547–554. https://doi.org/10.1038/s41587-019-0071-9

Sainz-Perez, A., Lim, A., Lemercier, B., & Leclerc, C. (2012). The T-cell Receptor Repertoire of Tumor-Infiltrating Regulatory T Lymphocytes Is Skewed Toward Public Sequences. *Cancer Research*, *72*(14), 3557–3569. https://doi.org/10.1158/0008-5472.CAN-12-0277

Sage, P. T., Francisco, L. M., Carman, C. v, & Sharpe, A. H. (2013). The receptor PD-1 controls follicular regulatory T cells in the lymph nodes and blood. Nature Immunology, 14(2), 152–161. https://doi.org/10.1038/ni.2496

Sakaguchi, S., Mikami, N., Wing, J. B., Tanaka, A., Ichiyama, K., & Ohkura, N. (2020). Regulatory T Cells and Human Disease. Annual Review of Immunology, 38(1), 541–566. https://doi.org/10.1146/annurev-immunol-042718-041717

Sakaguchi, S., Sakaguchi, N., Asano, M., Itoh, M., & Toda, M. (1995). Immunologic self-tolerance maintained by activated T cells expressing IL-2 receptor alpha-chains (CD25). Breakdown of a single mechanism of self-tolerance causes various autoimmune diseases. Journal of Immunology (Baltimore, Md. : 1950), 155(3), 1151–1164.

Sakaguchi, S., Yamaguchi, T., Nomura, T., & Ono, M. (2008). Regulatory T Cells and Immune Tolerance. Cell, 133(5), 775–787. https://doi.org/10.1016/j.cell.2008.05.009

Sampson, J. H., Schmittling, R. J., Archer, G. E., Congdon, K. L., Nair, S. K., Reap, E. A., Desjardins, A., Friedman, A. H., Friedman, H. S., Herndon, J. E., Coan, A., McLendon, R. E., Reardon, D. A., Vredenburgh, J. J., Bigner, D. D., & Mitchell, D. A. (2012). A Pilot Study of IL-2Rα Blockade during Lymphopenia Depletes Regulatory T-cells and Correlates with Enhanced Immunity in Patients with Glioblastoma. PLoS ONE, 7(2), e31046. https://doi.org/10.1371/journal.pone.0031046

Satija, R., Farrell, J. A., Gennert, D., Schier, A. F., & Regev, A. (2015). Spatial reconstruction of single-cell gene expression data. Nature Biotechnology, 33(5), 495–502. https://doi.org/10.1038/nbt.3192

Schaefer, T. S., Sanders, L. K., & Nathans, D. (1995). Cooperative transcriptional activity of Jun and Stat3 beta, a short form of Stat3. Proceedings of the National Academy of Sciences, 92(20), 9097–9101. https://doi.org/10.1073/pnas.92.20.9097

Schubert, D., Bode, C., Kenefeck, R., Hou, T. Z., Wing, J. B., Kennedy, A., Bulashevska, A., Petersen, B.-S., Schäffer, A. A., Grüning, B. A., Unger, S., Frede, N., Baumann, U., Witte, T., Schmidt, R. E., Dueckers, G., Niehues, T., Seneviratne, S., Kanariou, M., … Grimbacher, B. (2014). Autosomal dominant immune dysregulation syndrome in humans with CTLA4 mutations. Nature Medicine, 20(12), 1410–1416. https://doi.org/10.1038/nm.3746

Seglen, P. O. (1976). Chapter 4 Preparation of Isolated Rat Liver Cells (pp. 29–83). https://doi.org/10.1016/S0091-679X(08)61797-5

Selby, M. J., Engelhardt, J. J., Quigley, M., Henning, K. A., Chen, T., Srinivasan, M., & Korman, A. J. (2013). Anti-CTLA-4 Antibodies of IgG2a Isotype Enhance Antitumor Activity through Reduction of Intratumoral Regulatory

T Cells. Cancer Immunology Research, 1(1), 32–42. https://doi.org/10.1158/2326-6066.CIR-13-0013

Sen, D. R., Kaminski, J., Barnitz, R. A., Kurachi, M., Gerdemann, U., Yates, K. B., Tsao, H.-W., Godec, J., LaFleur, M. W., Brown, F. D., Tonnerre, P., Chung, R. T., Tully, D. C., Allen, T. M., Frahm, N., Lauer, G. M., Wherry, E. J., Yosef, N., & Haining, W. N. (2016). The epigenetic landscape of T cell exhaustion. Science, 354(6316), 1165–1169. https://doi.org/10.1126/science.aae0491

Serrels, A., Lund, T., Serrels, B., Byron, A., McPherson, R. C., von Kriegsheim, A., Gómez-Cuadrado, L., Canel, M., Muir, M., Ring, J. E., Maniati, E., Sims, A. H., Pachter, J. A., Brunton, V. G., Gilbert, N., Anderton, S. M., Nibbs, R. J. B., & Frame, M. C. (2015). Nuclear FAK Controls Chemokine Transcription, Tregs, and Evasion of Anti-tumor Immunity. Cell, 163(1), 160–173. https://doi.org/10.1016/j.cell.2015.09.001

Setoguchi, R., Hori, S., Takahashi, T., & Sakaguchi, S. (2005). Homeostatic maintenance of natural Foxp3+ CD25+ CD4+ regulatory T cells by interleukin (IL)-2 and induction of autoimmune disease by IL-2 neutralization. Journal of Experimental Medicine, 201(5), 723–735. https://doi.org/10.1084/jem.20041982

Sharma, A., Subudhi, S. K., Blando, J., Scutti, J., Vence, L., Wargo, J., Allison, J. P., Ribas, A., & Sharma, P. (2019). Anti-CTLA-4 Immunotherapy Does Not Deplete FOXP3+ Regulatory T Cells (Tregs) in Human Cancers. Clinical Cancer Research, 25(4), 1233–1238. https://doi.org/10.1158/1078-0432.CCR-18-0762

Sharma, P., & Allison, J. P. (2015). The future of immune checkpoint therapy. Science, 348(6230), 56–61. https://doi.org/10.1126/science.aaa8172

Sia, D., Hoshida, Y., Villanueva, A., Roayaie, S., Ferrer, J., Tabak, B., Peix, J., Sole, M., Tovar, V., Alsinet, C., Cornella, H., Klotzle, B., Fan, J., Cotsoglou, C., Thung, S. N., Fuster, J., Waxman, S., Garcia–Valdecasas, J. C., Bruix, J., … Llovet, J. M. (2013). Integrative Molecular Analysis of Intrahepatic Cholangiocarcinoma Reveals 2 Classes That Have Different Outcomes. Gastroenterology, 144(4), 829–840. https://doi.org/10.1053/j.gastro.2013.01.001

Simoni, Y., Becht, E., Fehlings, M., Loh, C. Y., Koo, S.-L., Teng, K. W. W., Yeong, J. P. S., Nahar, R., Zhang, T., Kared, H., Duan, K., Ang, N., Poidinger, M., Lee, Y. Y., Larbi, A., Khng, A. J., Tan, E., Fu, C., Mathew, R., … Newell, E. W. (2018a). Bystander CD8+ T cells are abundant and phenotypically distinct in human tumour infiltrates. Nature, 557(7706), 575–579. https://doi.org/10.1038/s41586-018-0130-2

Simoni, Y., Becht, E., Fehlings, M., Loh, C. Y., Koo, S.-L., Teng, K. W. W., Yeong, J. P. S., Nahar, R., Zhang, T., Kared, H., Duan, K., Ang, N., Poidinger, M., Lee, Y. Y., Larbi, A., Khng, A. J., Tan, E., Fu, C., Mathew, R., … Newell, E. W. (2018b). Bystander CD8+ T cells are abundant and phenotypically distinct in human tumour infiltrates. Nature, 557(7706), 575–579. https://doi.org/10.1038/s41586-018-0130-2

Simpson, T. R., Li, F., Montalvo-Ortiz, W., Sepulveda, M. A., Bergerhoff, K., Arce, F., Roddie, C., Henry, J. Y., Yagita, H., Wolchok, J. D., Peggs, K. S., Ravetch, J. v., Allison, J. P., & Quezada, S. A. (2013). Fc-dependent depletion of tumor-infiltrating regulatory T cells co-defines the efficacy of

anti–CTLA-4 therapy against melanoma. Journal of Experimental Medicine, 210(9), 1695–1710. https://doi.org/10.1084/jem.20130579

Solomon, I., Amann, M., Goubier, A., Arce Vargas, F., Zervas, D., Qing, C., Henry, J. Y., Ghorani, E., Akarca, A. U., Marafioti, T., Śledzińska, A., Werner Sunderland, M., Franz Demane, D., Clancy, J. R., Georgiou, A., Salimu, J., Merchiers, P., Brown, M. A., Flury, R., … Quezada, S. A. (2020). CD25-Treg-depleting antibodies preserving IL-2 signaling on effector T cells enhance effector activation and antitumor immunity. Nature Cancer, 1(12), 1153–1166. https://doi.org/10.1038/s43018-020-00133-0

Speiser, D. E., Ho, P.-C., & Verdeil, G. (2016). Regulatory circuits of T cell function in cancer. Nature Reviews Immunology, 16(10), 599–611. https://doi.org/10.1038/nri.2016.80

Spits, H. (2002). Development of αβ T cells in the human thymus. Nature Reviews Immunology, 2(10), 760–772. https://doi.org/10.1038/nri913

Spranger, S., Spaapen, R. M., Zha, Y., Williams, J., Meng, Y., Ha, T. T., & Gajewski, T. F. (2013). Up-Regulation of PD-L1, IDO, and T regs in the Melanoma Tumor Microenvironment Is Driven by CD8 + T Cells. Science Translational Medicine, 5(200). https://doi.org/10.1126/scitranslmed.3006504

Summers, C., Rankin, S. M., Condliffe, A. M., Singh, N., Peters, A. M., & Chilvers, E. R. (2010). Neutrophil kinetics in health and disease. *Trends in Immunology*, *31*(8), 318–324. https://doi.org/10.1016/j.it.2010.05.006

Starr, T. K., Jameson, S. C., & Hogquist, K. A. (2003). Positive and Negative Selection of T Cells. Annual Review of Immunology, 21(1), 139–176. https://doi.org/10.1146/annurev.immunol.21.120601.141107

Steinman, R. M., Hawiger, D., & Nussenzweig, M. C. (2003). Tolerogenic Dendritic Cells. Annual Review of Immunology, 21(1), 685–711. https://doi.org/10.1146/annurev.immunol.21.120601.141040

Takahashi, T., Kuniyasu, Y., Toda, M., Sakaguchi, N., Itoh, M., Iwata, M., Shimizu, J., & Sakaguchi, S. (1998). Immunologic self-tolerance maintained by CD25+CD4+ naturally anergic and suppressive T cells: induction of autoimmune disease by breaking their anergic/suppressive state. International Immunology, 10(12), 1969–1980. https://doi.org/10.1093/intimm/10.12.1969

Tan, M. C. B., Goedegebuure, P. S., Belt, B. A., Flaherty, B., Sankpal, N., Gillanders, W. E., Eberlein, T. J., Hsieh, C.-S., & Linehan, D. C. (2009). Disruption of CCR5-Dependent Homing of Regulatory T Cells Inhibits Tumor Growth in a Murine Model of Pancreatic Cancer. The Journal of Immunology, 182(3), 1746–1755. https://doi.org/10.4049/jimmunol.182.3.1746

Tanaka, A., & Sakaguchi, S. (2017). Regulatory T cells in cancer immunotherapy. Cell Research, 27(1), 109–118. https://doi.org/10.1038/cr.2016.151

Tariq, N.-A., McNamara, M. G., & Valle, J. W. (2019). Biliary tract cancers: current knowledge, clinical candidates and future challenges . Cancer Management and Research, Volume 11, 2623–2642. https://doi.org/10.2147/CMAR.S157092

Tay, C., Qian, Y., & Sakaguchi, S. (2020). Hyper-Progressive Disease: The Potential Role and Consequences of T-Regulatory Cells Foiling Anti-PD-1 Cancer Immunotherapy. Cancers, 13(1), 48. https://doi.org/10.3390/cancers13010048

Thornton, A. M., & Shevach, E. M. (1998). CD4+CD25+ Immunoregulatory T Cells Suppress Polyclonal T Cell Activation In Vitro by Inhibiting Interleukin 2 Production. Journal of Experimental Medicine, 188(2), 287–296. https://doi.org/10.1084/jem.188.2.287

Tirosh, I., Izar, B., Prakadan, S. M., Wadsworth, M. H., Treacy, D., Trombetta, J. J., Rotem, A., Rodman, C., Lian, C., Murphy, G., Fallahi-Sichani, M., Dutton-Regester, K., Lin, J.-R., Cohen, O., Shah, P., Lu, D., Genshaft, A. S., Hughes, T. K., Ziegler, C. G. K., … Garraway, L. A. (2016). Dissecting the multicellular ecosystem of metastatic melanoma by single-cell RNA-seq. Science, 352(6282), 189–196. https://doi.org/10.1126/science.aad0501

Togashi, Y., Kamada, T., Sasaki, A., Nakamura, Y., Fukuoka, S., Tada, Y., Kawazoe, A., Shitara, K., & Nishikawa, H. (2018). Clinicopathological, genomic and immunological features of hyperprogressive disease during PD-1 blockade in gastric cancer patients. Journal of Clinical Oncology, 36(15_suppl), 4106–4106. https://doi.org/10.1200/JCO.2018.36.15_suppl.4106

Togashi, Y., & Nishikawa, H. (2017). Regulatory T Cells: Molecular and Cellular Basis for Immunoregulation (pp. 3–27). https://doi.org/10.1007/82_2017_58

Topalian, S. L., Hodi, F. S., Brahmer, J. R., Gettinger, S. N., Smith, D. C., McDermott, D. F., Powderly, J. D., Carvajal, R. D., Sosman, J. A., Atkins, M. B., Leming, P. D., Spigel, D. R., Antonia, S. J., Horn, L., Drake, C. G., Pardoll, D. M., Chen, L., Sharfman, W. H., Anders, R. A., … Sznol, M. (2012). Safety, Activity, and Immune Correlates of Anti–PD-1 Antibody in Cancer. New England Journal of Medicine, 366(26), 2443–2454. https://doi.org/10.1056/NEJMoa1200690

Valzasina, B., Guiducci, C., Dislich, H., Killeen, N., Weinberg, A. D., & Colombo, M. P. (2005). Triggering of OX40 (CD134) on CD4+CD25+ T cells blocks their inhibitory activity: a novel regulatory role for OX40 and its comparison with GITR. *Blood*, *105*(7), 2845–2851. https://doi.org/10.1182/blood-2004-07-2959

Van der Leun, A. M., Thommen, D. S., & Schumacher, T. N. (2020). CD8+ T cell states in human cancer: insights from single-cell analysis. *Nature Reviews Cancer*, *20*(4), 218–232. https://doi.org/10.1038/s41568-019-0235-4

Vargas, F., Furness, A. J. S., Litchfield, K., Joshi, K., Rosenthal, R., Ghorani, E., Solomon, I., Lesko, M. H., Ruef, N., Roddie, C., Henry, J. Y., Spain, L., ben Aissa, A., Georgiou, A., Wong, Y. N. S., Smith, M., Strauss, D., Hayes, A., Nicol, D., … Kirk, A. (2018). Fc Effector Function Contributes to the Activity of Human Anti-CTLA-4 Antibodies. Cancer Cell, 33(4), 649-663.e4. https://doi.org/10.1016/j.ccell.2018.02.010

Vargas, F., Furness, A. J. S., Solomon, I., Joshi, K., Mekkaoui, L., Lesko, M. H., Miranda Rota, E., Dahan, R., Georgiou, A., Sledzinska, A., ben Aissa, A., Franz, D., Werner Sunderland, M., Wong, Y. N. S., Henry, J. Y., O'Brien, T., Nicol, D., Challacombe, B., Beers, S. A., … Asante-Siaw, J. (2017).

Fc-Optimized Anti-CD25 Depletes Tumor-Infiltrating Regulatory T Cells and Synergizes with PD-1 Blockade to Eradicate Established Tumors. Immunity, 46(4), 577–586. https://doi.org/10.1016/j.immuni.2017.03.013

Vasanthakumar, A., Liao, Y., Teh, P., Pascutti, M. F., Oja, A. E., Garnham, A. L., Gloury, R., Tempany, J. C., Sidwell, T., Cuadrado, E., Tuijnenburg, P., Kuijpers, T. W., Lalaoui, N., Mielke, L. A., Bryant, V. L., Hodgkin, P. D., Silke, J., Smyth, G. K., Nolte, M. A., … Kallies, A. (2017). The TNF Receptor Superfamily-NF-κB Axis Is Critical to Maintain Effector Regulatory T Cells in Lymphoid and Non-lymphoid Tissues. Cell Reports, 20(12), 2906–2920. https://doi.org/10.1016/j.celrep.2017.08.068

Vasanthakumar, A., Moro, K., Xin, A., Liao, Y., Gloury, R., Kawamoto, S., Fagarasan, S., Mielke, L. A., Afshar-Sterle, S., Masters, S. L., Nakae, S., Saito, H., Wentworth, J. M., Li, P., Liao, W., Leonard, W. J., Smyth, G. K., Shi, W., Nutt, S. L., … Kallies, A. (2015). The transcriptional regulators IRF4, BATF and IL-33 orchestrate development and maintenance of adipose tissue–resident regulatory T cells. Nature Immunology, 16(3), 276–285. https://doi.org/10.1038/ni.3085

Virgin, H. W., Wherry, E. J., & Ahmed, R. (2009). Redefining Chronic Viral Infection. Cell, 138(1), 30–50. https://doi.org/10.1016/j.cell.2009.06.036

Walker, L. S. K., & Sansom, D. M. (2011). The emerging role of CTLA4 as a cell-extrinsic regulator of T cell responses. Nature Reviews Immunology, 11(12), 852–863. https://doi.org/10.1038/nri3108

Wang, D., Quiros, J., Mahuron, K., Pai, C.-C., Ranzani, V., Young, A., Silveria, S., Harwin, T., Abnousian, A., Pagani, M., Rosenblum, M. D., van Gool, F., Fong, L., Bluestone, J. A., & DuPage, M. (2018). Targeting EZH2 Reprograms Intratumoral Regulatory T Cells to Enhance Cancer Immunity. Cell Reports, 23(11), 3262–3274. https://doi.org/10.1016/j.celrep.2018.05.050

Wang, R., Dillon, C. P., Shi, L. Z., Milasta, S., Carter, R., Finkelstein, D., McCormick, L. L., Fitzgerald, P., Chi, H., Munger, J., & Green, D. R. (2011). The Transcription Factor Myc Controls Metabolic Reprogramming upon T Lymphocyte Activation. Immunity, 35(6), 871–882. https://doi.org/10.1016/j.immuni.2011.09.021

Wei, W.-Z., Jacob, J. B., Zielinski, J. F., Flynn, J. C., Shim, K. D., Alsharabi, G., Giraldo, A. A., & Kong, Y. M. (2005). Concurrent Induction of Antitumor Immunity and Autoimmune Thyroiditis in CD4+CD25+ Regulatory T Cell–Depleted Mice. Cancer Research, 65(18), 8471–8478. https://doi.org/10.1158/0008-5472.CAN-05-0934

Wherry, E. J. (2011). T cell exhaustion. Nature Immunology, 12(6), 492–499. https://doi.org/10.1038/ni.2035

Williams, J. B., Horton, B. L., Zheng, Y., Duan, Y., Powell, J. D., & Gajewski, T. F. (2017). The EGR2 targets LAG-3 and 4-1BB describe and regulate dysfunctional antigen-specific CD8+ T cells in the tumor microenvironment. Journal of Experimental Medicine, 214(2), 381–400. https://doi.org/10.1084/jem.20160485

Wing, K., Onishi, Y., Prieto-Martin, P., Yamaguchi, T., Miyara, M., Fehervari, Z., Nomura, T., & Sakaguchi, S. (2008a). CTLA-4 Control over Foxp3 + Regulatory T Cell Function. Science, 322(5899), 271–275. https://doi.org/10.1126/science.1160062

Wolf, Y., Anderson, A. C., & Kuchroo, V. K. (2020). TIM3 comes of age as an inhibitory receptor. Nature Reviews Immunology, 20(3), 173–185. https://doi.org/10.1038/s41577-019-0224-6

Wooldridge, L., Ekeruche-Makinde, J., van den Berg, H. A., Skowera, A., Miles, J. J., Tan, M. P., Dolton, G., Clement, M., Llewellyn-Lacey, S., Price, D. A., Peakman, M., & Sewell, A. K. (2012). A Single Autoimmune T Cell Receptor Recognizes More Than a Million Different Peptides. Journal of Biological Chemistry, 287(2), 1168–1177. https://doi.org/10.1074/jbc.M111.289488

Yang, B.-H., Wang, K., Wan, S., Liang, Y., Yuan, X., Dong, Y., Cho, S., Xu, W., Jepsen, K., Feng, G.-S., Lu, L.-F., Xue, H.-H., & Fu, W. (2019). TCF1 and LEF1 Control Treg Competitive Survival and Tfr Development to Prevent Autoimmune Diseases. Cell Reports, 27(12), 3629-3645.e6. https://doi.org/10.1016/j.celrep.2019.05.061

Yu, G., Wang, L.-G., & He, Q.-Y. (2015). ChIPseeker: an R/Bioconductor package for ChIP peak annotation, comparison and visualization. Bioinformatics, 31(14), 2382–2383. https://doi.org/10.1093/bioinformatics/btv145

Zambelli, F., Pesole, G., & Pavesi, G. (2009). Pscan: finding over-represented transcription factor binding site motifs in sequences from co-regulated or co-expressed genes. Nucleic Acids Research, 37(suppl_2), W247–W252. https://doi.org/10.1093/nar/gkp464

Zarour, H. M. (2016). Reversing T-cell Dysfunction and Exhaustion in Cancer. Clinical Cancer Research, 22(8), 1856–1864. https://doi.org/10.1158/1078-0432.CCR-15-1849

Zhang, N., & Bevan, M. J. (2011). CD8+ T Cells: Foot Soldiers of the Immune System. Immunity, 35(2), 161–168. https://doi.org/10.1016/j.immuni.2011.07.010

Zheng, C., Zheng, L., Yoo, J.-K., Guo, H., Zhang, Y., Guo, X., Kang, B., Hu, R., Huang, J. Y., Zhang, Q., Liu, Z., Dong, M., Hu, X., Ouyang, W., Peng, J., & Zhang, Z. (2017). Landscape of Infiltrating T Cells in Liver Cancer Revealed by Single-Cell Sequencing. Cell, 169(7), 1342-1356.e16. https://doi.org/10.1016/j.cell.2017.05.035

Zheng, Y., Chaudhry, A., Kas, A., deRoos, P., Kim, J. M., Chu, T.-T., Corcoran, L., Treuting, P., Klein, U., & Rudensky, A. Y. (2009). Regulatory T-cell suppressor program co-opts transcription factor IRF4 to control TH2 responses. Nature, 458(7236), 351–356. https://doi.org/10.1038/nature07674

# 7. Appendices

## 7.1 List of abbreviations

| | |
|---|---|
| Ag | Antigen |
| ADCC | Antibody dependent cellular cytoxicity |
| AICE | AP-1 composite elements |
| ALRA | Adaptively-thresholded Low Rank Approximation |
| APCs | Antigen-presenting cells |
| ATAC-seq | Assay for Transposase-Accessible Chromatin using sequencing |
| AUC | Area Under Curve |
| BATF | Basic Leucine Zipper ATF-Like Transcription |
| BLIMP1 | B lymphocyte-induced maturation protein |
| BM | Bone marrow |
| Breg | regulatory B cells |
| CCR8 | Chemokine (C-C motif) receptor 8 |
| CFSE | 5-(and 6)-carboxyfluorescein diacetate succinimidyl ester |
| CD127 | IL7-receptor subunit |
| CD15s | syalyn Lewis x |
| CD244 | natural killer cell receptor 2B4 |
| CD25 | IL2-receptor α chain |
| CD39 | ectonucleoside triphosphate diphosphohydrolase 1 |
| CD73 | 5'-nucleotidase |
| cDC2 | type 2 dendritic cell |
| ChIP | Chromatin Immunoprecipitation sequencing |
| CSV | comma-separated |
| CTLA-4 | Cytotoxic T Lymphocyte Antigen 4 |
| CTV | Cell Trace Violet |
| d | Day |
| D | Diversity |
| DC | Dendritic cell |
| DEG | Differentially Expressed Gene |
| DFS | Disease Free Survival |
| DN | Double Negative |
| DP | Double Positive |

| | |
|---|---|
| EDTA | Ethylenediaminetetraacetic Acid |
| EZH2 | Enhancer of Zeste Homolog 2 |
| FAK | Fochal Adhesion kinase |
| FC | Fold Change |
| FCS | Flow Cytometry Standart |
| FOXP3 | Forkhead box transcription factor 3 |
| γc | Gamma chain |
| FDR | False Discovery Rate |
| FMO | Fluorescence Minus One |
| FOXO1 | Forkhead box protein O1 |
| GATA3 | GATA-binding protein 3 |
| GEO | Gene Expression Omnibus |
| GEPIA | Gene Expression Profiling Interactive Analysis |
| GFP | Green Fluorescent Protein |
| GITR | Glucorticoid-induced TNFR-related protein |
| GSEA | Gene Set Enrichment Analysis |
| HNSCC | squamous cell carcinoma |
| HBV | Hepatitis B Virus |
| HSC | Haematopoietic Stem Cell |
| iCCA | intrahepatic cholangiocarcinoma |
| IFN | Interferon |
| IPEX | X-linked syndrome |
| Ig | Immunoglobulin |
| ICOS | Inducibile T Cell Costimulator |
| ID3 | DNA-binding protein inhibitor 3 |
| IL | Interleukin |
| IL1R2 | Interleukin 1 Receptor Type 2 |
| IRF4 | Interferon regulatory factor 4 |
| LEF1 | Lymphoid Enhancer binding Factor 1 |
| mAb | Monoclonal antibody |
| J | Joining |
| LAG3 | Lymphocyte-activation gene 3 |
| LIHC | hepatocellular carcinoma |
| LUAD | Lung adenocarcinoma |
| LV | Lentiviral |
| MDSCs | Myeloid Derived Suppressor Cells |

| | |
|---|---|
| MFI | Median fluorescence intensity |
| MHC | Major histocompatibility complex |
| MAIT | Mucosal-Associated Invariant T cells |
| MEOX1 | Mesenchyme homeobox 1 |
| NK | Natural killer |
| NRP1 | Neuropilin-1 |
| NSCLC | Non Small Cell Lung Cancer |
| OE | Over Expression |
| OS | overall survival |
| PB | Peripheral blood |
| PBMCs | Peripheral blood mononuclear cells |
| PCA | Principal Component Analysis |
| PET | Positron Emission Tomography |
| PI | Proliferation Index |
| p:MHC | Peptide-MHC |
| PPAR-γ | Peroxisome Proliferator-Activated Receptor gamma |
| pTreg | peripheral Treg |
| RCC | Renal carcinoma |
| SCENIC | Single-Cell regulatory network Inference and Clustering |
| scRNA-seq | single cell RNA-sequecing |
| SD | Standard Deviation |
| SEM | Standard error of the mean |
| SKCM | melanoma dataset |
| SLO | Secondary Lymphoid Organ |
| SUVmax | maximum standardized value of fluorodeoxyglucose uptake |
| T-bet | T-box transcription factor TBX21 |
| TCF1 | T cell specific transcription factor 1 |
| TCGA | The Cancer Genome Atlas |
| $T_{CM}$ | Central memory T cells |
| TCR | T cell receptor |
| TGF-β | Transforming Growth Factor-Beta |
| TIM3 | T-Cell Membrane Protein 3 |
| $T_{EFF}$ | Effector T cells |
| $T_{EM}$ | Effector memory T cell |
| $T_{EX}$ | Exhausted T cells |
| TF | Transcription Factor |

| | |
|---|---|
| TFBM | Transcription Factor Binding Motif |
| $T_H$ | T Helper cells |
| $T_H17$ | T helper type-17 cells |
| $T_{MEM}$ | Memory T cells |
| TME | Tumor Microenvironment |
| $T_N$ | Naïve T cells |
| *TNFRSF4* | Tumor Necrosis Factor Receptor Superfamily member 4 |
| *TNFRSF9* | Tumor Necrosis Factor Receptor Superfamily member 9 |
| *TNFRSF18* | Tumor Necrosis Factor Receptor Superfamily member 18 |
| Tr1 | type 1 regulatory T cells |
| TREC | T cell Receptor Excision Circle |
| Treg | Regulatory T cells |
| tTreg | Thymus derived Treg |
| Tresp | T conv responder cells |
| $T_{RM}$ | Tissue Resident memory cells |
| TSDR | Treg-specific demethylation region |
| t-SNE | t-Distributed Stochastic Neighbor Embedding |
| TSS | Transcription Starting Site |
| $T_{TE}$ | Terminal effector memory T cells |
| UMAP | Uniform Manifold Approximation and Projection |
| UMI | Unique Molecular Identifier |
| UT | Untransduced cells |
| V | Variable |
| VAT | Visceral Adipose Tissue |
| WT | Wild-Type |

## 7.2 List of Figures

### Introduction



### Results

Results part 1



Results Part 2

## 7.3 List of Tables

## 7.4 List of PhD candidate publications

- Alvisi G, Puccio S, Scirgolea C, Lugli E. *High-dimensional single-cell profiling of tumor-infiltrating CD4+ regulatory T cells.* Methods Mol Biol. 2022

- Alvisi G*, Termanini* A, Soldani C, Portale F, Carriero R, Pilipow K, Polidoro M, Franceschini B, Malenica I, Puccio S, Lise V, Galletti G, Zanon V, Colombo FS, Tufano M, Peano C, Iannacone M, Roychoudhuri R, Donadon M, Torzilli G, Kunderfranco P, Di Mitri D, Lugli E, Lleo A. *Multimodal single-cell profiling of intrahepatic cholangiocarcinoma defines hyperactivated Tregs as a potential therapeutic target.* Journal of Hepatology. 2022

- Losurdo A*, Scirgolea C*, Alvisi G, Brummelman J, Errico V, Di Tommaso L, Pilipow K, Colombo FS, Bethania Fernandes B, Peano C, Testori A, Tinterri C, Roncalli M, Santoro A, Mazza EMC, Lugli E. *Single-cell profiling defines the prognostic benefit of CD39high tissue resident memory T cells in luminal-like breast cancer.* Communication Biology. Commun Biol. 2021

- Van Beek JJP*, Puccio S*, Roberto A*, De Paoli F, Graziano G, Salviato E, Alvisi G, Zanon V, Scarpa A, Zaghi E, Calvi M, Di Vito C, Mineri R, Sarina B, De Philippis C, Santoro A, Mariotti J, Bramanti J, Ferrari F, Castagna L, Mavilio D, Lugli E. *Single-cell profiling reveals the dynamics of cytomegalovirus-specific T cells in haploidentical hematopoietic stem cell transplantation*. Hematologica 2021.

- Bonnal RJP*, Rossetti G*, Lugli E*, De Simone M*, Gruarin P*, Brummelman J*, Drufuca L, Passaro M, Bason R, Gervasoni F, Della Chiara G, D'Oria C, Martinovic M, Curti S, Ranzani V, Cordiglieri C, Alvisi G, Mazza EMC, Oliveto S, Silvestri Y, Carelli E, Mazzara S, Bosotti R, Sarnicola ML, Godano C, Bevilacqua V, Lorenzo M, Siena S, Bonoldi E, Sartore-Bianchi A, Amatu A, Veronesi G, Novellis P, Alloisio M, Giani A, Zucchini N, Opocher E, Pisani Ceretti A, Mariani N, Biffo S, Prati D, Bardelli A, Geginat J, Lanzavecchia A, Abrignani S, Pagani M. *Clonally expanded EOMES+ Tr1-like cells in primary and metastatic tumors are associate with disease progression.* Nat Immunol. 2021 Jun;22(6):735-745.

- Galletti G*, De Simone G*, Mazza EMC*, Puccio S, Mezzanotte C, Bi TM, Davydov AN, Metsger M, Scamardella E, Alvisi G, De Paoli F, Zanon V, Scarpa A, Camisa B, Colombo FS, Anselmo A, Peano C, Polletti S, Mavilio D, Gattinoni L, Boi SK, Youngblood BA, Jones RE, Baird DM, Gostick E, Llewellyn-Lacey S, Ladell K, Price DA, Chudakov DM, Newell EW, Casucci M, Lugli E. *Two subsets of stem-like CD8+ memory T cell progenitors with distinct fate commitments in humans.* Nat Immunol. 2020 Dec;21(12):1552-1562.

- Bruzzone L*, Argüelles C*, Sanial M, Miled S, Alvisi G, Gonçalves-

Antunes M, Qasrawi F, Holmgren R, Smibert C, Lipshitz H, Boccaccio GL, Plessis A, Bécam I. *Regulation of the RNA-binding protein Smaug by the GPCR Smoothened via the kinase Fused.* EMBO Rep. 2020 Jul 3;21(7):e48425.

- Alvisi G*, Brummelman J*, Puccio S*, Mazza EMC, Paoluzzi Tomada E, Losurdo A, Zanon V, Peano C, Colombo FS, Scarpa A, Alloisio M, Vasanthakumar A, Roychoudhuri R, Kallikourdis M, Pagani M, Lopci E, Novellis P, Blume J, Kallies A, Veronesi G, Lugli E. *IRF4 instructs effector Treg differentiation and immune suppression in human cancer.* J Clinic Invest. 2020 Jun 1;130(6):3137-3150.

- Martini E*, Kunderfranco P*, Peano C, Carullo P, Cremonesi M, Schorn T, Carriero R, Termanini A, Colombo FS, Jachetti E, Panico C, Faggian G, Fumero A, Torracca L, Molgora M, Cibella J, Pagiatakis C, Brummelman J, Alvisi G, Mazza EMC, Colombo MP, Lugli E, Condorelli G, Kallikourdis M. *Single-Cell Sequencing of Mouse Heart Immune Infiltrate in Pressure Overload-Driven Heart Failure Reveals Extent of Immune Activation.* Circulation. 2019 Dec 17;140(25):2089-2107.

- Cossarizza A, Chang HD, Radbruch A, Acs A , Adam D, Adam-Klages S, Agace WW, Aghaeepour N, Akdis M, Allez M, Almeida LN, Alvisi G et al. (…) *Guidelines for the use of flow cytometry and cell sorting in immunological studies (Second edition)* Eur J Immunol. 2019 Oct, 49(10):1457-1973.

- Brummelman J, Haftmann C*, Núñez NG*, Alvisi G, Mazza EMC, Becher B, Lugli E. *Development, application and computational analysis of high-dimensional fluorescent antibody panels for single-cell flow cytometry.* Nat Protoc 2019 Jul;14(7):1946-1969.

- Brummelman J*, Mazza EMC*, Alvisi G, Colombo FS, Grilli A, Mikulak J, Mavilio D, Alloisio M, Ferrari F, Lopci E, Novellis P, Veronesi G, Lugli E. *High-Dimensional Single Cell Analysis Identifies Stem-Like Cytotoxic CD8+ T Cells Infiltrating Human Tumors.* J Exp Med, 2018 Oct 1;215(10):2520-2535.

- Mazza EMC*, Brummelman J*, Alvisi G, Roberto A, De Paoli F, Zanon V, Colombo F, Roederer M, Lugli E. *Background fluorescence and spreading error are major contributors of variability in high-dimensional flow cytometry data visualization by tSNE.* Cytometry A, 2018 Aug;93(8):785-792.

*these authors contributed equally

## 7.5 Author contribution

*Part 1:* E. Lugli, J. Brummelman and I conceived the study. J. Brummelman and I analyzed and interpreted the data. E. Lugli supervised the study. S. Puccio performed bulk RNA sequencing and ChIP data analysis. I performed high dimensional single cell analysis after previous training by Simone Puccio and Emilia Mazza. I perfomed all the experiments on human samples with the support of other members of the Laboratory of Translational Immunology, namely Elisa Paoluzzi Tomada (MD student) and Veronica Zanon (Lab technician). Jonas Blume performed all the mice experiments. I performed FACS sorting, after previous training by E. Lugli, F.S. Colombo. Clelia Peano and Javier Cibella performed sequencing experiments and supported RNA libraries generation. Marco Alloisio, Pierluigi Novellis, and Giulia Veronese performed surgery. Agnese Losurdo, Egesta Lopci and Giulia Veronesi provided clinical information and helped with clinical interpretation of the data. Rahul Roychoudhuri, Marinos Kallikourdis, Massimiliano Pagano and Axel Kallies provided expertise in data analysis. Giorgia Alvisi and Enrico Lugli wrote the manuscript related to these results (Alvisi et al., 2020).

*Part 2:* Alberto Termanini, Cristiana Soldani, Paolo Kunderfranco, Diletta Dimitri, Enrico Lugli, Ana Lleo and I, conceptulize and deisgned the study. I perfomed all the wet experiments with the support of other members of the Laboratory of Translational Immunology. The memebers of the Laboratory of Hepatobiliary Immunopathology collected and processed the samples. Clelia Peano and Javier Cibella performed sequencing experiments and supported RNA libraries generation. I performed high dimensional flow cytometric analysis after previous training by Simone

Puccio. I performed single cell RNA sequencing analysis with the support, menthorship and supervision of the Humanitas bioinformatic core (Alberto Termanini, Paolo Kunderfranco and Roberta Carriero). The division of Internal Medicine and Hepatology, Department of Gastroenterology, provided clinical data and provided a clinical interpretation of the data.